Light-Matter Interactions in a Single Josephson Junction Microwave Resonator

by Samuel Andersson

LUND
UNIVERSITY

Division of Mathematical Physics

Thesis for the degree of
Master of Science in Engineering Physics

Supervisor: Peter Samuelsson
Co-supervisor: Ville Maisi

Examiner: Gillis Carlsson

June 7, 2024

Abstract

This thesis models a superconducting device, known as a Transmon, from the perspective of a microwave resonator. The work is motivated by Ref. 1, where such a device was realised and characterised by its resonator properties, showing that it can be viewed as a high-impedance resonator. In the thesis, the resonator is symmetrically connected to two transmission lines: one input port and one output port. Both single tone and two-tone measurements are treated, where the two-tone case treats the limit of a weak probe. The measurements are simulated within the framework of input-output theory, however the Lindblad master equation is also used showcasing an alternative approach for solving the system dynamics. In the two-tone measurements we also find a coherent signal at a third frequency, other than the probe or drive frequencies. This leaves an open question of seeing if this signal can be measured in experiments and how to explain it. The thesis also raises the question of whether the perspective of a resonator with photons residing inside it is actually valid in this extreme case of a Transmon, often considered as an artificial atom. It is highlighted that an alternative picture than that of a 'dressed atom' should be presented in the highly non-linear regime in order to aid this interpretation.

Populärvetenskaplig Sammanfattning

Mikrovågsugnar på kvantnivå

Mikrovågsresonatorer används inom supraledande kvantsystem för avläsning och manipulation av kvantkomponenter. I avhandlingen analyseras en sådan där gränsdragningen mellan foton och exciterad 'atom' börjar suddas ut i dessa system.

De senaste decennierna har supraledande kretsar och komponenter haft stort intresse inom forskningen. Det finns flera orsaker till detta; bland annat tack vare att dessa kan uppvisa kvantfysikaliska fenomen, de kan konstrueras med hög precision och de erbjuder en möjlighet att studera hur ljus och materia interagerar med varandra under särskilda förhållanden. Att ett ämne är supraledande innebär att det kan leda ström utan någon resistans. Detta är en egenskap som några material får när de kyls ner till mycket låga temperaturer. Till exempel blir aluminium supraledande när det kyls ner till cirka 1.2 Kelvin, där 0 Kelvin är den absoluta nollpunkten (-273.15 °C). Detta är en väldigt låg temperatur, men i labb kan man med relativt god tillgänglighet numera kyla ner enheter till temperaturer av enstaka tusendelars Kelvin. Att använda kvantfenomenen som uppstår från supraledande effekter är ett av flera sätt man forskar på idag för att lyckas bygga en kvantdator, som skulle vara mycket effektivare på att lösa vissa specifika problem. För att åstadkomma detta krävs kvantversionen av en bit (något som antar värde 0 eller 1, principen som datorer är byggda på), en så kallad 'kvantbit'. En komponent i ansatsen att åstadkomma en qubit för supraledande kretsar har fått namnet Transmon. Denna kallas ibland för en 'artificiell atom', då den har egenskaper som atomer är kända för att ha. Bland annat kan den fånga upp, fotoner - enskilda paket av ljus - som den sedan kan skicka iväg. En viktig komponent för att manipulera och läsa av kvantbitar är det som kallas för mikrovågsresonatorer. Det är i princip känt hur man konstruerar dessa, men ständigt arbete pågår för att förbättra dem och hitta nya tillämpningar. Namnet är säkert bekant, då en mikrovågsugn är en typ av mikrovågsresonator, men vi behöver en mycket mindre och kontrollerad variant, med lite annan funktion. Fotonerna - ljuset - har ungefär samma våglängd men våra resonatorer vill hålla inne fotoner som matchar dess resonansfrekvens en liten stund och stänga ute resten.

Vad är då en resonansfrekvens? Tänk dig att du rullar ut en jojo hela vägen. Sedan sätter du den i svängning så att den svänger fram och tillbaka. Rör du dig fram och tillbaka i rätt tempo - med rätt frekvens - kommer den svänga mer, än om du försöker få den att svänga mycket långsammare eller mycket snabbare. Då svänger du i resonans med jojon.

I denna avhandling analyserar jag en resonator vars resonansfrekvens bestäms med hjälp av egenskaper hos Transmonen och är en teoretisk analys baserat på experiment jag utfört tidigare. Detta ger upphov till olinjära effekter som kan vara intressanta att undersöka för att få bättre förståelse för kvantfysiken. En sådan olinjär effekt som förutspås teoretiskt i uppsatsen är att när ljus med två olika frekvenser skickas in i resonatorn, kommer den under vissa förhållanden skicka ut ljus med en tredje våglängd. Detta återstår att observera i experiment.

Acknowledgements

I want to start by thanking both of my (very encouraging) supervisors, Peter Samuelsson and Ville Maisi, as this thesis would not be possible without them. Peter has an inspiring interest in physics, an incredible drive and shares my sense of discomfort when there are unresolved ”murky” details. Although he can sometimes be a little difficult to reach (he's a busy man), discussions with him are always a pleasure and he is very engaging. Ville has always had an open door, and his love for physics is infectious. He is an experienced experimentalist, while still being very skilled with theory and has provided a lot of feedback and ideas for the thesis. He always has an open door and has helped me untangle many knots ever since I first started working with him almost a year ago. It is comforting knowing that I will continue working with such a remarkable supervisor.

Thank you to my opponents Gustav, Andrea and Ferdinand for providing feedback and comments on the thesis. My apologies for giving you so much work.

Next I want to thank all of my friends from the F-guild who have made my five years at Lund University a memory that I will cherish dearly, with a shout out to Nördbordet and in particular Nils (NK) who has helped me resolve issues with VS Code.

Everyone I have shared an office with during my time here, thank you! The days are just brighter when you are around. Also while I am at it, the people at Solid States and Mathematical Physics, in particular everyone in Peter's and Ville's groups as well as the Germans!

I shall not forget my friends from Uddevalla, thank you for always showing me that there are more things to enjoy in life than just physics!

Last but not least, I want to thank my family. Hilda and Amanda, somewhere along the years you must have grown up as it seems like we never fight anymore. Keep on being as wonderful as you are (btw, you are very good at buying gifts, so I might continue leaving that responsibility to you...). Mum and dad, even though you might provide very little help when I have pondering questions about physics, it is thanks to your sacrifices and the support that you have provided throughout my life that has allowed me to get to where I am. I owe you everything.

Contents

Chapter 1

Introduction

We are the universe experiencing itself.
- Carl Sagan

Superconducting microwave resonators are used in for instance quantum optics and quantum information, where they are often based on a coplanar waveguide (CPW) design, the equivalent of a coaxial cable on a 2D surface [2, 3]. CPW microwave resonators have use in studying some metals [4], as well as coupling to quantum devices such as superconducting qubits [5] and quantum dots [6, 7]. CPW resonators are typically linear over several orders of magnitude, meaning that the number of photons stored in the resonator cavity can be varied several orders of magnitude without changing the resonance frequency. A typical design is schematically depicted in Fig. 1.1, which shows a finite transmission line on a Si wafer surrounded by a ground plane. The geometry of this (Fig. 1.1b) determines some capacitance and inductance per unit length. The length of the cavity L can then be used to choose the resonance frequency to high precision [3, 8]. The Hamiltonian for such a system can be modelled as an ideal harmonic oscillator [9], yielding the highly linear behaviour. CPWs have been proven useful for the study of light and matter, as they can be used to reach the strong coupling regime when coupled to artificial atoms [10].

One of the reasons that superconducting circuits allow for the study of interaction between light and matter is the introduction of a new non-linear circuit element known as the Josephson junction [11]. The properties of the Josephson junction have been used for achieving parametric amplification [12–14], realising artificial atoms [15, 16] and fabricating high-impedance resonators by using arrays of Josephson junctions in order to achieve strong and ultra-strong coupling [17, 18], among several other applications.

Taking the limit of only one junction as a resonator, which is what this thesis considers, you end up effectively with a Transmon. Transmon qubits are a modification of the original Cooper pair box (CPB) [15]. A CPB uses the non-linearity of a Josephson junction to achieve energy levels with anharmonicity, allowing them to be used as qubits. An issue with CPBs are that they are sensitive to charge noise, which the Transmon solves

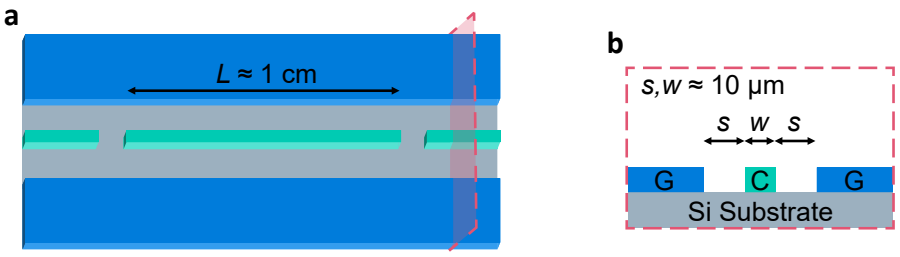

Figure 1.1: A schematic picture of a CPW resonator with insets of typical length scales. In **a** you can see the silicon substrate in grey. On top of this is a ground plane G (in blue) with a centre conductor C (in turquoise) where the separation defines a capacitive coupling between transmission lines on the left and right to the cavity in the middle. The length of the cavity L is one of the parameters defining the resonance frequency of the cavity. In **b** you see a linecut of the transmission line geometry, where the parameters s, w can be used to define some inductance and conductance per unit length.

by coupling a large capacitance to the CPB. The sensitivity to charge noise is reduced exponentially, while the anharmonicity is reduced according to a power law by this added capacitance [16]. These Transmons can be coupled to resonators for manipulation and readout [17, 19]. They are often considered as 'artificial atoms' due to their energy level structure and coupling to photons. Their energy level structure is similar to a harmonic oscillator, but with added anharmonicity. This means that the resonance frequency for a transition depends on which state the Transmon is in, for instance if it is in the ground state or some excited state. The resonance frequency decreases if it is in an excited state compared to the ground state. This shift in resonance frequency is a parameter that can be chosen in fabrication within some constraints [16].

During the summer of 2023 at Lund University, we made a microwave resonator using the properties of the well known Transmon [1]. High-impedance resonators have been fabricated previously using arrays of Josephson junctions in order to increase the coupling strength to circuit quantum electrodynamics (cQED) elements, such as Transmons or quantum dots [17, 18, 20, 21], however the limit of one junction had not been viewed in the light of a resonator before. The resonator became highly non-linear in the sense that it saturated at one photon in the resonator at the bare resonance frequency. The next photon that could be stored in the resonator had to have a lower frequency to be resonant with the Transmon again. This was observed using two-tone measurements, where two radio frequency (RF) signals are sent into the resonator. One that is measured (the probe) and one that drives the system to a certain desired state (the drive). This method has been used when measuring similar devices [22–26].

The main goal of this thesis is to use the established theoretical framework of analysing quantum electrical circuits, in order to test the agreement with theory and experiment. A secondary goal in this is to give an introduction to the theory, by deriving many of the relations in order to give a connection between the theory and the actual physics, which

will hopefully give some intuition for the theoretical formulas. Furthermore many of the calculations will be presented in detail so that the steps will be easier to follow. This will hopefully serve also as an introduction on how the theoretical toolbox may be used. The thesis also tries to view the Transmon from the perspective of a high-impedance resonator. This is different from the usual picture of an artificial atom, however as we will see, this distinction is seldom going to be of relevance in theoretical considerations. It will rather come as a short discussion in Chapter 8. Due to the strong anharmonicity of the Transmon compared to the linewidth of the system, a reduction to a simpler two-level system will become useful in understanding some of the observed features of the Transmon resonator.

The structure of the thesis is as follows. Chapter 2 has a short introduction on the experimental setup that the theory aims to simulate. After that, in Chapter. 3, I will introduce circuit quantisation and the Josephson element, as well as other building blocks that will be needed, such as the Transmon. In Chapter 4 input-output theory is introduced, first in a general case when studying a system weakly coupled to a bosonic bath before before deriving the equations of motion for the Transmon symmetrically coupled to transmission lines. In Chapter 5 the Lindblad master equation is introduced as an additional tool for studying the dynamics of quantum systems, where also the two-level system will be analysed within this framework in preparation for understanding some of the observed features of the Transmon. With all of the theory necessary presented, the methods of the theoretical simulations as well as results for single tone measurements (Chapter 6) and two-tone measurements (Chapter 7) will be presented, comparing the theoretical prediction with the experimental data. In these chapters, I will provide an explanation for some of the observed non-linear features. Then finally in Chapter 8, there will be some conclusions drawn from and discussion about the results from the thesis, as well as some outlook on future work that could be done. One of the interesting results of the thesis is the appearance of a coherent signal at a third frequency in the two-tone measurements, leaving an open question of whether or not this could be measured in experiments.

Chapter 2

Background

Leave the atom alone.
- Edgar "Yip" Harburg

Since the thesis project was motivated by experiments made [1], let us first get acquainted with what it is that we are trying to model and how measurements are carried out. The system is a microwave resonator, which means that the system has some eigenmode with a resonance frequency f_r in the microwave regime. In our particular system $\mathcal{S}$ which was studied, the resonance frequency was $f_r = 4.715\,\text{GHz}$, and photons carrying that frequency could enter the resonator from the left, and leave it to the right. This is depicted in Fig. 2.1, which shows a scanning electron microscope (SEM) image of the system. The turquoise part in the middle makes the island part of the resonator, the blue highlighted parts are transmission lines carrying microwave signals generated from an RF generator (RF In) and to a measurement device (RF Out), the brighter grey areas are the silicon wafer that the system was fabricated on and the darker grey areas are the ground plane. The light blue rectangle highlights the Josephson junction and is the main source of capacitance and inductance for this resonator. Since the blue and turquoise parts are never in touch, they

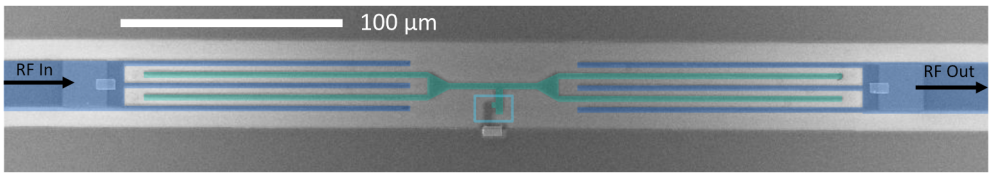

Figure 2.1: An SEM image of the microwave resonator that was studied in Ref. 1. Microwave photons are sent in through the left coupler in blue (RF In) and if they are resonant with the system they can travel across to the resonator island (turquoise) and then leave on the right coupler, also in blue (RF Out), where the signal is then measured. The measurement setup is illustrated in Fig. 2.2. The light grey areas of the image is the Si wafer that the system is fabricated on and the darker grey areas make up the ground plane. The light blue rectangle highlights the Josephson junction, which in this device defines the main inductance and capacitance, working effectively as an LC resonator as a single element. This will be further explained in Chapter 3.

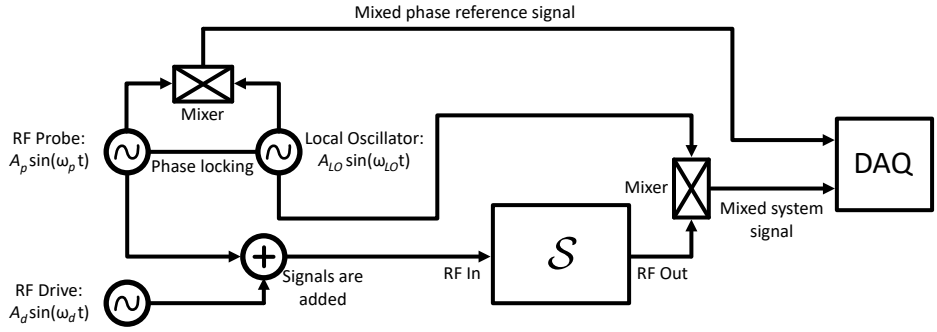

Figure 2.2: A schematic representation of how a measurement is made on the microwave resonator considered in Ref. 1. Three RF generators are sending signals into different transmission lines. The probe and LO signals are mixed in one branch directly without having entered the system. This is used as a phase reference when digitally analysing the signal from the system. The probe and drive signals are added before entering the system, and the outgoing signal is mixed with the LO before being digitised in the DAQ.

are only capacitively coupled, which means that photons generally cannot travel through unobstructed, unless they carry a frequency matching the eigenmode of the resonator. Photons that do not enter the resonator are reflected. If the microwaves are sufficiently close to the resonance frequency, they can still enter the resonator and be transmitted through, however with a lower probability, so the transmitted signal at such a frequency will be lower than on resonance. Or at least this is the case for a linear resonator. The experiments were conducted on a non-linear resonator, which means that if the input signal is twice as strong, the output signal is not necessarily twice as strong as well. As we will see, non-linear effects need to be taken into account and then it becomes relevant what is referred to when saying 'signal'. What is it that we actually measure for our signal? In the measurements, a setup for heterodyne detection was used. This will be explained in a little more detail in Sec. 4.5, but what it means is that the coherent part of the signal was measured. This will be defined more thoroughly in the thesis, however a familiar example of a source of coherent light would be that of a laser compared to a source of incoherent light such as an LED. There is clearly a difference which could be seen by for instance looking at diffraction patterns from each light source. The non-linearity of the resonator makes it so that the coherent amplitude can in some instances be lower on resonance than slightly off. This is due to a non-linear effect of destroying some of the coherence, unlike a linear resonator in which all of the coherence is preserved.

What does the measurement setup look like then, and what do we need to take into account in the theory? A simplified version is depicted in Fig. 2.2, which essentially contains all the relevant parts to consider in the theory. There are three RF generators (RF Probe, RF Drive and the Local Oscillator (LO)), all in the left part of the figure. They each send out a signal, in general with different amplitudes and frequencies, into transmission lines. The probe and the LO are phase locked, which essentially means that their internal clocks are synchronised and they have a stable phase relation. They both send a signal to a mixer,

which can be thought of as 'multiplying' the signals (more on this in Sec. 4.5). This mixed signal will be used as a phase reference for the signal that has gone through the system. The mixed phase reference signal is connected via a cable to a data acquisition (DAQ) system, which will digitise the signal for processing. Now if we consider what signal is sent into the system $\mathcal{S}$, we see that the RF Probe and RF Drive signals are added together before entering the system. Two types of measurement will be considered: one-tone and two-tone measurements. A one-tone measurement essentially just means that the RF Drive is turned off. The signal transmitted through the system is then sent into a mixer together with a signal from the LO. This mixed signal is then also sent into the DAQ and here the amplitude and phase of the component oscillating with frequency ω_p is extracted and compared to the phase from the phase reference signal. This is in order to be able to detect phase shifts in the signal.

The described measurement setup contains important parts of what is needed to be considered in the theory, as it tells us what quantity it is that we actually measure. The way the outgoing signal is depicted in Fig. 2.1 means that we measure the transmitted signal.

As this thesis has such a close connection to experiments, and is based on well established theory, figures will often be in units that make sense from an experimentalist's point of view, rather than in unitless parameters which are often something that a theoretician might be interested in. An example is the use of dBm as a unit. If you have not encountered it before, it is defined as $P(\text{dBm}) = 10\log_{10}\left(\frac{P(\text{mW})}{1\,\text{mW}}\right)$, so for instance $1\,\text{mW} = 0\,\text{dBm}$ and $100\,\text{mW} = 20\,\text{dBm}$.

Chapter 3

cQED

It's the irony of fate that the kinetic energy of the inductor is the potential energy in phase space..
- Ville F. Maisi

Circuit quantum electrodynamics (cQED or circuit QED) is the study of light-matter interactions in electrical circuits and borrows a number of techniques from the field by which the name was inspired; cavity QED, the study of interaction between light and individual atoms [27]. In cQED electrical circuits on the size of a few millimeters, with the smallest components the size of a few nanometers, are quantised. This means that continuous classical varibales like voltage and charge are turned into quantum operators. This is possible due to the fact that we are able to cool down these circuits to a a temperature of a few mK [28] such that $kT \ll \hbar\omega$ where ω is the typical resonance frequency of the circuit, making thermal fluctuations very small as well as turning some metals into superconductors. When a metal transitions into a superconducting state, it goes through a phase transition that changes some properties of the material. Famously, conduction without resistance is one of these properties [29]. Although superconductivity requires BCS theory to fully describe it [30], the tools that superconductivity provide can be understood without a full BCS theory description. A consequence of more fundamental properties of superconductors, is the possibility of creating a new circuit element: the Josephson junction (sometimes called Josephson element) [11], which has become of huge importance within the field of cQED with some of the applications already mentioned in Chapter 1.

The system that we will be interested in is know as a Transmon, a type of superconducting charge qubit [16]. In principle its Hamiltonian is well known within the community of superconducting qubits and the thesis will mostly be treating the Hamiltonian, so it could just be stated here. Doing this would however give no physical insight in how we end up with this Hamiltonian. There will therefore be some instructive introduction on how to quantise circuits, inspired by Ref. 9, and the Josephson junction before introducing the Transmon.

3.1 Setting up the Lagrangian

In quantum mechanics we know that the dynamics of a system is described by the Schrödinger equation. For this we need the Hamiltonian of our system, which can be derived from the Lagrangian. In cQED, our physical system can often be represented by a circuit diagram containing lumped and/or distributed elements of capacitors, resistors, conductors and inductors (and Josephson junctions). Initially these circuits are considered purely classical before 'promoting' conjugate variables to quantum operators. This method is in fact a common way to introduce quantum mechanics from the perspective of classical mechanics, where typically a mass is connected to a spring. Then we have the Hamiltonian

$$H = \frac{p^2}{2m} + \frac{1}{2}m\omega^2 x^2, \tag{3.1}$$

where p is the momentum of the mass, m is its mass, x is the displacement of the mass from the natural length of the spring and $\omega = \sqrt{k/m}$. Here x and p are conjugate variables, such that if we consider the Poisson bracket $[;]$, we have the relation

$$[x; p] = 1, \tag{3.2}$$

and we can promote our conjugate variables by letting $x \to \hat{x}$ and $p \to \hat{p}$, while giving them the commutation relation

$$[\hat{x}, \hat{p}] = i\hbar, \tag{3.3}$$

yielding the quantum version of the Hamiltonian for a mechanical oscillator

$$\hat{H} = \frac{\hat{p}^2}{2m} + \frac{1}{2}m\omega^2\hat{x}^2, \tag{3.4}$$

which can for instance come from a particle of mass m in a harmonic potential.

This time we did not start from the Lagrangian since it was just to provide a familiar example, however to see how one might go about this in cQED, we will start with setting up the Lagrangian for an LC oscillator (Fig. 3.1), as this is the typical example of a harmonic oscillator in circuit theory, bridging the gap between the mechanical harmonic oscillator case and the cQED equivalent. As we will see, the variables that we will want to quantise are the charge and flux. To find the Lagrangian we use node analysis. In

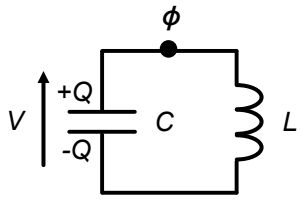

Figure 3.1: Circuit diagram of an LC circuit with parameter ϕ defined according to Eq. (3.5) and charge $\pm Q$ on the capacitor plates.

preparation for later, instead of charge q as the analogue of a position coordinate with flux Φ as its conjugate variable which is what is classically used, we will define our position coordinate as

$$\phi = \int_{t_0}^{t} V(\tau)\mathrm{d}\tau, \tag{3.5}$$

where $V(t)$ is the voltage at the node at time t. This is a little out of the blue for now, but this will be more natural when we get to the CPB. Since $V(t) = \dot{\phi}$, the potential energy stored in the capacitor with capacitance C is

$$E_{kin} = \frac{1}{2}C\dot{\phi}^2, \tag{3.6}$$

which looks like a kinetic energy term in the coordinate ϕ that we have defined. One thing to note is that ϕ is in the case of an LC oscillator still the magnetic flux Φ, which we can see from

$$\dot{\phi} = V = L\dot{I}, \tag{3.7}$$

where I is the current through the inductor and the last inequality is the voltage-current relation for an inductor. This is important in order to determine the kinetic energy stored in the inductor:

$$E_{pot} = \frac{1}{2L}\phi^2, \tag{3.8}$$

which now has the appearance of potential energy. Our Lagrangian is then

$$\mathcal{L} = E_{kin} - E_{pot} = \frac{1}{2}C\dot{\phi}^2 - \frac{1}{2L}\phi^2, \tag{3.9}$$

from which we find the conjugate variable

$$Q = \frac{\partial \mathcal{L}}{\partial \dot{\phi}} = C\dot{\phi} = CV, \tag{3.10}$$

where we see from the last equality that this corresponds to a charge. Analogous to position and momentum as conjugate variables in a mass connected to a spring, we can turn ϕ and Q into quantum operators with the conjugate variable commutation relation

$$[\hat{\phi}, \hat{Q}] = i\hbar. \tag{3.11}$$

There is a subtlety here which is that in order to get this sign convention, we need to define $Q = -q$ (so this commutation relation is almost like defining the charge of the electron to be positive). The Hamiltonian for the system is then readily obtained as

$$H = Q\dot{\phi} - \mathcal{L} = \frac{1}{2L}\phi^2 + \frac{1}{2C}Q^2, \tag{3.12}$$

where we see that as expected it is the total energy stored in the capacitor and inductor. Proceeding with the analogy of position and momentum, the Hamiltonian can be written as an operator by turning the flux and charge into quantum operators. Furthermore, you

can see a close resemblance to the Hamiltonian of a harmonic oscillator. This should come to no surprise, as the LC circuit is a very common example of such a system. The Hamiltonian can then be written in two ways:

$$\hat{H} = \frac{1}{2L}\hat{\phi}^2 + \frac{1}{2C}\hat{Q}^2 = \hbar\Omega\left(\hat{a}^\dagger\hat{a} + \frac{1}{2}\right), \tag{3.13}$$

where $\hat{a}, \hat{a}^\dagger$ are step operators which is exactly analogous to the mechanical harmonic oscillator and $\Omega = \sqrt{1/LC}$. This analogy will be made again later with the Transmon, and the likeness will then also be considered in a slightly more detailed manner.

Here a specific example has been used, but the approach is quite general. Electronic components like capacitors and inductors can be made very small, and by making them superconducting by cooling them to very low temperatures, quantum effects become relevant. This also allows for close to ideal circuits of purely reactive elements (like the LC circuit). Then the general method of node analysis and quantising the circuit can be used to derive quantum Hamiltonians for a system of interest.

3.2 Josephson relations and the Josephson junction

The Josephson junction that has already been mentioned a couple of times, consists of two superconducting leads with some 'weak link'. This weak link typically consists of a resistive material as a tunnel barrier, however can also be a normal conducting metal or entirely superconducting with a much thinner segment [29]. Cooper pairs are essentially paired up electrons, such that they become composite bosons. Cooper pairs in low temperature superconductors can be phenomenologically understood as electrons of opposite spin pairing up at low temperatures due to one electron attracting positively charged ions in a lattice, such that they in turn attract a new electron. Since Cooper pairs are composite bosons, several of them can occupy the same state. The Cooper pairs can then condense into the same ground state, forming an energy gap of 2Δ between the condensed state and the quasiparticle states. Due to this, the condensate has a macroscopic coherent wavefunction with one specific phase, which we will soon encounter, applying for all particles. The energy gap of 2Δ is known as the superconducting gap, and is the energy needed to break up a Cooper pair [29]. There is a critical temperature associated with superconducting materials, indicating at which temperature they become superconducting. Aluminium for instance has a critical temperature of about 1.2 K and a superconducting gap of about $\Delta = 200\,\mu\text{eV}$ (depending on the thickness of the metal) [31]. A good reference point to have is also the energy relation between frequency and temperature, where 1 K corresponds to a frequency of about 21 GHz. This shows the motivation for using microwave photons in superconducting resonators, where typical ranges are in the GHz regime as we want to be in a regime where $k_B T \ll \hbar\omega \ll 2\Delta$ in order to avoid breaking the Cooper pairs and

also avoid thermal fluctuations to the resonator mode.

I will start here by naming the two Josephson relations for tunnel junctions [11]:

$$\begin{cases} I(t) &= I_c \sin(\varphi(t)) \\ \frac{\partial \varphi}{\partial t} &= \frac{2eV(t)}{\hbar}, \end{cases} \tag{3.14}$$

where φ is interpreted as the phase difference between the Cooper pair wave equations of the superconductors separated by the junction (the phase mentioned in the previous paragraph), I_c is a quantity known as the 'critical current', the current at which the junction becomes normal conducting instead of superconducting and $V(t)$ and $I(t)$ are the voltage across and current through the junction. Note here that φ is proportional to ϕ defined in Eq. (3.5). It can therefore be interpreted as some flux. If we differentiate the first Josephson relation with respect to t, we see that we get

$$\frac{\partial I(t)}{\partial t} = I_c \cos(\varphi(t)) \frac{\partial \varphi}{\partial t} = \frac{2eI_c \cos(\varphi(t))}{\hbar} V(t), \tag{3.15}$$

which we can interpret as an inductance by

$$V(t) = \frac{L_J}{\cos(\varphi)} \frac{\mathrm{d}I(t)}{\mathrm{d}t} \Rightarrow L_J = \frac{\hbar}{2eI_c}. \tag{3.16}$$

Following this interpretation, we can find the energy E_M stored in the magnetic field at time t from some time t_0 as

$$\begin{aligned} E_M &= \int_{t_0}^{t} V(\tau) I(\tau) \mathrm{d}\tau = \int_{\varphi(t_0)}^{\varphi(t)} I_c \sin(\varphi) \frac{\hbar}{2e} \mathrm{d}\varphi \\ &= -\frac{I_c \hbar}{2e} \cos(\varphi(t)) + \frac{I_c \hbar}{2e} \cos(\varphi(t_0)) \\ &= -E_J \cos(\varphi(t)) + \text{const}, \end{aligned} \tag{3.17}$$

where the Josephson energy (sometimes referred to as the Josephson coupling) E_J has been defined as $L_J I_c^2$, which in these terms is very reminiscent of the energy stored in an inductor.

We see that the Josephson energy is dependent on the critical current I_c, but have not yet said anything about how this is determined. In case of a tunnel junction, for instance when there is an oxide layer between the superconducting leads, the Ambegaokar-Baratoff relation [32]

$$I_c = \frac{\pi}{2e} \frac{\Delta}{R_N} \tanh\left(\frac{\Delta}{2k_B T}\right) \tag{3.18}$$

becomes very useful, where R_N is the normal state resistance over the junction. Also, since we are at very low temperatures, $\tanh\left(\frac{\Delta}{2k_B T}\right) \approx 1$. With this formula we can now determine the Josephson energy E_J of a single junction in the case of a tunnel junction by measuring its normal state resistance. We are now ready to consider the Cooper pair

box and derive its Hamiltonian.

3.3 Cooper pair box

In order to derive a Hamiltonian for the Cooper pair box, we need to know its equivalent circuit diagram. One way of representing it is shown in Fig. 3.2, where also the circuit element representation for both an ideal and a non-ideal Josephson junction are shown. In Fig. 3.2b, the non-ideal Josephson junction is also represented as a parallel LCR circuit, where the resistance R_J can be used to represent internal losses. It is important not to confuse this with the $RCSJ$ (resistively capacitance shunted junction) model, which describes the junction at some bias voltage [29]. The resistance considered in that case is the normal state resistance, acting as a resistor for current flowing through the junction. When deriving the system Hamiltonian, losses from the junction will be neglected ($R_J = 0$) and internal losses will be added in later sections when the system is coupled to an environment, so the Josephson junction will be considered to have just a capacitance C_J and a non-linear inductance L_J from the Josephson relations.

If we now initially consider the variable ϕ (as we know from the LC oscillator that this can be thought of as the familiar flux) at the node indicated in Fig. 3.2c by a black dot, we can find the potential energy of the system by relating it to its adjacent nodes, receiving the energy stored in the capacitors as

$$U = \frac{1}{2}C_J\dot{\phi}^2 + \frac{1}{2}C_g(\dot{\phi} - V_g)^2, \tag{3.19}$$

and the energy stored by the Josephson junction is as we have seen (ignoring constant terms)

$$T = -E_J \cos\left(\frac{2e}{\hbar}\phi\right), \tag{3.20}$$

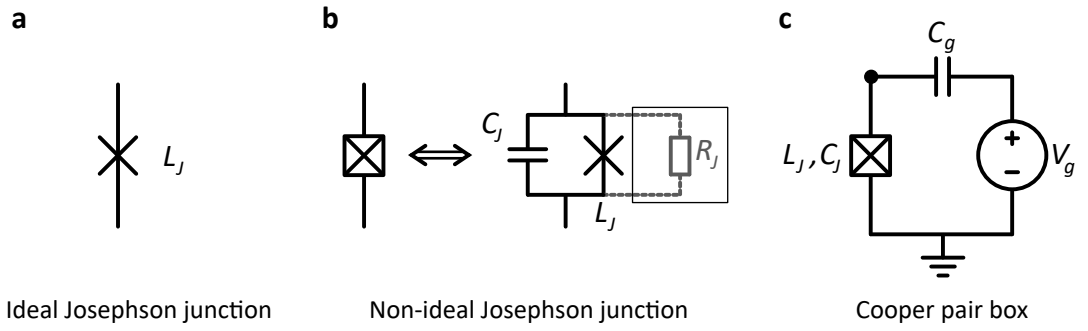

Figure 3.2: a. The circuit diagram symbol representing an ideal Josephson junction satisfying the Josephson relations (3.14). **b.** A non-ideal Josephson junction (left) can be equivalently represented as a capacitance, ideal Josephson junction and resistance in parallel. The resistance mainly acts as a damping/dissipative element and will be assumed negligible. Note that a non-ideal Josephson junction is very reminiscent of an LC oscillator as an alone element. **c.** A circuit diagram of the Cooper pair box. A dot is placed in the top left corner as the node from which the circuit is quantised. It is this 'island' that constitutes the Cooper pair box.

where the proportionality between φ and ϕ has been inserted. This yields the Lagrangian

$$\mathcal{L} = U - T = \frac{1}{2}C_J\dot{\phi}^2 + \frac{1}{2}C_g(\dot{\phi} - V_g)^2 + E_J \cos\left(\frac{2e}{\hbar}\phi\right), \tag{3.21}$$

from which we can find the conjugate variable

$$Q_I = \frac{\partial \mathcal{L}}{\partial \dot{\phi}} = C_J\dot{\phi} + C_g(\dot{\phi} - V_g). \tag{3.22}$$

Using this, we can express $\dot{\phi}$ as

$$\dot{\phi} = \frac{Q_I + C_g V_g}{C_J + C_g}, \tag{3.23}$$

allowing us to express the Hamiltonian as

$$\begin{aligned} H &= Q_I\dot{\phi} - \mathcal{L} \\ &= \frac{Q_I^2 + Q_I C_g V_g}{C_J + C_g} - \frac{1}{2(C_J + C_g)}(Q_I + C_g V_g)^2 + \frac{C_g V_g (Q_I + C_g V_g)}{C_J + C_g} \\ &\quad - \frac{1}{2}C_g V_g^2 - E_J \cos\left(\frac{2e}{\hbar}\phi\right) \\ &= \frac{1}{2C_\Sigma}(Q_I + C_g V_g)^2 - E_J \cos\left(\frac{2e}{\hbar}\phi\right) + \text{const.} \\ &= 4E_C(n - n_g)^2 - E_J \cos\varphi \quad (+ \text{ const.}), \end{aligned} \tag{3.24}$$

where some definitions have been made in order to arrive at the form most commonly used. The defined variables are $Q_I \equiv 2en$, where n is the number of excess Cooper pairs on the island, $n_g \equiv -\frac{C_g V_g}{2e}$ is the charge bias which is considered as a continuous variable and in practice is affected both by an applied gate voltage V_g, but also random charge noise, and furthermore the charging energy $E_C \equiv \frac{e^2}{2C_\Sigma}$, where $C_\Sigma = C_J + C_g$, has been defined which is the energy associated with transferring a single electron. The sign change to n_g is once again a result of sign convention for out conjugate variable Q_I in order to arrive at the correct sign for the commutation relation. Also, we now went back to the variable φ in preparation for the quantisation.

The variables we wish to quantise are the number of Cooper pairs n and the Josephson phase φ, similarly to how we did with the LC oscillator. They have the commutation relation

$$[\hat{\varphi}, \hat{n}] = \left[\frac{2e}{\hbar}\hat{\phi}, \frac{1}{2e}\hat{Q}\right] = i, \tag{3.25}$$

where the second equality is just to show the close connection to our previous commutator of Eq. 3.11, however one should be careful when using this as only periodic functions of φ have an unambiguous interpretation [33]. This will become slightly more clear when looking at the base kets, as we will see that they are periodic, and this periodicity stems from the fact that n is a discrete variable. We finally have the Cooper pair box Hamiltonian

$$\hat{H} = 4E_C(\hat{n} - n_g)^2 - E_J \cos\hat{\varphi}. \tag{3.26}$$

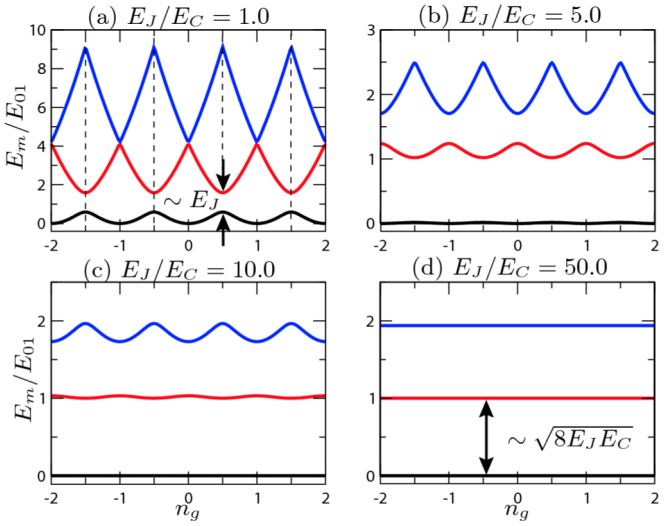

Figure 3.3: The three lowest energy levels of a Cooper pair box as a function of the charge bias n_g for the four values $E_J/E_C = 1, 5, 10, 50$. The energy levels are normalised such that the difference in energy between the ground state and the first excited state at $n_g = 0.5$ is unity, and the ground state is 0 at its lowest point. Figure from Ref. 16.

Now that we have the Hamiltonian and quantum operators $\hat{n}, \hat{\varphi}$, it is worth considering their eigenbases, how they act on them and how to transform between them. First of all we remind ourselves that n can only take integer values, as it represents the number of Cooper pairs tunneling which has to be an integer number. If $|n\rangle$ is the eigenket for $\hat{n}$ with relation $\hat{n}|n\rangle = n|n\rangle$, then we can more generally write

$$\hat{n} = \sum_{n=-\infty}^{\infty} = |n\rangle n\langle n|. \tag{3.27}$$

Now in analogy with transferring between position and momentum, we have the relation that

$$|\varphi\rangle = \sum_{n=-\infty}^{\infty} e^{in\varphi}|n\rangle, \tag{3.28}$$

where instead of an integral (as with position and momentum) we have a sum since n is discrete. Note that all shifts of φ by 2π leave $|\varphi\rangle$ unaffected, so it is periodic. In the derivation it was originally not specified that φ could only take on values in the range $\varphi \in [0, 2\pi)$. The reason this did not hurt us is that it only appeared inside a cosine, which effectively takes care of this for us. It also made the analogy to the flux in the case of the LC oscillator closer at hand.

The transfer back to the $|n\rangle$-basis is done using the relation

$$|n\rangle = \frac{1}{2\pi}\int_0^{2\pi} e^{-in\varphi}|\varphi\rangle \mathrm{d}\varphi. \tag{3.29}$$

We already know how to express our Cooper pair box Hamiltonian in the φ-representation:

$$\hat{H} = 4E_C \left(-i\frac{\partial}{\partial\varphi} - n_g\right)^2 - E_J \cos(\hat{\varphi}), \tag{3.30}$$

(see that $\hat{n}$ turns into $-i\frac{\partial}{\partial\varphi}$ similarly to how $\hat{p}$ turns into $-i\hbar\frac{\partial}{\partial x}$) but what does it look like in the $|n\rangle$-basis representation? In order to find this, we need to know the matrix elements of $\cos\hat{\varphi}$ in this representation. We find them to be

$$\begin{aligned}
\langle m|\cos\hat{\varphi}|n\rangle &= \langle m|\frac{1}{2\pi}\int_0^{2\pi}\cos\hat{\varphi}|\varphi\rangle\langle\varphi|n\rangle \mathrm{d}\varphi \\
&= \langle m|\frac{1}{2}\frac{1}{2\pi}\int_0^{2\pi}(e^{-i\varphi}+e^{-i\varphi})|\varphi\rangle e^{in\varphi}\mathrm{d}\varphi \\
&= \frac{1}{2}\left(\langle m|\frac{1}{2\pi}\int_0^{2\pi}(e^{-i(n-1)\varphi}+e^{-i(n+1)\varphi})|\varphi\rangle\mathrm{d}\varphi\right) \\
&= \frac{1}{2}\left(\langle m|n-1\rangle + \langle m,|n+1\rangle\right) \\
&= \frac{1}{2}(\delta_{m,n-1}+\delta_{m,n+1}),
\end{aligned} \tag{3.31}$$

where $\delta_{m,n}$ is the Kronecker delta function. From this we can deduce that

$$\cos\hat{\varphi} = \frac{1}{2}\sum_n \left(|n-1\rangle\langle n| + |n+1\rangle\langle n|\right), \tag{3.32}$$

in the n representation, from which we can see that indeed the effect of $\cos\hat{\varphi}$ is that Cooper pairs tunnel through the junction as the operator changes the number of Cooper pairs on each side of the junction. From this we have now recovered our Hamiltonian in the number representation

$$\hat{H} = 4E_C(\hat{n}-n_g)^2 - \frac{E_J}{2}\sum_n \left(|n-1\rangle\langle n| + |n+1\rangle\langle n|\right). \tag{3.33}$$

In Fig. 3.3 the three lowest energy levels are shown as a function of n_g for different values of E_J/E_C, showing that when this quantity is higher, the energy level spacing is less sensitive to fluctuations in the charge noise, but at the cost of reduced anharmonicity [16]. The regime of $E_J \gg E_C$ is what will be explored from now on in the thesis and is what is known as the Transmon regime.

3.4 The Transmon regime

Even though the results of the Transmon regime could be taken from the original paper of Ref. 16, I will write the derivation how I did it myself. This way it will hopefully be more clear what is lost in the approximations and give a view of what we are doing to arrive at the final Hamiltonian. In the case when the Josephson energy is much larger than the charging energy ($E_J \gg E_C$), the CPB Hamiltonian can be expanded in $\hat{\varphi}$ to quartic

order, and be considered as a harmonic oscillator with some anharmonicity. This can be understood by considering $\hat{\varphi}$ as the position coordinate in the analogy of a particle, which then translates into $-E_J \cos\hat{\varphi}$ being potential energy and the E_C term then behaves like a kinetic energy term. We then have a low kinetic energy particle in a strong cosine-shaped potential, which close to the origin looks like a quadratic potential. This is the motivation for the expansion of $\hat{\varphi}$, which we will later see is valid in the regime $E_J \gg E_C$. Since E_C is considered to be much lower than E_J, the simplification of ignoring n_g is made in the derivation as well, which in Fig. 3.3 you can see that not much is lost with this approximation. What we end up with is

$$\hat{H} \approx 4E_C\hat{n}^2 - E_J\left(1 - \frac{\hat{\varphi}^2}{2} + \frac{\hat{\varphi}^4}{24}\right), \tag{3.34}$$

so we have a harmonic oscillator with some constant offset $-E_J$ (which will not contribute to any dynamics), as well as a term of quartic order in $\hat{\varphi}$. The next step is to find step operators $\hat{a}, \hat{a}^\dagger$, such that we can write

$$\hat{H}' = 4E_C\hat{n}^2 + \frac{E_J}{2}\hat{\varphi}^2 = \hbar\omega\left(\hat{a}^\dagger\hat{a} + \frac{1}{2}\right), \tag{3.35}$$

where

$$[\hat{a}, \hat{a}^\dagger] = 1, \tag{3.36}$$

all in analogy with usual harmonic oscillator systems. By these requirements and comparing with the well studied case of a (quantum) mechanical harmonic oscillator (the quantum mechanical version of a mass connected to a spring):

$$\hat{H}_{HO} = \frac{\hat{p}^2}{2m} + \frac{1}{2}m\omega^2\hat{x}^2, \tag{3.37}$$

which has the step operators

$$\hat{a}_{HO} = \sqrt{\frac{m\omega}{2\hbar}}\left(\hat{x} + i\frac{\hat{p}}{m\omega}\right) \tag{3.38}$$

$$\hat{a}^\dagger_{HO} = \sqrt{\frac{m\omega}{2\hbar}}\left(\hat{x} - i\frac{\hat{p}}{m\omega}\right), \tag{3.39}$$

one can be inspired to make the ansatz

$$\hat{a} = A(\hat{\varphi} + iB\hat{n}). \tag{3.40}$$

Then by comparison of terms with the mechanical harmonic oscillator, or by imposing the requirements (3.35),(3.36), one finds that the operators $\hat{a}, \hat{a}^\dagger$ are (with a certain choice of phase)

$$\hat{a} = \left(\frac{E_J}{32E_C}\right)^{(1/4)}\left(\hat{\varphi} + i\sqrt{\frac{8E_C}{E_J}}\hat{n}\right) \tag{3.41}$$

$$\hat{a}^\dagger = \left(\frac{E_J}{32E_C}\right)^{(1/4)} \left(\hat{\varphi} - i\sqrt{\frac{8E_C}{E_J}}\hat{n}\right), \tag{3.42}$$

where $\hbar\omega = \sqrt{8E_C E_J}$. The transformation back to the operators $\hat{n}, \hat{\varphi}$ then have the form

$$\hat{\varphi} = \left(\frac{8E_C}{E_J}\right)^{(1/4)} \frac{1}{\sqrt{2}}(\hat{a} + \hat{a}^\dagger) \tag{3.43}$$

$$\hat{n} = \left(\frac{E_J}{8E_C}\right)^{(1/4)} \frac{-i}{\sqrt{2}}(\hat{a} - \hat{a}^\dagger), \tag{3.44}$$

where we also see that the expansion is valid as an approximation for $\cos\hat{\varphi}$ when $E_J \gg E_C$.

We now have our Hamiltonian in the form

$$\hat{H} = -E_J + \sqrt{8E_C E_J}\left(\hat{a}^\dagger\hat{a} + \frac{1}{2}\right) - \frac{E_J}{24}\hat{\varphi}^4 = \hat{H}_0 - \frac{E_C}{12}(\hat{a} + \hat{a}^\dagger)^4, \tag{3.45}$$

where $\hat{H}_0 = -E_J + \sqrt{8E_C E_J}\left(\hat{a}^\dagger\hat{a} + \frac{1}{2}\right)$ is the harmonic part. The term $(\hat{a} + \hat{a}^\dagger)^4$ can be expanded and ordered in terms that couple the state $|m\rangle$ with $|m\rangle$,
$|m \pm 2\rangle, |m \pm 4\rangle$, where $|m\rangle$ is a Fock state s.t $\hat{a}^\dagger\hat{a}|m\rangle = m|m\rangle$, not an eigenstate of the $\hat{n}$ operator:

$$\begin{aligned}
&|m\rangle \leftrightarrow |m+4\rangle : \hat{a}^{\dagger 4} \\
&|m\rangle \leftrightarrow |m+2\rangle : \hat{a}^{\dagger 2}(4\hat{a}^\dagger\hat{a} + 6) \\
&|m\rangle \leftrightarrow |m\rangle \quad\;\; : 6(\hat{a}^\dagger\hat{a})^2 + 6\hat{a}^\dagger\hat{a} + 3 \\
&|m\rangle \leftrightarrow |m-2\rangle : \hat{a}^2(4\hat{a}^\dagger\hat{a} - 2) \\
&|m\rangle \leftrightarrow |m-4\rangle : \hat{a}^4.
\end{aligned} \tag{3.46}$$

If we do first order perturbation theory, where $\hat{V} = -E_C/12(\hat{a} + \hat{a}^\dagger)^4$, we can find how much the eigenstates change due to the perturbation. Let $|m\rangle = |m^0\rangle + |m^1\rangle$, where $|m^0\rangle$ are the eigenstates of the unperturbed Hamiltonian $\hat{H}_0$ and $|m^1\rangle$ is the first order correction. Then, since the eigenenergies of the harmonic oscillator are non-degenerate, $|m^1\rangle$ is given by

$$|m^1\rangle = \sum_{n,n\neq m} \frac{\langle n^0|\hat{V}|m^0\rangle}{E_m^0 - E_n^0}|n^0\rangle. \tag{3.47}$$

Using this relation and the above results we find

$$
\begin{aligned}
|m^1\rangle = -\frac{E_C}{12}\Bigg(&\frac{\langle m^0+4|(\hat{a}^\dagger)^4|m^0\rangle}{(m-(m+4))\sqrt{8E_CE_J}}|m^0+4\rangle + \frac{\langle m^0+2|\hat{a}^{\dagger 2}(4\hat{a}^\dagger\hat{a}+6)|m^0\rangle}{(m-(m+2))\sqrt{8E_CE_J}}|m^0+2\rangle \\
&+ \frac{\langle m^0-2|\hat{a}^2(4\hat{a}^\dagger\hat{a}-2)|m^0\rangle}{(m-(m-2))\sqrt{8E_CE_J}}|m^0-2\rangle + \frac{\langle m^0-4|\hat{a}^4|m^0\rangle}{(m-(m-4))\sqrt{8E_CE_J}}|m^0-4\rangle\Bigg) \\
= \frac{1}{12}\sqrt{\frac{E_C}{8E_J}}\Bigg(&\frac{\sqrt{(m+1)(m+2)(m+3)(m+4)}}{4}|m^0+4\rangle \\
&+ \frac{\sqrt{(m+1)(m+2)}(4m+6)}{2}|m^0+2\rangle - \frac{\sqrt{m(m-1)}(4m-2)}{2}|m^0-2\rangle \\
&- \frac{\sqrt{m(m-1)(m-2)(m-3)}}{4}|m^0-4\rangle\Bigg),
\end{aligned}
\tag{3.48}
$$

so for small m, these corrections will be small. Therefore these corrections to the states will be neglected. Then we make the rotating wave approximation (RWA), meaning that we only keep terms which are energy conserving in terms of the creation and annihilation operators (the $|m\rangle \leftrightarrow |m\rangle$ terms). After this approximation we end up with

$$
\hat{H} = -E_J + \sqrt{8E_CE_J}\left(\hat{a}^\dagger\hat{a} + \frac{1}{2}\right) - \frac{E_C}{4}\Big(2(\hat{a}^\dagger\hat{a})^2 + 2\hat{a}^\dagger\hat{a} + 1\Big), \tag{3.49}
$$

where the term proportional to $(\hat{a}^\dagger\hat{a})^2/2$ is known as a Kerr non-linearity. The eigenenergies for this perturbation approach is

$$
E_m = -E_J + \sqrt{8E_CE_J}\left(m + \frac{1}{2}\right) - \frac{E_C}{4}(2m^2 + 2m + 1). \tag{3.50}
$$

Note that these eigenenergies are the ones that are received by a lowest order Rayleigh-Schrödinger perturbation series where one has instead defined $\hat{H}_0$ as in equation (3.49) and the other terms from equation (3.45) as the potential $\hat{V}$. In this sense, what we are doing can be seen as making a "0:th" order expansion of the eigenenergies and eigenstates, however it is perhaps more natural to see this as a RWA.

The states $|m\rangle$ can now be interpreted as the number of photons stored inside the Transmon, similarly to the number state in CPW resonators corresponing to the number of photons stored inside them. Thus the operators $\hat{a}, \hat{a}^\dagger$ correspond to removing or adding a photon in the resonator respectively. One more thing that should be highlighted now since it will be used later, is the anharmonicity of the energy levels. Let $E_{m,n} = E_m - E_n$, then we find that $E_{m+2,m+1} - E_{m+1,m} = -E_C$ [16] i.e. the charging energy E_C determines the anharmonicity. In other words the photon energy required to excite the state $|m+1\rangle$ is lowered by E_C as compared to exciting the state $|m\rangle$.

3.5 Coherent states

Before moving on to connecting the system to an environment in order to model measurements, a short section about coherent states is appropriate. It serves both as an introduction to what it refers to and to make a distinction between what is meant with coherence or a coherent state in the thesis. There could otherwise be some confusion with what is typically meant when calling a state 'coherent'. Typically what you learn in textbooks as an example of a coherent state is a state that is in a superposition of states [34], for instance a wavefunction $|\Psi\rangle$ that is in a superposition of spin up $|\uparrow\rangle$ and spin down $|\downarrow\rangle$

$$|\Psi\rangle = \frac{1}{\sqrt{2}}\Big(|\uparrow\rangle + |\downarrow\rangle\Big), \tag{3.51}$$

however this is not what we will refer to in the thesis as a coherent state. A coherent state here refers to the quantised electromagnetic field (sometimes referred to as a Glauber state) and was extensively treated by R. Glauber (see Ref. 35). It is an eigenstate of the annihilation operator $\hat{a}$, such that

$$\hat{a}|\alpha\rangle = \alpha|\alpha\rangle, \tag{3.52}$$

where $|\alpha\rangle$ is the coherent state of a single oscillator mode relating to $\hat{a}$. It is such a state that is considered as coherent within quantum optics. When quantising electromagnetic fields, the state $|0\rangle$ is the vacuum state and the operators $\hat{a}^\dagger, \hat{a}$, the creation and annihilation operators connected to some mode, are fundamental building blocks. Acting with these operators directly on the vacuum state will not create a coherent state, however there exists an operator known as a displacement operator $\hat{D}_\alpha$, such that

$$|\alpha\rangle = \hat{D}_\alpha|0\rangle, \tag{3.53}$$

so it turns or 'displaces' the vacuum state into a coherent state. It turns out that the operator that achieves this is

$$\hat{D}_\alpha = e^{-\frac{1}{2}|\alpha|^2} e^{\alpha\hat{a}^\dagger} e^{-\alpha^*\hat{a}}. \tag{3.54}$$

A coherent state is in quantum optics a state that is "the most classical", since photon fields generated by arbitrary distributions of classical currents have a simple description in terms of coherent states [35]. If we consider the Schrödinger picture, the coherent state evolves as

$$|\alpha(t)\rangle = |e^{-i\Omega t}\alpha(0)\rangle = e^{-\frac{1}{2}|\alpha|^2} e^{\alpha e^{-i\Omega t}\hat{a}^\dagger}|0\rangle, \tag{3.55}$$

where Ω is the (angular) frequency of the oscillator mode relating to $\hat{a}$. You see from this that the real and imaginary parts of α oscillate sinusoidally in time, and α is then considered to be the classical amplitude of the motion [9]. This classical amplitude could for instance be a voltage amplitude in the case of a microwave RF drive.

Another property of the coherent state is that it shows that the occupation number n of the modes (photons in the case of light) is given by a Poisson distribution [35]:

$$P_n = |\langle n|\alpha\rangle|^2 = \frac{|\alpha|^{2n}}{n!}e^{-|\alpha|^2}, \tag{3.56}$$

where we see that the mean photon number is $|\alpha|^2$.

If the coherent amplitude α is large $|\alpha| \gg 1$, then quantum fluctuations can often be ignored as they become negligibly small [27], simplifying some calculations. For the system that we will consider, photon numbers inside the resonator will be of order 1, however we will consider continuous weak measurements, meaning that if we increase the integration time, it effectively acts as increasing $|\alpha|$. If the integration time is long enough then we can reach this limit where the quantum fluctuations will be negligible in our measurement.

This section has kept a very complicated subject very dense. For more details I refer to chapter 2 in Ref. 27, or for a more formal mathematical treatment Ref. 36. The main takeaway from this section should be that a Glauber state can be viewed as state that is as close to classical as possible in some sense and it is this state we mean when talking about a coherent state. We will consider voltage signals from our RF drives as these coherent states.

3.6 Semi-infinite transmission lines as baths

In preparation for Chapter 4, where we will look into connecting our system to a transmission line, we want to have a quantum description of it. Taking inspiration from Ref. 37, the picture that we will start from is depicted in Fig. 3.4, where the transmission line initially is of finite length l terminated at $x = 0$ and $x = l$ by capacitors on either side. Furthermore it is segmented into inductors and capacitors with inductance ℓ and capacitance c respectively, each node separated by δx with N nodes such that $N\delta x = l$. With this we implicitly assume that the transmission line is homogeneous. With flux and charge defined as in Sec. 3.1, the energies associated to each capacitance and inductance at node n is $Q_n^2/2c$ and $(\phi_{n+1} - \phi_n)^2/2\ell$. Skipping some steps that we have already seen and writing the classical Hamiltonian for this system we have

$$H = \sum_{n=0}^{N-1}\left(\frac{1}{2c}Q_n^2 + \frac{1}{2\ell}(\phi_{n+1} - \phi_n)^2\right). \tag{3.57}$$

We want to take this to the continuum limit ($\delta x \to 0$), which we can do by defining $c = \delta x c_0$, $\ell = \delta x \ell_0$, where c_0, ℓ_0 are the capacitance and inductance per unit length respectively, as well as defining the flux field as $\phi(x_n) = \phi_n$ and charge density field as

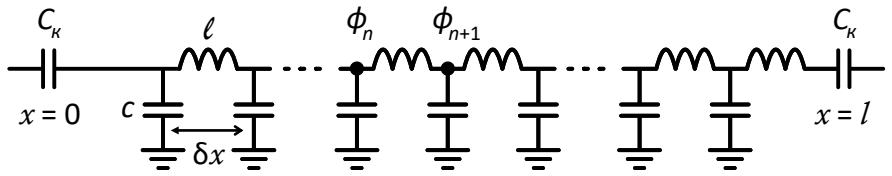

Figure 3.4: A transmission line of length l segmented into a series of N lumped elements such that $l = N\delta x$ that is terminated at the ends by some coupling capacitors. The capacitors have capacitance c and the inductors inductance ℓ. ϕ_n represents the flux at node n. For finite l, this schematic can represent for instance a CPW resonator.

$Q(x_n) = Q_n/\delta x$. Now taking the limit as we keep $l = N\delta x$ constant yields

$$H = \int_0^l \frac{1}{2c_0} Q(x)^2 + \frac{1}{2l_0}\left(\frac{\partial\phi(x)}{\partial x}\right)^2 \mathrm{d}x, \tag{3.58}$$

where so far the time dependence of Q and ϕ have not been explicitly written out for brevity. Again, the charge $Q(x,t) = c_0\partial_t\phi(x,t)$ is the canonical momentum and $\phi(x,t) = \int_{-\infty}^t V(x,t')\,\mathrm{d}t'$ now is continuous and dependent on x. Hamilton's equations (alternatively also the Euler-Lagrange equation) yield the wave equation for the propagation along the transmission line

$$v_0^2\partial_x^2\phi - \partial_t^2\phi = 0, \tag{3.59}$$

where the mode wave velocity $v_0^2 = 1/c_0\ell_0$ has been defined, i.e. the speed with which the modes propagate in the transmission line. This equation is separable and can be solved in terms of normal modes as

$$\phi(x,t) = \sum_{m=0}^{\infty} u_m(x)\phi_m(t), \tag{3.60}$$

where $\phi_m(t)$ is not to be confused with ϕ_n and has the relation $\ddot{\phi}_m(t) = -\omega_m^2\phi_m(t)$. Furthermore

$$u_m(x) = A_m\cos(k_m x + \alpha_m), \tag{3.61}$$

where A_m is the amplitude of the mode and α_m as well as $k_m = \omega_m/v_0$ are set by the boundary conditions at $x = 0$ and $x = l$. More specifically the boundary conditions for this case is that there is no current at those points, giving the condition

$$-\frac{1}{\ell_0}\frac{\partial\phi(x,t)}{\partial x}\bigg|_{x=0,l} = 0, \tag{3.62}$$

which tells us that $\alpha_m = 0$ and $k_m = m\pi/l$ becomes discrete. Choosing the normalisation of u_m (by choosing the constant A_m) such that

$$\frac{1}{l}\int_0^l u_m(x)u_{m'}(x)\,\mathrm{d}x = \delta_{x,x'}, \tag{3.63}$$

giving $A_m = \sqrt{2}$. With this work done, we can rewrite our Hamiltonian using our normal mode decomposition as

$$H = \sum_{m=0}^{\infty} \left(\frac{Q_m^2}{2C_r} + \frac{1}{2} C_r \omega_m^2 \phi_m^2 \right), \tag{3.64}$$

where $C_r = lc_0$ is the total capacitance of the transmission line. Now the charge conjugate to ϕ_m is $Q_m = C_r \dot{\phi}_m$. Here we can see that we have a sum of harmonic oscillators which we can promote to quantum operators similarly to how it was done in Sec. 3.1. We can then write our Hamiltonian as a sum of harmonic oscillators

$$\hat{H} = \sum_{m=0}^{\infty} \hbar \omega_m \hat{a}_m^\dagger \hat{a}_m, \tag{3.65}$$

where

$$[\hat{a}_m, \hat{a}_n^\dagger] = \delta_{m,n}. \tag{3.66}$$

This Hamiltonian in the form of Eq. 3.65 will be used as the Hamiltonian in Chapter 4 representing a semi-infinite transmission line, then in the language of a bath connected to our system, containing bosonic modes. Some comments should also be made here. In no step did we let $l \to \infty$, so for any finite l what we have modelled is a transmission line resonator, for instance a CPW resonator. The coupling capacitances C_κ have however been ignored, which would enter as coupling terms in our Hamiltonian. Another way of viewing it is that C_κ is considered as 0. Taking $l \to \infty$ should be done carefully. If we consider our Hamiltonian (Eq. (3.65)) we see that formally it turns the bath into a continuum of frequencies. For more details on this limit, see e.g. Ref. 37.

Chapter 4

Input-Output Theory

This looks kind of murky... We'll have to think more about this, yes.
- Peter Samuelsson

So far everything we have considered is an isolated system, describing its quantum states and properties. Now we want to connect this system to some measurement setup, so that we can do measurements on it. This is the motivation for this section, as quantum input-output theory is a theory describing how information about a system can be extracted from sending in a signal to the system and then measuring the signal coming out. This is done by describing interactions between an environment and a system; how they affect each other. The idea is that if we want to get information out from a system, we must allow for information to go from the system to the environment. By doing this, we also must allow for the environment to let noise into the system, but it also allows us to affect the system from the outside in a more deliberate way. We will consider a system which will be referred to as a 'cavity' in analog with quantum optics. In quantum optics, one considers a cavity with weakly transparent mirrors such that the cavity can let out photons trapped in the cavity for measurement, at the expense of letting in noise from photons in the environment. This is similar to the case which will be studied, where microwave photons are residing in a 'bath' that is connected to the cavity. The cavity is considered to have high 'quality factor' Q, a measure of how many times a photon oscillates on average inside the cavity before escaping. This is the same as saying that the system is weakly coupled to the environment, or in other words well isolated. The total Hamiltonian of the system can then be divided up into three parts since we can think of the system as separated from the environment, in contrast to if we would have strong coupling. The Hamiltonian with its three parts is

$$\hat{H} = \hat{H}_{\mathcal{S}} + \hat{H}_{int} + \hat{H}_{bath}, \tag{4.1}$$

where $\hat{H}_{\mathcal{S}}$ is the cavity (system) Hamiltonian, $\hat{H}_{int}$ is the interaction Hamiltonian between the system and the bath and $\hat{H}_{bath}$ is the bath Hamiltonian which in our case comes from

connecting the system to a semi-infinite transmission line. More formally what is done is that we consider the two spaces $\mathcal{H}_S$ and $\mathcal{H}_E$ as separate Hilbert spaces, where $\mathcal{H}_S$ is the Hilbert space of the system and $\mathcal{H}_E$ is the Hilbert space of the environment. Then $\hat{H}$ acts on $\mathcal{H}_S \otimes \mathcal{H}_E$, where $\hat{H}_S$ acts on $\mathcal{H}_S \otimes \mathbb{1}$, $\hat{H}_{bath}$ acts on $\mathbb{1} \otimes \mathcal{H}_E$ and $\hat{H}_{int}$ acts on $\mathcal{H}_S \otimes \mathcal{H}_E$.

We will see that this separation with a few assumptions allows us to make measurements of the system by sending in photons via the bath, and then measure how the bath is affected by the interaction with the system.

4.1 Coupling semi-infinite transmission lines to a system

We know from electronics that a semi-infinite transmission line can act as a dissipative element, even if it only consists of reactive elements (has no resistance). This is because a signal can be transmitted from a system into the transmission line on one end and then never get reflected back, so that energy is dissipated from the system. We will see that we have an analogous situation here, where we will be considering modes in the bath that we will be interpreting as ingoing or outgoing. These travelling waves will be considered as independent everywhere except where the transmission lines terminate at the system, where a relation will be derived to relate the ingoing and outgoing modes to each other and the system. This section and the next will mostly follow the derivation made in Appendix E from Ref. 38, however there are other standard references for this, for instance Refs. 27, 39, 40 and 41. The results from Sec. 4.3 can be found in these, however I have connected the gap a little bit. Later I found that this is also done in Ref. 42.

We will consider the case where we have a coherent drive connected to the system Hamiltonian. The bath Hamiltonian, motivated by the derivation in Sec. 3.6, will be assumed to be of form

$$\hat{H}_{bath} = \sum_q \hbar\omega_q \hat{b}_q^\dagger \hat{b}_q, \tag{4.2}$$

where q labels the quantum numbers of the bath, which are assumed to be independent harmonic oscillator (or bosonic) modes, obeying

$$[\hat{b}_q, \hat{b}_{q'}^\dagger] = \delta_{qq'}. \tag{4.3}$$

This is reasonable, as we can think of these harmonic modes as photons residing in the bath. Each photon has a certain frequency ω_q, and the number of photons with a certain frequency are governed by the bosonic step operators $\hat{b}_q, \hat{b}_q^\dagger$ connected to that particular frequency. Because the bath terminates at the system (semi-infinite instead of infinite), there is no translational invariance and we do not have running waves, but standing.

The coupling Hamiltonian between the two systems is of the form

$$\hat{H}_{int} = -i\hbar \sum_q (\hat{a}^\dagger - \hat{a})(f_q \hat{b}_q + f_q^* \hat{b}_q^\dagger), \tag{4.4}$$

where f_q is the coupling strength between the bath and the system which in general can be dependent on the frequency ω_q. This term you can get from coupling the voltage operator of the transmission line to the number operator of the CPB for instance. Note that the form of it is a gauge choice, for instance with a different gauge choice the number operator is proportional to $\hat{a} + \hat{a}^\dagger$ instead.

For the interaction term, we make the RWA which means that terms that are rotating at high frequency in the interaction representation are neglected, such as $\hat{a}\hat{b}_q$. These will have a much smaller effect on the dynamics of the system. Another way of viewing it, which is perhaps more intuitive, is that we keep the terms that conserve the photon number. We then end up with

$$\hat{H}_{int} = -i\hbar \sum_q \Big(f_q \hat{a}^\dagger \hat{b}_q - f_q^* \hat{b}_q^\dagger \hat{a} \Big). \tag{4.5}$$

The system Hamiltonian can be assumed more general when only one degree of freedom is considered, for which the bosonic relation will still hold:

$$[\hat{a}, \hat{a}^\dagger] = 1. \tag{4.6}$$

The derivation of the expressions will be kept as general as possible. However, assuming that the system is a harmonic oscillator can in some cases be used to carry out further calculations. This will be considered in Sec. 4.2. In the case of an empty cavity, this can be assumed to hold for the lowest mode. The operators will be considered in the Heisenberg picture, so they have some time dependence and the equation of motion (EoM) is for a general operator $\hat{A}$ given by

$$\frac{\mathrm{d}}{\mathrm{d}t}\hat{A} = \frac{i}{\hbar}[\hat{H}, \hat{A}]. \tag{4.7}$$

Using this we find

$$\dot{\hat{b}}_q = \frac{i}{\hbar}[\hat{H}, \hat{b}_q] = -i\omega_q \hat{b}_q + f_q^* \hat{a}, \tag{4.8}$$

which is the EoM for the drive modes. The first term is the same as the EoM for a harmonic oscillator, while the second term acts like a drive or force connected to the harmonic oscillator. The system is linear and can be solved exactly by integration. Starting from a time t_0 far into the past long before any wavepacket going towards the cavity has reached it, we have the solution

$$\hat{b}_q(t) = e^{-i\omega_q(t-t_0)}\hat{b}_q(t_0) + \int_{t_0}^{t} e^{-i\omega_q(t-\tau)} f_q^* \hat{a}(\tau)\, \mathrm{d}\tau. \tag{4.9}$$

The first term is just the time evolution of the free bath, while the second term governs

the waves absorbed and radiated by the cavity from and into the bath respectively. We can also find the EoM of the cavity:

$$\dot{\hat{a}} = \frac{i}{\hbar}[H_{\mathcal{S}}, \hat{a}] - \sum_q f_q \hat{b}_q + \frac{i}{\hbar}\underbrace{[\hat{H}_{bath}, \hat{a}]}_{=0}. \tag{4.10}$$

We can insert Eq. (4.9) into the last term yielding

$$\begin{aligned}\sum_q f_q \hat{b}_q =& \sum_q f_q e^{-i\omega_q(t-t_0)}\hat{b}_q(t_0) \\ &+ \sum_q |f_q|^2 \int_{t_0}^{t} e^{-i(\omega_q-\omega_r)(t-\tau)}\{e^{+i\omega_r(\tau-t)}\hat{a}(\tau)\}\,\mathrm{d}\tau.\end{aligned} \tag{4.11}$$

The last term in the curly brackets is a slowly varying function of τ. The decay rate between two states where the difference in energy is $E = \hbar\omega_r$ is given by a version of the Fermi Golden Rule [34]:

$$\kappa(\omega_r) = 2\pi \sum_q |f_q|^2 \delta(\omega_r - \omega_q). \tag{4.12}$$

In order to be able to simplify our expression in Eq. (4.11), we note that

$$\begin{aligned}\int_{-\infty}^{+\infty} \frac{\kappa(\omega_r+\nu)}{2\pi} e^{-i\nu(t-\tau)}\,\mathrm{d}\nu &= \int_{-\infty}^{+\infty} \sum_q |f_q|^2 \delta\Big(\nu - (\omega_q - \omega_r)\Big) e^{-i\nu(t-\tau)}\,\mathrm{d}\nu \\ &= \sum_q |f|_q^2 e^{-i(\omega_q-\omega_r)(t-\tau)}.\end{aligned} \tag{4.13}$$

To proceed further, we make the Markov approximation, which means that $\kappa(\nu) = \kappa$ is considered to be constant over the range of frequencies relevant to the cavity. With this assumption, we have

$$\int_{-\infty}^{+\infty} \frac{\kappa}{2\pi} e^{-i\nu(t-\tau)}\,\mathrm{d}\nu = \kappa\delta(t-\tau). \tag{4.14}$$

Therefore, we make the approximation

$$\sum_q |f_q|^2 e^{-i(\omega_q-\omega_r)(t-\tau)} = \kappa\delta(t-\tau). \tag{4.15}$$

One final relation that will be used is

$$\int_{-\infty}^{x_0} \delta(x - x_0)\,\mathrm{d}x = \frac{1}{2}, \tag{4.16}$$

which if we insert all of these results back into Eq. (4.11) yields

$$\dot{\hat{a}} = \frac{i}{\hbar}[\hat{H}_{\mathcal{S}}, \hat{a}] - \frac{\kappa}{2}\hat{a} - \sum_q f_q e^{-i\omega_q(t-t_0)}\hat{b}_q(t_0). \tag{4.17}$$

The second term in Eq. (4.10) which had a quite complicated expression before, has under the approximations become a simple damping term in the EoM. For further simplification

and in the spirit of the Markov approximation, we consider $f = \sqrt{|f_q|^2}$ to be constant over the bath modes q relevant to the interaction with the cavity. Defining the density of states, treated as a constant, as

$$\rho = \sum_q \delta(\omega_r - \omega_q), \tag{4.18}$$

we can write the Golden Rule rate from Eq. (4.12) as

$$\kappa = 2\pi f^2 \rho, \tag{4.19}$$

and this allows us to define the input mode

$$\hat{b}_{in}(t) \equiv \frac{1}{\sqrt{2\pi\rho}} \sum_q e^{-i\omega_q(t-t_0)} \hat{b}_q(t_0). \tag{4.20}$$

The input mode evolves as though no cavity was present until it arrives at the system and acts as a drive. Since the evolution of the mode evolves long before it interacts with the system, it is interpreted as an input; it evolves from a time t_0, where it does not interact with the cavity up until time t, when it drives it.

Before proceeding, a distinction should be made between the rates κ in Eq. (4.17) and Eq. (4.18). So far, these have been considered to be the same, as we have assumed that the modes decaying in the cavity end up in the bath. A more general and physical assumption is to allow for some internal losses, which means that there is an environment outside of the transmission line where the modes can end up. With this additional way of relaxation of the cavity, we can denote the rate κ_c as the decay rate from the cavity to the bath and κ_i as internal losses, the decay rate to the outside environment. We also for simplicity re-define $\kappa \equiv \kappa_c + \kappa_i$. Then we end up with the total equation of motion

$$\dot{\hat{a}} = \frac{i}{\hbar}[\hat{H}_{\mathcal{S}}, \hat{a}] - \frac{\kappa}{2}\hat{a} - \sqrt{\kappa_c}\hat{b}_{in}(t). \tag{4.21}$$

Formally, what one does to arrive at this is to add another bath connected to the system (similarly as to how it is done in section 4.3). One then needs to consider the effect that the additional bath has on the system. Since we consider the case $kT \ll \hbar\omega$, we say that the thermal fluctuations from the environment do not affect the system. We also ignore vacuum fluctuations, as the cases we will consider from experiments is doing many weak measurements, which will average out the vacuum fluctuations. The amplifiers also provide more noise than vacuum fluctuations in the experiments. Therefore, the input term from the environment (”loss” bath) will be considered as 0, and the output term is not something that can be measured directly, so this will also be ignored.

We now want to consider the outgoing modes from the system residing in the bath. For these we have the contrary scenario; we assume that we measure them at a time t_1 long

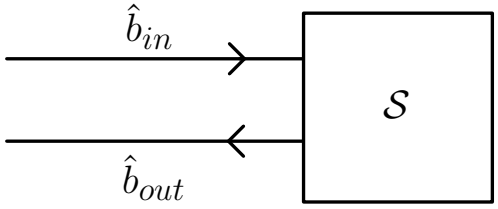

Figure 4.1: A very general schematic of a bath connected to a system $\mathcal{S}$, where the bath can be divided up into input and output modes $\hat{b}_{in}$ and $\hat{b}_{out}$ respectively, similarly to a semi-infinite transmission line connected to a system.

after they interacted with the system at time t, such that at time t_1, the modes no longer affect the system. We then integrate the EoM (Eq. (4.9)) backwards from t_1 to t, in order to arrive at the time when the bath and system interacted. This gives the expression

$$\hat{b}_q(t) = e^{-i\omega_q(t-t_1)}\hat{b}_q(t_1) - \int_t^{t_1} e^{-i\omega_q(t-\tau)} f_q^* \hat{a}(\tau)\,\mathrm{d}\tau. \tag{4.22}$$

The minus sign on the second term appears since we first integrate from t_1 to t (since we integrate backwards), then the direction of the integration is interchanged with the compensation of changing the sign. We now perform all steps similarly to the input mode. Defining

$$\hat{b}_{out}(t) \equiv \frac{1}{\sqrt{2\pi\rho}} \sum_q e^{-i\omega_q(t-t_1)}\hat{b}_q(t_1), \tag{4.23}$$

which is the free evolution of the bath, but now it evolves from $\hat{b}_q(t_1)$ in the future backwards toward the time of interaction t. Inserting Eq. (4.22) into Eq. (4.10) yields, with the same approximations

$$\dot{\hat{a}} = \frac{i}{\hbar}[\hat{H}_{\mathcal{S}}, \hat{a}] + \frac{\kappa_c - \kappa_i}{2}\hat{a} - \sqrt{\kappa_c}\hat{b}_{out}(t). \tag{4.24}$$

Subtracting Eq. (4.21) from Eq. (4.24) yields

$$\hat{b}_{out}(t) = \hat{b}_{in}(t) + \sqrt{\kappa_c}\hat{a}(t), \tag{4.25}$$

where we see that at the point where the system and bath interact, the outgoing field is the reflected ingoing field together with the field radiated from the system. A schematic of this bath connected to a system $\mathcal{S}$ is depicted in Fig. 4.1.

4.2 Coupling a harmonic oscillator to a transmission line

The results so far are valid for a general system Hamiltonian, but as stated before we can assume a harmonic oscillator system. The system Hamiltonian is then

$$\hat{H}_{\mathcal{S}} = \hbar\omega_r \hat{a}^\dagger \hat{a}, \tag{4.26}$$

where ω_r is the resonance frequency of the harmonic oscillator. Then we find the EoM

$$\dot{\hat{a}} = -i\omega_r \hat{a} - \frac{\kappa}{2}\hat{a} - \sqrt{\kappa_c}\hat{b}_{in}(t), \tag{4.27}$$

which is linear and can therefore be Fourier transformed to describe the spectral domain of $\hat{a}$:

$$\hat{a}[\omega] = \frac{-i\sqrt{\kappa_c}}{(\omega - \omega_r) + i\kappa/2}\hat{b}_{in}[\omega]. \tag{4.28}$$

Inserting this into the Fourier transformed version of Eq. (4.25) yields

$$\hat{b}_{out}[\omega] = \frac{\omega - \omega_r + i(\kappa_i - \kappa_c)/2}{\omega - \omega_r + i\kappa/2}\hat{b}_{in}[\omega] = r[\omega]\hat{b}_{in}[\omega], \tag{4.29}$$

where the reflection amplitude $r[\omega]$ has implicitly been defined as

$$r[\omega] = \frac{\omega - \omega_r + i(\kappa_i - \kappa_c)/2}{\omega - \omega_r + i\kappa/2}. \tag{4.30}$$

When measuring the spectral response of a system, the reflected signal will depend on the ingoing power and the reflection coefficient

$$|r|^2 = \frac{(\omega - \omega_r)^2 + \left(\frac{\kappa_i - \kappa_c}{2}\right)^2}{(\omega - \omega_r)^2 + (\kappa/2)^2}, \tag{4.31}$$

which we recognise as a Lorentzian with line width κ. We see that there is no reflection when driving on resonance when the internal losses and the coupling to the transmission line have the same rates. The measured amplitude of the signal is symmetric in κ_i and κ_c, however, the phase of the response can be used to determine which of them is larger This can be seen from Eq. (4.30), where in the case $\kappa_c > \kappa_i$ the phase of the signal shifts with 2π when going from $\omega = -$"∞" to $\omega = +$"∞".

A general expression for the input power P_{in} that the cavity is driven with can be expressed as

$$P_{in}(t) = \hbar\omega\langle\hat{b}_{in}^\dagger(t)\hat{b}_{in}(t)\rangle, \tag{4.32}$$

where we consider the drive as a monochromatic beam with frequency ω. A steady state solution can be found given a constant drive. We can relate the ingoing and outgoing powers for a given frequency to the state of our cavity by using Eqs. (4.25) and (4.28),

arriving at

$$P_{in} = \hbar\omega\langle\hat{b}_{in}^{\dagger}\hat{b}_{in}\rangle = \hbar\omega\frac{4(\omega-\omega_r)^2+\kappa^2}{4\kappa_c}\langle\hat{a}^{\dagger}\hat{a}\rangle \tag{4.33}$$

and

$$P_{out} = \hbar\omega\langle\hat{b}_{out}^{\dagger}\hat{b}_{out}\rangle = \hbar\omega\frac{4(\omega-\omega_r)^2+(\kappa_c-\kappa_i)^2}{4\kappa_c}\langle\hat{a}^{\dagger}\hat{a}\rangle. \tag{4.34}$$

This yields a way of determining the average number of photons residing in a resonator $\langle\hat{a}^{\dagger}\hat{a}\rangle$ depending on the drive. If the denote the detuning by $\Delta = \omega_r - \omega$, Eq. (4.33) yields

$$\langle\hat{a}^{\dagger}\hat{a}\rangle = \frac{\kappa_c}{\Delta^2+\kappa^2}\frac{P_{in}}{\hbar\omega}. \tag{4.35}$$

If we consider the case of a lossless cavity driven on resonance, the steady state is

$$P = \hbar\omega\langle\hat{b}_{in}^{\dagger}\hat{b}_{in}\rangle = \hbar\omega\langle\hat{b}_{out}^{\dagger}\hat{b}_{out}\rangle = \hbar\omega\frac{\kappa_c}{4}\langle\hat{a}^{\dagger}\hat{a}\rangle, \tag{4.36}$$

which is different then what one would initially expect, which is $P = \hbar\omega\kappa_c\langle\hat{a}^{\dagger}\hat{a}\rangle$. This discrepancy is due to interference between the field radiated by the cavity and the incoming drive modes. If the drive is turned off ($\hat{b}_{in} = 0$) the outgoing waves yield this expected power.

4.3 Two-port cavity

So far, the system has only been connected to a bath by a single weak coupling term. An example of such a case is when a cavity is coupled to an external drive using a partially transparent mirror on one side, while on the other using a reflecting mirror. It is in some cases interesting to consider the case of two partially transparent mirrors. In order to treat this, we have to open up the system to an additional bath, schematically represented in Fig. 4.2. The treatment is essentially equivalent. One distinction we have to make is that the couplings need not be of the same strength, but can be asymmetric. This is taken care of by labelling κ_L to be the coupling between the left bath and the system and κ_R the coupling between the system and the right bath, where 'left' and 'right' refer to their locations in Fig. 4.2. The bath modes on the right are

$$\hat{H}_{bath,R} = \sum_q \hbar\omega_q\hat{c}_q^{\dagger}\hat{c}_q, \tag{4.37}$$

similarly to the bath modes on the left. The interaction Hamiltonian is just interchanging $\hat{b}_q$ and $\hat{b}_q^{\dagger}$ in Eq. (4.2) with $\hat{c}_q$ and $\hat{c}_q^{\dagger}$ respectively, and also allowing for some different coupling strength f_q' instead of f_q (this is what leads to κ_L and κ_R). The final result is

$$\dot{\hat{a}} = \frac{i}{\hbar}[\hat{H}_{\mathcal{S}},\hat{a}] - \frac{\kappa}{2}\hat{a} - \kappa_L\hat{b}_{in} - \kappa_R\hat{c}_{in}, \tag{4.38}$$

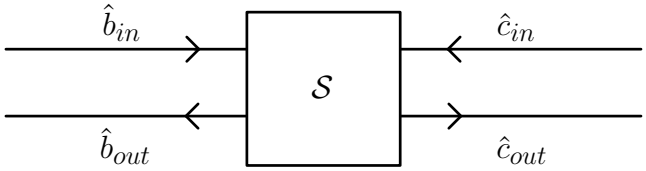

Figure 4.2: Schematic figure where an additional semi-infinite transmission line is added on the right in order to be able to describe a two-port cavity resonator, for instance a cavity with two partially transparent mirrors.

where here $\kappa = \kappa_L + \kappa_R + \kappa_i$. We also arrive at the expression

$$\hat{c}_{out}(t) = \hat{c}_{in}(t) + \sqrt{\kappa_R}\hat{a}. \tag{4.39}$$

Once again, assuming that the system is a harmonic oscillator, we can Fourier transform Eq. (4.38), arriving at the solution

$$\hat{a}[\omega] = -i\frac{\sqrt{\kappa_L}\hat{b}_{in}[\omega] + \sqrt{\kappa_R}\hat{c}_{in}[\omega]}{(\omega - \omega_r) + i\kappa/2}, \tag{4.40}$$

and then by inserting this into Eq. (4.39) receive

$$\begin{aligned}\hat{c}_{out}[\omega] &= \frac{-i\sqrt{\kappa_L\kappa_R}}{(\omega - \omega_r) + i\kappa/2}\hat{b}_{in}[\omega] + \frac{(\omega - \omega_r) + i(\kappa/2 - \kappa_R)}{(\omega - \omega_r) + i\kappa/2}\hat{c}_{in}[\omega] \\ &= \tilde{t}[\omega]\hat{b}_{in}[\omega] + \tilde{r}_R[\omega]\hat{c}_{in}[\omega],\end{aligned} \tag{4.41}$$

where now the transmission and reflection amplitudes $\tilde{t}[\omega]$ and $\tilde{r}_R[\omega]$ have been defined as

$$\tilde{t}[\omega] = \frac{-i\sqrt{\kappa_L\kappa_R}}{(\omega - \omega_r) + i\kappa/2} \tag{4.42}$$

and

$$\tilde{r}_R[\omega] = \frac{(\omega - \omega_r) + i(\kappa/2 - \kappa_R)}{(\omega - \omega_r) + i\kappa/2}. \tag{4.43}$$

Note that the transmission amplitude is symmetric with respect to the two ports, i.e. the expression is the same whether the transmission is considered from left to right or right to left. This is not true for the reflection amplitude, where if the reflection from the left port is considered, κ_R should be interchanged with κ_L.

In two-port measurements, it is common to only send in a signal from one side. This means that $\hbar\omega\langle\hat{b}_{in}^\dagger\hat{b}_{in}\rangle = P_{in}, \langle\hat{c}_{in}^\dagger\hat{c}_{in}\rangle = 0$ and we can derive expressions similar to what

was done in Eqs. (4.33),(4.34). Using Eqs. (4.40),(4.42), we find

$$\begin{aligned}
\langle \hat{a}^\dagger \hat{a} \rangle &= \left\langle \left(\frac{\tilde{t}^*}{\sqrt{\kappa_R}} \hat{b}_{in}^\dagger + \frac{\tilde{t}^*}{\sqrt{\kappa_L}} \hat{c}_{in}^\dagger \right) \left(\frac{\tilde{t}}{\sqrt{\kappa_R}} \hat{b}_{in} + \frac{\tilde{t}}{\sqrt{\kappa_L}} \hat{c}_{in} \right) \right\rangle \\
&= \frac{|\tilde{t}|^2}{\kappa_R} \langle \hat{b}_{in}^\dagger \hat{b}_{in} \rangle + \frac{|\tilde{t}|^2}{\kappa_L} \langle \hat{c}_{in}^\dagger \hat{c}_{in} \rangle + \frac{|\tilde{t}|^2}{\sqrt{\kappa_R \kappa_L}} \langle \hat{b}_{in}^\dagger \hat{c}_{in} \rangle + \frac{|\tilde{t}|^2}{\sqrt{\kappa_R \kappa_L}} \langle \hat{c}_{in}^\dagger \hat{b}_{in} \rangle \\
&= \frac{|\tilde{t}|^2}{\kappa_R} \langle \hat{b}_{in}^\dagger \hat{b}_{in} \rangle \\
&= \frac{|\tilde{t}|^2}{\kappa_R} \frac{P_{in}}{\hbar\omega} \\
&= \frac{\kappa_L}{(\omega - \omega_r)^2 + (\kappa/2)^2} \frac{P_{in}}{\hbar\omega},
\end{aligned} \tag{4.44}$$

where the assumption $\langle \hat{b}_{in}^\dagger \hat{c}_{in} \rangle = \langle \hat{c}_{in}^\dagger \hat{b}_{in} \rangle = 0$ has been made, since these are considered to be uncorrelated. This is then an expression for the number of photons residing in a linear resonator. If we now consider the outgoing power, we can find this for both ports. For the right port we can use Eq. (4.39) to get

$$P_{out,R} = \hbar\omega \langle \hat{c}_{out}^\dagger \hat{c}_{out} \rangle = \hbar\omega \kappa_R \langle \hat{a}^\dagger \hat{a} \rangle, \tag{4.45}$$

where again it is assumed that $\langle \hat{c}_{in}^\dagger \hat{c}_{in} \rangle = 0$. For the left port we receive

$$\begin{aligned}
\frac{P_{out,L}}{\hbar\omega} &= \langle \hat{b}_{out}^\dagger \hat{b}_{out} \rangle \\
&= \langle (\hat{b}_{in}^\dagger + \sqrt{\kappa_L} \hat{a}^\dagger)(\hat{b}_{in} + \sqrt{\kappa_L} \hat{a}) \rangle \\
&= \langle (\tilde{r}_L^* \hat{b}_{in}^\dagger + \tilde{t}^* \hat{c}_{in}^\dagger)(\tilde{r}_L \hat{b}_{in} + \tilde{t} \hat{c}_{in} \rangle \\
&= |\tilde{r}_L|^2 \langle \hat{b}_{in}^\dagger \hat{b}_{in} \rangle \\
&= \frac{(\omega - \omega_r)^2 + (\kappa/2 - \kappa_L)^2}{(\omega - \omega_r)^2 + (\kappa/2)^2} \langle \hat{b}_{in}^\dagger \hat{b}_{in} \rangle,
\end{aligned} \tag{4.46}$$

which is what one would intuitively expect, that the reflected power is the input power times the reflection coefficient.

4.4 Transmon symmetrically coupled to two transmission lines

Now I will apply this to our Transmon in the case where $\kappa_L = \kappa_R = \kappa_c$, i.e. that we have a symmetric coupling to our system. We will consider the system Hamiltonian to be the

one defined in Eq. (3.49). With this, we have

$$\begin{aligned}\frac{i}{\hbar}[\hat{H}_{\mathcal{S}},\hat{a}] &= \frac{i}{\hbar}\left(\sqrt{8E_CE_J}[\hat{a}^\dagger\hat{a},\hat{a}] - \frac{E_C}{4}[2(\hat{a}^\dagger\hat{a})^2 + 2\hat{a}^\dagger\hat{a},\hat{a}]\right)\\ &= -i\omega\hat{a} - \frac{i\omega_C}{4}(2(\hat{a}^\dagger\hat{a}[\hat{a}^\dagger\hat{a},\hat{a}] + [\hat{a}^\dagger\hat{a},\hat{a}]\hat{a}^\dagger\hat{a}) - 2\hat{a})\\ &= -i\omega\hat{a} - \frac{i\omega_C}{4}(-2\hat{a}^\dagger\hat{a}\hat{a} - 2(\hat{a}^\dagger\hat{a}\hat{a} + \hat{a}) - 2\hat{a})\\ &= -i(\omega_r - \omega_C\hat{a}^\dagger\hat{a})\hat{a},\end{aligned} \tag{4.47}$$

where the definitions $\hbar\omega = \sqrt{8E_CE_J}, \hbar\omega_C = E_C$ and $\omega_r = \omega - \omega_C$ have been made. We can compare this to a harmonic oscillator and see that if the system is in the state $|m\rangle$, then the resonance frequency shifts by an amount equal to $-m\omega_C$. This result is consistent with the perturbative result from calculating the resonance frequencies of the Transmon as discussed at the end of Sec. 3.4, and it is thus this term that governs the non-linearity. The full EoM for $\hat{a}$ is then

$$\dot{\hat{a}} = -i\omega_r\hat{a} + i\omega_C\hat{a}^\dagger\hat{a}\hat{a} - \frac{\kappa}{2}\hat{a} - \sqrt{\kappa_c}(\hat{b}_{in} + \hat{c}_{in}), \tag{4.48}$$

where $\kappa = 2\kappa_c + \kappa_i$. Unlike the linear case, we cannot do a Fourier transform to receive the transmission spectrum. What we can do however is to find the EoM for $\hat{a}^\dagger\hat{a}\hat{a}$. This EoM will, as soon shall be seen, be dependent on terms of both higher and lower order. This will be true for all EoMs, thus there is not much hope in finding a solution in closed finite form. The terms of higher order will however most likely have decreasing amplitude, meaning that we can eventually truncate terms of some high order while keeping the error small. What is needed is a general expression for the EoM of $(\hat{a}^\dagger)^m\hat{a}^n$, which is what is done in Ref. 25. To find this we again need the full Hamiltonian from Eq. (4.1). The full expression is

$$\begin{aligned}\frac{\mathrm{d}}{\mathrm{d}t}((\hat{a}^\dagger)^m\hat{a}^n) &= \frac{i}{\hbar}[\hat{H},(\hat{a}^\dagger)^m\hat{a}^n]\\ &= \frac{i}{\hbar}[\hat{H}_{\mathcal{S}},(\hat{a}^\dagger)^m\hat{a}^n] + \left[\sum_q\left(f_q\hat{a}^\dagger\hat{b}_q - f_q^*\hat{b}_q^\dagger\hat{a}\right),(\hat{a}^\dagger)^m\hat{a}^n\right] + \frac{i}{\hbar}\underbrace{[\hat{H}_{bath},(\hat{a}^\dagger)^m\hat{a}^n]}_{=0}.\end{aligned} \tag{4.49}$$

It will be useful to have the commutation relations $[\hat{a},(\hat{a}^\dagger)^m]$ as well as $[\hat{a}^\dagger,\hat{a}^n]$ readily available. We find these to be

$$\begin{aligned}[\hat{a},(\hat{a}^\dagger)^m] &= \hat{a}(\hat{a}^\dagger)^m - (\hat{a}^\dagger)^m\hat{a}\\ &= (\hat{a}^\dagger)^{m-1} + \hat{a}^\dagger\hat{a}(\hat{a}^\dagger)^{m-1} - (\hat{a}^\dagger)^m\hat{a}\\ &= \cdots = m(\hat{a}^\dagger)^{m-1} + (\hat{a}^\dagger)^m\hat{a} - (\hat{a}^\dagger)^m\hat{a}\\ &= m(\hat{a}^\dagger)^{m-1}\end{aligned} \tag{4.50}$$

$$\begin{aligned}[\hat{a}^\dagger, \hat{a}^n] &= \hat{a}^\dagger \hat{a}^n - \hat{a}^n \hat{a}^\dagger \\ &= \hat{a}^\dagger \hat{a}^n - \hat{a}^{n-1}\hat{a}^\dagger \hat{a} - \hat{a}^{n-1} = \cdots = \\ &= -n\hat{a}^{n-1}.\end{aligned} \tag{4.51}$$

Treating one term in the Hamiltonian (4.49) at a time, we find

$$\begin{aligned}[\hat{a}^\dagger \hat{a}, (\hat{a}^\dagger)^m \hat{a}^n] &= \hat{a}^\dagger \hat{a}(\hat{a}^\dagger)^m \hat{a}^n - (\hat{a}^\dagger)^m \hat{a}^n \hat{a}^\dagger \hat{a} \\ &= \hat{a}^\dagger \Big((\hat{a}^\dagger)^m \hat{a} + m(\hat{a}^\dagger)^{m-1}\Big)\hat{a}^n - (\hat{a}^\dagger)^m \Big(\hat{a}^\dagger \hat{a}^n + n\hat{a}^{n-1}\Big)\hat{a}\hat{a}^\dagger \hat{a} \\ &= (\hat{a}^\dagger)^{m+1}\hat{a}^{n+1} - (\hat{a}^\dagger)^{m+1}\hat{a}^{n+1} + m(\hat{a}^\dagger)^m \hat{a}^n - n(\hat{a}^\dagger)^m \hat{a}^n \\ &= (m-n)(\hat{a}^\dagger)^m \hat{a}^n\end{aligned} \tag{4.52}$$

$$\begin{aligned}[(\hat{a}^\dagger \hat{a})^2, (\hat{a}^\dagger)^m \hat{a}^n] &= \hat{a}^\dagger \hat{a}[\hat{a}^\dagger \hat{a}, (\hat{a}^\dagger)^m \hat{a}^n] + [\hat{a}^\dagger \hat{a}, (\hat{a}^\dagger)^m \hat{a}^n]\hat{a}^\dagger \hat{a} \\ &= (m-n)\Big(\hat{a}^\dagger \hat{a}(\hat{a}^\dagger)^m \hat{a}^n + (\hat{a}^\dagger)^m \hat{a}^n \hat{a}^\dagger \hat{a}\Big) \\ &= (m-n)\Big(\hat{a}^\dagger((\hat{a}^\dagger)^m \hat{a} + m(\hat{a}^\dagger)^{m-1})\hat{a}^n + (\hat{a}^\dagger)^m(\hat{a}^\dagger \hat{a}^n + n\hat{a}^{n-1})\hat{a}\Big) \\ &= 2(m-n)(\hat{a}^\dagger)^{m+1}\hat{a}^{n+1} + (m^2 - n^2)(\hat{a}^\dagger)^m \hat{a}^n.\end{aligned} \tag{4.53}$$

With these two relations, the first term on the right hand side of Eq. (4.49) is readily obtained:

$$\begin{aligned}\frac{i}{\hbar}[\hat{H}_{\mathcal{S}}, (\hat{a}^\dagger)^m \hat{a}^n] &= \frac{i}{\hbar}\left(\Big(\sqrt{8E_C E_J} - \frac{E_C}{2}\Big)[\hat{a}^\dagger \hat{a}, (\hat{a}^\dagger)^m \hat{a}^n] - \frac{E_C}{2}[(\hat{a}^\dagger \hat{a})^2, (\hat{a}^\dagger)^m \hat{a}^n]\right) \\ &= \Big(i(m-n)\omega_r - i\frac{(m-n)(m+n-1)}{2}\omega_C\Big)(\hat{a}^\dagger)^m \hat{a}^n \\ &\quad - i(m-n)\omega_C(\hat{a}^\dagger)^{m+1}\hat{a}^{n+1},\end{aligned} \tag{4.54}$$

where the definitions for the variables are the same as in Eq. (4.47). For the interaction Hamiltonian $\hat{H}_{int}$, it is rather trivial given the relations (4.50),(4.51) to find that

$$\frac{i}{\hbar}[\hat{H}_{int}, (\hat{a}^\dagger)^m \hat{a}^n] = -n(\hat{a}^\dagger)^m \hat{a}^{n-1} \sum_q f_q \hat{b}_q - m \sum_q f_q^* \hat{b}_q^\dagger (\hat{a}^\dagger)^{m-1}\hat{a}^n. \tag{4.55}$$

Treating this the same way (with the same approximations) as in section 4.1 we find that

$$\sum_q f_q \hat{b}_q = \sqrt{\kappa_c}\hat{b}_{in}(t) + \frac{\kappa}{2}\hat{a}, \tag{4.56}$$

and similarly

$$\sum_q f_q^* \hat{b}_q^\dagger = \sqrt{\kappa_c}\hat{b}_{in}^\dagger(t) + \frac{\kappa}{2}\hat{a}^\dagger. \tag{4.57}$$

Note here that some steps have been skipped that were derived before. Since adding losses and a second port is completely analogous to adding the first port those details are skipped here. We further assume $\langle \hat{c}_{in}(t) \rangle = 0$ since we are not driving the system from this side and thus ignore this term, so we will only consider the influence from $\hat{b}_{in}(t)$ on the system.

The effect is then in principle to let $\kappa = 2\kappa_c + \kappa_i$. The total EoM for $(\hat{a}^\dagger)^m\hat{a}^n$ is now

$$\begin{aligned}\frac{\mathrm{d}}{\mathrm{d}t}(\hat{a}^\dagger)^m\hat{a}^n = &\Big(i(m-n)\omega_r - i\frac{(m-n)(m+n-1)}{2}\omega_C - \frac{m+n}{2}\kappa\Big)(\hat{a}^\dagger)^m\hat{a}^n \\ &- i(m-n)\omega_C(\hat{a}^\dagger)^{m+1}\hat{a}^{n+1} - n\sqrt{\kappa_c}(\hat{a}^\dagger)^m\hat{a}^{n-1}\hat{b}_{in}(t) \\ &- m\sqrt{\kappa_c}\hat{b}_{in}^\dagger(t)(\hat{a}^\dagger)^{m-1}\hat{a}^n.\end{aligned} \tag{4.58}$$

If you are attentive about the details, then you might become suspicious about blindly inserting Eqs. (4.56),(4.57) into Eq. (4.55). The operators $\hat{b}_q$ commute with all system operators, in particular $\hat{a}^\dagger$, since their Hilbert spaces are separated. The right hand side (RHS) of Eq. (4.56) however, contains $\hat{a}$ which does not commute with $\hat{a}^\dagger$. It seems at first as though something has broken down in our approximations. It is resolved by the fact that a single term on the RHS need not commute with a system operator, but all terms together on the RHS do. In other words, $\hat{b}_{in}$ does not commute with $\hat{a}^\dagger$ for instance. One can even find an expression for the EoM of a general system operator $\hat{O}_\mathcal{S}$:

$$\dot{\hat{O}}_\mathcal{S} = \frac{i}{\hbar}[\hat{H}_\mathcal{S}, \hat{O}_\mathcal{S}] + \left([\hat{a}^\dagger, \hat{O}_\mathcal{S}]\left(\frac{\kappa}{2}\hat{a} + \sqrt{\kappa}\hat{b}_{in}(t)\right) - \left(\frac{\kappa}{2}\hat{a}^\dagger + \sqrt{\kappa}\hat{b}_{in}^\dagger(t)\right)[\hat{a}, \hat{O}_\mathcal{S}]\right). \tag{4.59}$$

This is known as the quantum Langevin equation, and is in fact what we have used letting $\hat{O}_\mathcal{S} = (\hat{a}^\dagger)^m\hat{a}^n$ [39]. With Eq. (4.58) we now have a relation between all combinations of step operators. Since a complete solution would require an infinite number of coupled differential equations, m and n need to be truncated at some point. Then it becomes possible to solve using numerical methods. It is a natural question to wonder about what is lost when truncating at some finite m, n. For now the equation is only stated in terms of operators, but later we will consider the expectation value of these. Then unless higher order terms $\to 0$, they will become increasingly important for the dynamics. I will not prove that this condition really is fulfilled, but rather provide an argument for it in the limit that will be considered ($\omega_C \gg \kappa$): When acting on a state $|k\rangle$ with $(\hat{a}^\dagger)^m\hat{a}^n$ it is only non-zero if $k \geq n$. As the system is highly anharmonic and only driven on at most two frequencies, the system can only get excited to higher states with multi-photon processes. Multi-photon processes are somewhat unlikely events unless the drive is very strong, so they might occur occasionally, and they require approximately $n\hbar\omega \approx E_n - E_0$, where ω is the frequency of the RF signal and $E_n - E_0$ is the difference in energy between the n:th excited state and the ground state. I will only consider frequencies reasonably close to the resonance frequency, where these excitations are negligible for about $n \geq 5$ due to the strong anharmonicity, even with a strong drive. Since the excitations are essentially negligible, the states have low probability of occupancy which means that $\langle(\hat{a}^\dagger)^m\hat{a}\rangle$ will be small for higher m, n.

This reasoning is clearly not valid for systems where $\omega_C/\kappa \ll 1$, as then the system behaves closer to a linear system in which the higher states have a higher occupancy. Also, of course the strength of the drive is relevant but at sufficiently strong drive some of

the approximations made in the derivation of the input-output formulas start becoming less valid, such as the RWA.

In Chapter 6 a steady state solution for $\langle \hat{a} \rangle$ will be found numerically with this method for single tone measurements. It will also be used in Chapter 7, where the system dynamics will be analysed when a strong drive and a weak probe is injected into the system.

4.5 Heterodyne detection

With the output operators in our toolbox, we can start to look at what the measured signal will be. The measurement setup used in the original experiments utilises heterodyne detection. In order to understand what this means we first introduce what are called quadratures. If we have a cavity with annihilation operator $\hat{a}$, then we can define the quadrature operators [27]

$$\hat{X} \equiv \frac{1}{2}(\hat{a} + \hat{a}^\dagger) \tag{4.60}$$

$$\hat{Y} \equiv \frac{i}{2}(\hat{a}^\dagger - \hat{a}), \tag{4.61}$$

which are Hermitian operators and therefore correspond to some observable. They are effectively the real and imaginary parts of $\hat{a}$, which can be seen from $\langle \hat{X} \rangle = \mathrm{Re}\,\langle \hat{a} \rangle$ and $\langle \hat{Y} \rangle = \mathrm{Im}\,\langle \hat{a} \rangle$, where $\langle \hat{a}^\dagger \rangle = \langle \hat{a} \rangle^*$ has been used. These are canonically conjugate operators, satisfying

$$[\hat{X}, \hat{Y}] = +\frac{i}{2}, \tag{4.62}$$

and for coherent states they for instance obey

$$\langle \alpha | \hat{X} | \alpha \rangle = \mathrm{Re}\,(\alpha(t)) \tag{4.63}$$

$$\langle \alpha | \hat{Y} | \alpha \rangle = \mathrm{Im}\,(\alpha(t)). \tag{4.64}$$

Since they are conjugate, they cannot be measured by a projective measurement simultaneously. They are however measured simultaneously in a heterodyne measurement, which also means that such a measurement is limited in precision, determined by the Heisenberg uncertainty relation. This uncertainty can be thought of in terms of quantum noise where the output from the measurement contains some vacuum noise such that the uncertainty relation is preserved [9]. This is opposed to a homodyne measurement, where only one of these quadratures are measured.

When a heterodyne measurement is made, the signal from the system can be considered as being multiplied together with the signal from a local oscillator (LO) in a mixer, where the LO has some frequency ω_{LO}. If we first consider the transmitted response of a two-port linear resonator driven at frequency ω_d where $\hat{a}$ is considered in the rotating frame of the

drive, then the voltage signal from the mixer will be [43]

$$\begin{aligned} V_m &= \alpha\langle \hat{c}_{out}(t) + \hat{c}_{out}^\dagger(t)\rangle \cos\omega_{LO}t \\ &= \frac{\alpha\sqrt{\kappa_c}}{2}\langle \hat{a}e^{-i\omega_d t} + \hat{a}^\dagger e^{i\omega_d t}\rangle(e^{i\omega_{LO}t} + e^{-i\omega_{LO}t}) \\ &= \frac{\alpha\sqrt{\kappa_c}}{2}\Big\langle \hat{a}(e^{-i\omega_{IF}t} + e^{-i(\omega_d+\omega_{LO})t}) + \hat{a}^\dagger(e^{i\omega_{IF}t} + e^{i(\omega_d+\omega_{LO})t})\Big\rangle, \end{aligned} \tag{4.65}$$

where α is some amplitude and $\omega_{IF} = \omega_d - \omega_{LO}$ is some known intermediate frequency. This is then filtered through a low pass filter, removing the terms rotating with $e^{\pm i(\omega_d+\omega_{LO})}$, yielding a signal

$$V_{LPF} = \beta(\langle\hat{a}\rangle e^{-i\omega_{IF}t} + \langle\hat{a}^\dagger\rangle e^{i\omega_{IF}t}), \tag{4.66}$$

from which the quadratures $I = V_0\langle\hat{a} + \hat{a}^\dagger\rangle$ and $Q = iV_0\langle\hat{a}^\dagger - \hat{a}\rangle$ can be extracted. We are mainly interested in the steady state solution of $\langle\hat{a}\rangle$, so any phase difference when mixing the signals can here be ignored. With the choice made now, at $t = 0$ the I quadrature is extracted, but we can consider the case where we also have a $\sin\omega_{LO}t$ component as well. Then we can see that at $t = 0$, this component will yield the Q quadrature. With these we can find the steady state amplitude A of the signal in the measurement

$$A = \sqrt{I^2 + Q^2}. \tag{4.67}$$

This quantity corresponds here is then proportional to $|\langle\hat{a}\rangle|$. This sounds a bit strange, as $\hat{a}$ is not a Hermitian operator and can therefore not directly be measured. Now comes the important remark that was made earlier, we cannot measure I and Q simultaneously with perfect precision even though it might seem that way from our expressions. From the quantum noise perspective, we can consider that if the signal from $\hat{a}$ oscillates with $e^{-i(\omega_{LO}+\omega_{IF})t}$, then the output is subject to vacuum noise at frequency $e^{-i(\omega_{LO}-\omega_{IF})t}$ which prevents us from measuring both quadratures exactly at the same time. We need to make several measurements over time and take the average to get $\langle\hat{a}\rangle$.

Chapter 5

Master Equation

We carry out the calculation as if it is allowed and then see afterwards that it is. This is most often a good method.
- Tomas Persson

The input-output theory is very powerful and useful, as it tells us what our measured signal will be. It is however sometimes lacking when simulating quantum systems. Adding effects like pure dephasing that occurs due to interaction with the environment can be difficult, and sometimes it can be difficult to calculate quantities entirely within input-output theory. This is where master equations come in. Master equations are an efficient way of studying the internal dynamics of a system over time (which usually requires numerical simulations), or finding steady states solutions (which can sometimes be done analytically as I have in some cases in the thesis). The idea is that if we have a system $\mathcal{S}$ which is weakly coupled to an environment, it is a subsystem of some much larger, much more complicated total system. This total system has some dynamics and, since it is a Hilbert space, you can find some density of states matrix ρ_{tot} that properly describes everything. Since solving this would generally be virtually impossible, we instead make the approximation that the system $\mathcal{S}$ is weakly coupled and separable from the total system, such that we have $\rho_{tot} = \rho_{\mathcal{S}} \otimes \rho_E$, where $\rho_{\mathcal{S}}$ is the density of states of the system $\mathcal{S}$ and ρ_E is the density of states of the environment. This approximation was already made in the input-output formalism, however now we will trace out the environment, such that we are only left with the Hamiltonian for the system. This is what allows us to get access to the internal dynamics of the system. It is possible to derive an appropriate master equation from input-output theory, telling us that the same approximations are made on the system in the derivations [39]. This means that other than the separation of the two Hilbert spaces, only coupled via some weak interaction, the Markov approximation is used in the derivation of master equations.

The famous Lindblad master equation will be introduced and assumed as given. There are several derivations of it available with a few different approaches, see e.g. Ref. 44. In

order to arrive at the Lindblad master equation, the so called secular approximation has to be made. Essentially it means that terms that are fast rotating in the interaction picture and terms that lead to a small renormalisation of the system energy levels are ignored.

Master equations also have an edge against input-output theory in doing numerical simulations, as there are powerful toolboxes developed to do this, one of which will be used in this thesis known as Quantum Toolbox in Pyhton (QuTiP). Since master equations also give you access to the density matrix, information about coherences between states and their populations can also be obtained.

5.1 Lindblad master equation on a harmonic oscillator

We will start acquainting ourselves with the Lindblad master equation and how one can utilise it by applying it to a regular harmonic oscillator, more specifically some cavity where the number states correspond to how many photons are residing in the cavity. Notable changes compared to the input-output theory is that we will now be working in the Schrödinger picture instead of the Heisenberg picture, and instead of having a Hamiltonian connecting the system and the environment, this will be traced out yielding a driving term in the system Hamiltonian instead.

Our system Hamiltonian that we will study now has the form

$$\hat{H} = \hbar\omega_r \hat{a}^\dagger \hat{a} + \hbar\gamma \left(\hat{a}^\dagger e^{-i\omega_d t} + \hat{a} e^{i\omega_d t} \right), \tag{5.1}$$

where ω_r is the resonance frequency of the cavity, $\hat{a}$ and $\hat{a}^\dagger$ are the annihilation and creation operators respectively, ω_d is the frequency of the drive and γ is the coupling between the drive and the resonator. Note here again that we have made a gauge choice, similarly as to in Sec. 4.1, however this time a different one. It is mostly a matter of taste and convention, however one needs to be a bit careful as the input-output relations 4.25, 4.39 changes slightly (by some phase factor in front of $\langle \hat{a} \rangle$) due to the different gauge choices.

An issue with this Hamiltonian is that it is indeed an operator with time dependence, making it tricky to deal with. We can however get rid of this by moving to a frame which is co-rotating with the drive by performing a unitary transformation. This is described in Sec. 5.2. Our Hamiltonian in this frame is then

$$\hat{H} = \hbar\Delta \hat{a}^\dagger \hat{a} + \hbar\gamma \left(\hat{a}^\dagger + \hat{a} \right), \tag{5.2}$$

where $\Delta = \omega_r - \omega_d$ is the detuning of the drive frequency with respect to the resonance frequency of the harmonic oscillator. This is the Hamiltonian that will be inserted into the Lindblad master equation.

The Lindblad master equation for our system is

$$\dot{\hat{\rho}} = -\frac{i}{\hbar}[\hat{H}, \hat{\rho}] + \kappa \mathcal{D}[\hat{a}]\hat{\rho}, \tag{5.3}$$

where κ is some real parameter indicating the relaxation (de-excitation) rate from the system and $\mathcal{D}[\hat{a}]\hat{\rho}$ is the Lindblad dissipator which is defined for a general operator $\hat{A}$ as

$$\mathcal{D}[\hat{A}]\hat{\rho} = \frac{1}{2}\left([\hat{A}\hat{\rho}, \hat{A}^\dagger] + [\hat{A}, \hat{\rho}\hat{A}^\dagger]\right). \tag{5.4}$$

This will correspond to relaxations or de-excitations in the harmonic oscillator to the environment. Note here that in equation (5.3), we have implicitly defined $\hat{\rho}$ to be in the frame that is co-rotating with the system, and therefore if we wish to know the states in the original basis, we need to transform back to the original frame. One can also define $\hat{\rho}$ in the original frame, transform it to the co-rotating frame and carry out the calculations in a similar manner.

Let us now say that we want to look at steady state solutions for the average number of photons inside the cavity $\langle \hat{a}^\dagger \hat{a} \rangle$. To do this we make the requirement

$$0 \stackrel{!}{=} \frac{\mathrm{d}}{\mathrm{d}t}\langle \hat{a}^\dagger \hat{a} \rangle = \frac{\mathrm{d}}{\mathrm{d}t}\mathrm{tr}\{\hat{\rho}(\hat{a}^\dagger \hat{a})\} = \mathrm{tr}\{\dot{\hat{\rho}}(\hat{a}^\dagger \hat{a})\}, \tag{5.5}$$

where $\mathrm{tr}\{\hat{A}\}$ is the trace of an operator $\hat{A}$ and the last inequality follows from the fact that we are in the Schrödinger picture so the operators are time independent.

First, we find $\dot{\hat{\rho}}$ using equation (5.3):

$$\begin{aligned} \dot{\hat{\rho}} &= -\frac{i}{\hbar}\Big(\hbar\Delta(\hat{a}^\dagger \hat{a}\hat{\rho} - \hat{\rho}\hat{a}^\dagger \hat{a}) + \hbar\gamma(\hat{a}^\dagger \hat{\rho} - \hat{\rho}\hat{a}^\dagger + \hat{a}\hat{\rho} - \hat{\rho}\hat{a})\Big) + \frac{1}{2}\Big([\hat{a}\hat{\rho}, \hat{a}^\dagger] + [\hat{a}, \hat{\rho}\hat{a}^\dagger]\Big) \\ &= -i\Delta[\hat{a}^\dagger \hat{a}, \hat{\rho}] - i\gamma[\hat{a}^\dagger + \hat{a}, \hat{\rho}] + \frac{1}{2}\kappa\Big([\hat{a}\hat{\rho}, \hat{a}^\dagger] + [\hat{a}, \hat{\rho}\hat{a}^\dagger]\Big). \end{aligned} \tag{5.6}$$

This is about as far as we can go here, but when calculating $\langle \hat{a}^\dagger \hat{a} \rangle$ we can make further progress by using linearity and the cyclic property of the trace ($\mathrm{tr}\{\hat{A}\hat{B}\} = \mathrm{tr}\{\hat{B}\hat{A}\}$), as

well as $[\hat{a}, \hat{a}^\dagger] = 1$:

$$\begin{aligned}
\frac{\mathrm{d}}{\mathrm{d}t}\langle \hat{a}^\dagger \hat{a}\rangle &= \mathrm{tr}\{\dot{\hat{\rho}}\hat{a}^\dagger\hat{a}\} \\
&= \mathrm{tr}\Big\{ -i\Delta[\hat{a}^\dagger\hat{a},\hat{\rho}]\hat{a}^\dagger\hat{a} - i\gamma[\hat{a}^\dagger+\hat{a},\hat{\rho}]\hat{a}^\dagger\hat{a} + \frac{1}{2}\kappa\Big([\hat{a}\hat{\rho},\hat{a}^\dagger]\hat{a}^\dagger\hat{a} + [\hat{a},\hat{\rho}\hat{a}^\dagger]\hat{a}^\dagger\hat{a}\Big)\Big\} \\
&= \mathrm{tr}\Big\{-i\Delta(\hat{a}^\dagger\hat{a}\hat{\rho}\hat{a}^\dagger\hat{a} - \hat{\rho}\hat{a}^\dagger\hat{a}\hat{a}^\dagger\hat{a}) - i\gamma(\hat{a}^\dagger\hat{\rho}\hat{a}^\dagger\hat{a} - \hat{\rho}\hat{a}^\dagger\hat{a}^\dagger\hat{a} + \hat{a}\hat{\rho}\hat{a}^\dagger\hat{a} - \hat{\rho}\hat{a}\hat{a}^\dagger\hat{a}) \\
&\quad + \frac{1}{2}\kappa(\hat{a}\hat{\rho}\hat{a}^\dagger\hat{a}^\dagger\hat{a} - \hat{a}^\dagger\hat{a}\hat{\rho}\hat{a}^\dagger\hat{a} + \hat{a}\hat{\rho}\hat{a}^\dagger\hat{a}^\dagger\hat{a} - \hat{\rho}\hat{a}^\dagger\hat{a}\hat{a}^\dagger\hat{a})\Big\} \\
&= \mathrm{tr}\{-i\Delta(\hat{\rho}\hat{a}^\dagger\hat{a}\hat{a}^\dagger\hat{a} - \hat{\rho}\hat{a}^\dagger\hat{a}\hat{a}^\dagger\hat{a})\} + \mathrm{tr}\{-i\gamma(\hat{\rho}\hat{a}^\dagger\hat{a}\hat{a}^\dagger - \hat{\rho}\hat{a}^\dagger\hat{a}^\dagger\hat{a})\} \\
&\quad + \mathrm{tr}\{-i\gamma(\hat{\rho}\hat{a}^\dagger\hat{a}\hat{a} - \hat{\rho}\hat{a}\hat{a}^\dagger\hat{a})\} + \mathrm{tr}\left\{\frac{1}{2}\kappa(\hat{\rho}\hat{a}^\dagger\hat{a}^\dagger\hat{a}\hat{a} - \hat{\rho}\hat{a}^\dagger\hat{a}\hat{a}^\dagger\hat{a} + \hat{\rho}\hat{a}^\dagger\hat{a}^\dagger\hat{a}\hat{a} - \hat{\rho}\hat{a}^\dagger\hat{a}\hat{a}^\dagger\hat{a})\right\} \\
&= 0 - i\gamma\,\mathrm{tr}\{\hat{\rho}\hat{a}^\dagger[\hat{a},\hat{a}^\dagger]\} - i\gamma\,\mathrm{tr}\{\hat{\rho}(-[\hat{a},\hat{a}^\dagger])\hat{a}\} + \kappa\,\mathrm{tr}\{\hat{\rho}\hat{a}^\dagger(-[\hat{a},\hat{a}^\dagger])\hat{a}\} \\
&= -i\gamma\,\mathrm{tr}\{\hat{\rho}\hat{a}^\dagger\} - i\gamma\,\mathrm{tr}\{-\hat{\rho}\hat{a}\} - \kappa\,\mathrm{tr}\{\hat{\rho}\hat{a}^\dagger\hat{a}\} \\
&= -i\gamma\langle\hat{a}^\dagger\rangle + i\gamma\langle\hat{a}\rangle - \kappa\langle\hat{a}^\dagger\hat{a}\rangle.
\end{aligned} \tag{5.7}$$

We see that we need to find the steady state solutions to both $\langle\hat{a}\rangle$ and $\langle\hat{a}^\dagger\rangle$ in order to solve this. By similar calculations as above, we find

$$\begin{aligned}
\frac{\mathrm{d}}{\mathrm{d}t}\langle\hat{a}^\dagger\rangle &= \mathrm{tr}\{\dot{\hat{\rho}}\hat{a}^\dagger\} \\
&= \mathrm{tr}\Big\{-i\Delta(\hat{a}^\dagger\hat{a}\hat{\rho}\hat{a}^\dagger - \hat{\rho}\hat{a}^\dagger\hat{a}\hat{a}^\dagger) - i\gamma(\hat{a}^\dagger\hat{\rho}\hat{a}^\dagger - \hat{\rho}\hat{a}^\dagger\hat{a}^\dagger + \hat{a}\hat{\rho}\hat{a}^\dagger - \hat{\rho}\hat{a}\hat{a}^\dagger) \\
&\quad + \frac{1}{2}\kappa(\hat{a}\hat{\rho}\hat{a}^\dagger\hat{a}^\dagger - \hat{a}^\dagger\hat{a}\hat{\rho}\hat{a}^\dagger + \hat{a}\hat{\rho}\hat{a}^\dagger\hat{a}^\dagger - \hat{\rho}\hat{a}^\dagger\hat{a}\hat{a}^\dagger)\Big\} \\
&= \mathrm{tr}\{i\Delta\hat{\rho}\hat{a}^\dagger\} + \mathrm{tr}\{i\gamma\hat{\rho}\} - \mathrm{tr}\left\{\frac{1}{2}\kappa\hat{\rho}\hat{a}^\dagger\right\} \\
&= i\Delta\langle\hat{a}^\dagger\rangle + i\gamma - \frac{\kappa}{2}\langle\hat{a}^\dagger\rangle \stackrel{!}{=} 0 \\
\Rightarrow \langle\hat{a}^\dagger\rangle &= \frac{i\gamma}{\kappa/2 - i\Delta},
\end{aligned} \tag{5.8}$$

as well as

$$\begin{aligned}
\frac{\mathrm{d}}{\mathrm{d}t}\langle\hat{a}\rangle &= \mathrm{tr}\{\dot{\hat{\rho}}\hat{a}\} \\
&= \mathrm{tr}\Big\{-i\Delta(\hat{a}^\dagger\hat{a}\hat{\rho}\hat{a} - \hat{\rho}\hat{a}^\dagger\hat{a}\hat{a}) - i\gamma(\hat{a}^\dagger\hat{\rho}\hat{a} - \hat{\rho}\hat{a}^\dagger\hat{a} + \hat{a}\hat{\rho}\hat{a} - \hat{\rho}\hat{a}\hat{a}) \\
&\quad + \frac{1}{2}\kappa(\hat{a}\hat{\rho}\hat{a}^\dagger\hat{a} - \hat{a}^\dagger\hat{a}\hat{\rho}\hat{a} + \hat{a}\hat{\rho}\hat{a}^\dagger\hat{a} - \hat{\rho}\hat{a}^\dagger\hat{a}\hat{a})\Big\} \\
&= \mathrm{tr}\{-i\Delta\hat{\rho}\hat{a}\} + \mathrm{tr}\{-i\gamma\hat{\rho}\} - \mathrm{tr}\left\{\frac{1}{2}\kappa\hat{\rho}\hat{a}\right\} \\
&= -i\Delta\langle\hat{a}\rangle - i\gamma - \frac{\kappa}{2}\langle\hat{a}\rangle \stackrel{!}{=} 0 \\
\Rightarrow \langle\hat{a}\rangle &= \frac{-i\gamma}{\kappa/2 + i\Delta}.
\end{aligned} \tag{5.9}$$

This is, as is expected, just the complex conjugate of $\langle \hat{a}^\dagger \rangle$. Inserting this into equation (5.7) now yields the steady state solution

$$\begin{aligned} \frac{\mathrm{d}}{\mathrm{d}t}\langle \hat{a}^\dagger \hat{a} \rangle &= \frac{\gamma^2}{\kappa/2 - i\Delta} + \frac{\gamma^2}{\kappa/2 + i\Delta} - \kappa \langle \hat{a}^\dagger \hat{a} \rangle \\ &= \frac{\gamma^2(\kappa/2 - i\Delta + \kappa/2 + i\Delta)}{(\kappa/2)^2 + \Delta^2} - \kappa \langle \hat{a}^\dagger \hat{a} \rangle \stackrel{!}{=} 0 \\ &\iff \langle \hat{a}^\dagger \hat{a} \rangle = \frac{\gamma^2}{(\kappa/2)^2 + \Delta^2}. \end{aligned} \tag{5.10}$$

Comparison with this expression and Eq. (4.33) from input-output theory, we find after some manipulation that $\gamma^2 = \kappa_c \dot{N}$, where $\dot{N} = P/\hbar\omega_d$. A remark for the case of the harmonic oscillator is that in the steady state solution $\langle \hat{a}^\dagger \hat{a} \rangle = \langle \hat{a}^\dagger \rangle \langle \hat{a} \rangle$. This means that the coherence of the drive is conserved within the system, something that will be discussed in more detail in later sections.

5.2 Moving to a frame rotating with the drive

We want to eliminate the time dependence of the Hamiltonian in equation (5.1). This can be done via a unitary transformation of our states:

$$|\tilde{\Psi}(t)\rangle = \hat{U}(t)|\Psi(t)\rangle. \tag{5.11}$$

In order to see how our Hamiltonian changes under this transformation, we need to derive this by requiring that

$$i\hbar \frac{\mathrm{d}}{\mathrm{d}t}|\tilde{\Psi}(t)\rangle = \hat{H}'|\tilde{\Psi}(t)\rangle, \tag{5.12}$$

where $\hat{H}'$ is the Hamiltonian after the unitary transformation (which in general may or may not have some time dependence). We then find

$$\begin{aligned} i\hbar \frac{\mathrm{d}}{\mathrm{d}t}|\tilde{\Psi}(t)\rangle &= i\hbar \frac{\mathrm{d}}{\mathrm{d}t}(\hat{U}(t)|\Psi(t)\rangle) = i\hbar \dot{\hat{U}}(t)|\Psi(t)\rangle + \hat{U}(t)\left(i\hbar \frac{\mathrm{d}}{\mathrm{d}t}|\Psi(t)\rangle\right) \\ &= i\hbar \dot{\hat{U}}(t)|\Psi(t)\rangle + \hat{U}(t)\hat{H}|\Psi(t)\rangle \\ &= i\hbar \dot{\hat{U}}(t)\hat{U}^\dagger(t)|\tilde{\Psi}(t)\rangle + \hat{U}(t)\hat{H}\hat{U}^\dagger(t)|\tilde{\Psi}(t)\rangle \\ &= \left(i\hbar \dot{\hat{U}}(t)\hat{U}^\dagger(t) + \hat{U}(t)\hat{H}\hat{U}^\dagger(t)\right)|\tilde{\Psi}(t)\rangle \\ &= \hat{H}'|\tilde{\Psi}(t)\rangle. \end{aligned} \tag{5.13}$$

Where in the last equality, we have defined

$$\hat{H}' \equiv i\hbar \dot{\hat{U}}\hat{U}^\dagger + \hat{U}\hat{H}\hat{U}^\dagger, \tag{5.14}$$

where I have now skipped explicitly writing a time dependence for the unitary transformation operator. The unitary operator that changes the frame to one co-rotating with

the drive is

$$\hat{U}(t) = e^{i\omega_d \hat{a}^\dagger \hat{a} t}, \tag{5.15}$$

which we will see when we have derived the expression for the transformed Hamiltonian. For the calculations we need two commutation relations, namely

$$[\hat{a}^\dagger \hat{a}, \hat{a}^\dagger] = \hat{a}^\dagger \tag{5.16}$$

$$[\hat{a}^\dagger \hat{a}, \hat{a}] = -\hat{a}. \tag{5.17}$$

We are now ready to transform the Hamiltonian from equation (5.1) to the co-rotating frame.

$$\begin{aligned}
\hat{H}' &= i\hbar \dot{\hat{U}} \hat{U}^\dagger + \hat{U} \hat{H} \hat{U}^\dagger \\
&= i\hbar (i\omega_d \hat{a}^\dagger \hat{a}) \hat{U} \hat{U}^\dagger + \hbar \omega_r \hat{U} \hat{a}^\dagger \hat{a} \hat{U}^\dagger + \gamma e^{-i\omega_d t} \hat{U} \hat{a}^\dagger \hat{U}^\dagger + \gamma e^{i\omega_d t} \hat{U} \hat{a} \hat{U}^\dagger \\
&= \hbar(\omega_r - \omega_d) \hat{a}^\dagger \hat{a} + \gamma e^{-i\omega_d t} \hat{U} \hat{a}^\dagger \hat{U}^\dagger + \gamma e^{i\omega_d t} \hat{U} \hat{a} \hat{U}^\dagger.
\end{aligned} \tag{5.18}$$

For the last two terms, we will treat one of them thoroughly then transfer the result to the other case. We start by treating

$$\begin{aligned}
\hat{U}\hat{a}^\dagger &= e^{i\omega_d \hat{a}^\dagger \hat{a} t} \hat{a}^\dagger \\
&= \sum_{k=0}^{\infty} \frac{(i\omega_d t)^k}{k!} (\hat{a}^\dagger \hat{a})^k \hat{a}^\dagger \\
&= \sum_{k=0}^{\infty} \frac{(i\omega_d t)^k}{k!} (\hat{a}^\dagger \hat{a})^{(k-1)} (\hat{a}^\dagger + \hat{a}^\dagger (\hat{a}^\dagger \hat{a})) \\
&= \sum_{k=0}^{\infty} \frac{(i\omega_d t)^k}{k!} (\hat{a}^\dagger \hat{a})^{(k-1)} \hat{a}^\dagger (1 + \hat{a}^\dagger \hat{a})) \\
&= \hat{a}^\dagger \sum_{k=0}^{\infty} \frac{(i\omega_d t)^k}{k!} (1 + \hat{a}^\dagger \hat{a})^k = \hat{a}^\dagger e^{i\omega_d (1 + \hat{a}^\dagger \hat{a}) t} \\
&= e^{i\omega_d t} \hat{a}^\dagger \hat{U}.
\end{aligned} \tag{5.19}$$

Similarly, one finds

$$\hat{U}\hat{a} = e^{-i\omega_d t} \hat{a} \hat{U}. \tag{5.20}$$

Putting these back into equation (5.18) yields the Hamiltonian presented in (5.2) (where $\omega_r - \omega_d$ has been replaced with Δ), which I repeat here for readability:

$$\hat{H} = \hbar \Delta \hat{a}^\dagger \hat{a} + \hbar \gamma \left(\hat{a}^\dagger + \hat{a} \right). \tag{5.21}$$

5.3 Lindblad master equation on Transmon

After having gotten aqcuainted with the Lindblad master equation on a harmonic oscillator it is time to use it on the system which we wish to study, namely the Transmon. We will

again try to find the steady state solution, except this time for the Transmon Hamiltonian from equation (3.49). This will be modified slightly, such that we ignore the constants as these do not affect the dynamics of the system. We will also add the driving term, finally yielding the system Hamiltonian

$$\hat{H}_{\mathcal{S}} = \left(\sqrt{8E_C E_J} - \frac{E_C}{2}\right)\hat{a}^\dagger\hat{a} - \frac{E_C}{2}\hat{a}^\dagger\hat{a}\hat{a}^\dagger\hat{a} + \hbar\gamma\left(\hat{a}^\dagger e^{-i\omega_d t} + \hat{a}^{i\omega_d t}\right), \tag{5.22}$$

which, after changing to a frame co-rotating with the drive becomes

$$\hat{H}_{\mathcal{S}} = \hbar\Delta\hat{a}^\dagger\hat{a} + \frac{E_C}{2}(\hat{a}^\dagger\hat{a} - \hat{a}^\dagger\hat{a}\hat{a}^\dagger\hat{a}) + \hbar\gamma(\hat{a}^\dagger + \hat{a}), \tag{5.23}$$

where $\hbar\Delta = (\sqrt{8E_C E_J} - E_C) - \hbar\omega_d = \hbar\omega_r - \hbar\omega_d$. We wish now to find an expression for $\langle\dot{\hat{a}}\rangle$. Terms proportional to $\hat{a}, \hat{a}^\dagger$ and $\hat{a}^\dagger\hat{a}$ have already been treated in Sec. 5.1, so we only need to treat the term $\hat{a}^\dagger\hat{a}\hat{a}^\dagger\hat{a}$:

$$\begin{aligned}
\mathrm{tr}\{-\frac{i}{\hbar}[\hat{a}^\dagger\hat{a}\hat{a}^\dagger\hat{a},\hat{\rho}]\hat{a}\} &= -\frac{i}{\hbar}\mathrm{tr}\{\hat{a}^\dagger\hat{a}\hat{a}^\dagger\hat{a}\hat{\rho}\hat{a} - \hat{\rho}\hat{a}^\dagger\hat{a}\hat{a}^\dagger\hat{a}\hat{a}\} \\
&= -\frac{i}{\hbar}\mathrm{tr}\{\hat{\rho}(\hat{a}\hat{a}^\dagger\hat{a}\hat{a}^\dagger\hat{a} - \hat{a}^\dagger\hat{a}\hat{a}^\dagger\hat{a}\hat{a})\} \\
&= -\frac{i}{\hbar}\mathrm{tr}\{\hat{\rho}(\hat{a}\hat{a}^\dagger\hat{a} + \hat{a}^\dagger\hat{a}\hat{a}\hat{a}^\dagger\hat{a} - \hat{a}^\dagger\hat{a}\hat{a}^\dagger\hat{a}\hat{a})\} \\
&= -\frac{i}{\hbar}\mathrm{tr}\{\hat{\rho}(\hat{a}\hat{a}^\dagger\hat{a} + \hat{a}^\dagger\hat{a}\hat{a} + \hat{a}^\dagger\hat{a}\hat{a}^\dagger\hat{a}\hat{a} - \hat{a}^\dagger\hat{a}\hat{a}^\dagger\hat{a}\hat{a})\} \\
&= -\frac{i}{\hbar}\mathrm{tr}\{\hat{\rho}(\hat{a} + 2\hat{a}^\dagger\hat{a}\hat{a})\} \\
&= -\frac{i}{\hbar}(\langle\hat{a}\rangle + 2\langle\hat{a}^\dagger\hat{a}\hat{a}\rangle).
\end{aligned} \tag{5.24}$$

With this, we now find by once again defining $\omega_C \equiv E_C/\hbar$

$$\frac{\mathrm{d}}{\mathrm{d}t}\langle\hat{a}\rangle = -i\Delta\langle\hat{a}\rangle + i\omega_C\langle\hat{a}^\dagger\hat{a}\hat{a}\rangle - i\gamma - \frac{\kappa}{2}\langle\hat{a}\rangle, \tag{5.25}$$

and by a similar calculation

$$\frac{\mathrm{d}}{\mathrm{d}t}\langle\hat{a}^\dagger\rangle = i\Delta\langle\hat{a}^\dagger\rangle - i\omega_C\langle\hat{a}^\dagger\hat{a}^\dagger\hat{a}\rangle + i\gamma - \frac{\kappa}{2}\langle\hat{a}^\dagger\rangle. \tag{5.26}$$

Trying to calculate a steady state for $\langle\hat{a}^\dagger\hat{a}\hat{a}\rangle$ and $\langle\hat{a}^\dagger\hat{a}^\dagger\hat{a}\rangle$ will yield terms of even higher order. One can see the similarity again with the input-output equation, as Eq. (5.25) is exactly what we get when taking the expectation value of Eq. (4.48), only that the drive term differs by a factor of i due to our gauge choice for the drive. In principle, one could again derive an expression for $\langle(\hat{a}^\dagger)^m\hat{a}^n\rangle$ using the master equation, but instead of taking this further we simply leave this here and move over to a system that will be of interest for gaining understanding of the Transmon resonator. This shows both that the two methods within the specific form of the Lindblad master equation we have chosen (Eq. (5.3)) are equivalent. The Lindblad master equation will later instead be used for

numerical simulations rather than have the same approach as the input-output method. More on this in the next chapter.

5.4 Driving the two-level system

Due to the large Kerr non-linearity ($E_C \gg \kappa$) the system is expected to behave similarly to a two-level system, especially when driven in a non-linear regime (i.e. for not too strong drive). It will therefore be useful to have insight in how the well studied two-level system behaves from the point of view that we are interested in. This section will use the Lindblad master equation to find analytical expressions for some quantities of interest, that will later be used to draw conclusions about the Transmon. In order to analyse the two-level system, we use the system Hamiltonian

$$\hat{H}_{\mathcal{S}} = \hbar\frac{\Delta}{2}\hat{\sigma}_z + \hbar\gamma(\hat{\sigma}^+ + \hat{\sigma}^-), \tag{5.27}$$

which is yielded by changing $\hat{a} \to \hat{\sigma}^-$ and $\hat{a}^\dagger \to \hat{\sigma}^+$ and moving to a frame co-rotating with the drive. The Lindblad Master equation considered is

$$\dot{\hat{\rho}} = -\frac{i}{\hbar}[\hat{H}_{\mathcal{S}}, \hat{\rho}] + \kappa\mathcal{D}[\hat{\sigma}^-]\hat{\rho}, \tag{5.28}$$

similar to equation (5.3). Useful relations in the calculations are

$$[\hat{\sigma}^+, \hat{\sigma}^-] = \hat{\sigma}_z \tag{5.29}$$

$$[\hat{\sigma}^+, \hat{\sigma}_z] = -2\hat{\sigma}^+ \tag{5.30}$$

$$[\hat{\sigma}^-, \hat{\sigma}_z] = 2\hat{\sigma}^- \tag{5.31}$$

$$\hat{\sigma}^+\hat{\sigma}^- = \frac{1+\hat{\sigma}_z}{2}. \tag{5.32}$$

Using all of these, we find

$$\begin{aligned}
\langle\dot{\hat{\sigma}_z}\rangle &= \mathrm{tr}\{\dot{\hat{\rho}}\hat{\sigma}_z\} \\
&= \mathrm{tr}\{-\frac{i}{\hbar}\hbar\frac{\Delta}{2}[\hat{\sigma}_z, \hat{\rho}]\hat{\sigma}_z - \frac{i}{\hbar}\hbar\gamma[\hat{\sigma}^+ + \hat{\sigma}^-, \hat{\rho}]\hat{\sigma}_z + \kappa\mathcal{D}[\hat{\sigma}^-]\hat{\rho})\\
&= -2i\gamma\mathrm{tr}\{\hat{\rho}\hat{\sigma}^+\} + 2i\gamma\mathrm{tr}\{\hat{\rho}\hat{\sigma}^-\} - 2\kappa\mathrm{tr}\{\hat{\rho}\hat{\sigma}^+\hat{\sigma}^-\} \\
&= -2i\gamma\langle\hat{\sigma}^+\rangle + 2i\gamma\langle\hat{\sigma}^-\rangle - 2\kappa\langle\hat{\sigma}^+\hat{\sigma}^-\rangle
\end{aligned} \tag{5.33}$$

as well as

$$\langle\dot{\hat{\sigma}^+}\rangle = -\left(\frac{\kappa}{2} - i\Delta\right)\langle\hat{\sigma}^+\rangle - i\gamma\langle\hat{\sigma}_z\rangle \tag{5.34}$$

$$\langle\dot{\hat{\sigma}^-}\rangle = -\left(\frac{\kappa}{2} + i\Delta\right)\langle\hat{\sigma}^-\rangle + i\gamma\langle\hat{\sigma}_z\rangle, \tag{5.35}$$

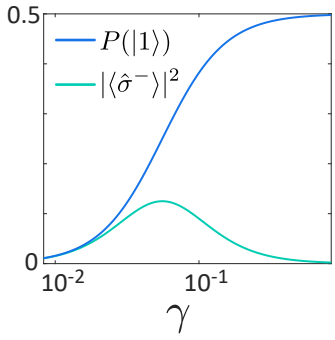

Figure 5.1: The population of the excited state $P(|1\rangle)$ (blue) and the coherent amplitude modulus squared $|\langle\hat{\sigma}^-\rangle|^2$ (turquoise) as functions of the coupling strength γ when driven on resonance ($\Delta = 0$). In the figures, $\kappa = 2\pi \cdot 0.025$ has been used. As one can clearly see, the population of the excited state $P(|1\rangle)$ converges to the expected value of $1/2$, and the coherent part increases similarly to $P(|1\rangle)$ for lower coupling strengths, while for higher coupling strengths it approaches 0.

which in steady state yields

$$\langle\hat{\sigma}^+\rangle = \frac{-i\gamma}{\kappa/2 - i\Delta}\langle\hat{\sigma}_z\rangle \tag{5.36}$$

$$\langle\hat{\sigma}^-\rangle = \frac{i\gamma}{\kappa/2 + i\Delta}\langle\hat{\sigma}_z\rangle \tag{5.37}$$

$$0 = -2i\gamma\langle\hat{\sigma}^+\rangle + 2i\gamma\langle\hat{\sigma}^-\rangle - 2\kappa\langle\hat{\sigma}^+\hat{\sigma}^-\rangle, \tag{5.38}$$

which, after inserting equations (5.36) and (5.37) into equation (5.38) yields, after some rearranging:

$$\langle\hat{\sigma}_z\rangle = -\frac{(\kappa/2)^2 + \Delta^2}{\gamma^2}\langle\hat{\sigma}^+\hat{\sigma}^-\rangle. \tag{5.39}$$

Using equation (5.32), this can be further simplified to

$$\langle\hat{\sigma}_z\rangle = -\frac{(\kappa/2)^2 + \Delta^2}{2\gamma^2 + (\kappa/2)^2 + \Delta^2}. \tag{5.40}$$

This is perhaps even better understood in terms of the probabilities that the ground and excited states are occupied. If we label the states $|0\rangle$ and $|1\rangle$, we have

$$P(|0\rangle) = \frac{\gamma^2 + (\kappa/2)^2 + \Delta^2}{2\gamma^2 + (\kappa/2)^2 + \Delta^2} \tag{5.41}$$

$$P(|1\rangle) = \frac{\gamma^2}{2\gamma^2 + (\kappa/2)^2 + \Delta^2}, \tag{5.42}$$

which you can get by using Eq. (5.32) on Eq. (5.40) as $\langle\hat{\sigma}^+\hat{\sigma}^-\rangle = P(|1\rangle)$ and $P(|0\rangle) + P(|1\rangle) = 1$.

From these equations we can see that if the drive is off ($\gamma = 0$), then the steady state of the system is in its ground state ($P(|0\rangle) = 1$), while in the limit of infinite drive ($\gamma \to \infty$)

we have $P(|0\rangle) = P(|1\rangle) = 1/2$, which is what we expect from a two-level system (it is assumed that κ is finite and non-zero, and Δ is also finite). These cases can already be seen from equation (5.40) (as the trace of the density function only has one degree of freedom), but the population distribution is more directly clear in terms of these probabilities. One thing to note here is that when doing heterodyne measurements it is the coherent response that is measured, which means that the output power will be proportional to $|\langle\hat{\sigma}^-\rangle|^2$ and not $\langle\hat{\sigma}_z\rangle$. From equation (5.37) we see that if the system is driven strongly, such that $\langle\hat{\sigma}_z\rangle$ is close to 0, then the measured signal will also approach 0. Note that the prefactor in equation (5.37) scales linearly with γ, and $\langle\hat{\sigma}_z\rangle$ scales (for large γ) like $1/\gamma^2$, so $\langle\hat{\sigma}_z\rangle$ does indeed approach 0 faster than the prefactor. These results can be seen in Fig. 5.1, which plots Eq. (5.37) modulus squared and Eq. (5.42) as functions of γ for $\Delta = 0$ and $\kappa = 2\pi \cdot 0.025$, showing quantitatively what has been qualitatively discussed here.

Chapter 6

Single Tone Measurements

Ohhh, look at me, I looked up a quote!
- Randall Munroe (xkcd.com)

In this section, I will present what results the different approaches yield for the response of the system. Firstly, the methods for determining the output from the system will be explained briefly. One of the methods utilises the Quantum Toolbox in Python (QuTiP), a toolbox containing functions that simulate quantum systems. The other method uses an input-output approach. Then the results from the two approaches will be compared with each other as well as the experimental results obtained previously in Ref. 1. I will also compare the results to the two-level system as this provides some insight in the observed effects. After this the coherence of the transmitted signal will be further discussed, which will serve as a motivation for investigating the emission spectrum of the system. This will initially be done for a two-level system, again in order to gain understanding for the Transmon resonator. The spectrum analysis of the two-level system will show that when the system is driven strongly, photons are emitted at three different frequencies. This feature is known as the Mollow triplet, after the theoretical discovery of this by B. R. Mollow in 1969 [45]. The emission spectrum will then be numerically determined using QuTiP.

6.1 Method

The general approach will be to find $\langle \hat{a} \rangle$, which is motivated by the use of heterodyne detection in the original experiments. This will be used to extract other important quantities, such as the coherent output power $P_{out,coh}$ (discussed in Sec. 4.5) from the right port of Fig. 4.2

$$P_{out,coh} = \hbar\omega |\langle \hat{c}_{out} \rangle|^2 = \hbar\omega\kappa_c |\langle \hat{a} \rangle|^2, \tag{6.1}$$

as well as the transmission amplitude

$$t \equiv \frac{\langle \hat{c}_{out} \rangle}{\langle \hat{b}_{in} \rangle} = \frac{\sqrt{\kappa_c}\langle \hat{a} \rangle}{\langle \hat{b}_{in} \rangle}, \tag{6.2}$$

where $\hat{b}_{in}$ is, as before, the input RF signal from the left port of Fig. 4.2. In the single tone measurements, we will consider an RF signal generated with an amplitude at a single frequency. This signal will be referred to as a "probe", indicating that it probes the system response. It is the probe signal that is presented in the figures, unless stated otherwise. In Chapter 7, another signal will be added on top of the probe. This will be referred to as the "drive", as it drives the system to a certain state, which is then probed via the probe RF signal. The drive and the probe will in general have different amplitudes and frequencies. This will be further explained in the two-tone measurements section (Chapter 7). One final remark is that in for instance Eq. (5.2), what is now referred to as probe was then referred to as drive. This made sense at the time, since from the perspective of the system the external RF source drives the internal system dynamics. It was not at this stage important to make a distinction in what the input was called, but now a distinction will help with clarity when it comes to the two-tone measurements. For now we are satisfied with considering only the probe which allows us to write $\langle \hat{b}_{in} \rangle$ as

$$\langle \hat{b}_{in} \rangle = \sqrt{\dot{N}} e^{-i\omega_p t}, \tag{6.3}$$

where $\dot{N}$ is the rate of incoming photons from the probe and ω_p is the probe signal frequency. From this we get the important quantity $P_p = \hbar\omega_p \langle \hat{b}_{in}^\dagger \hat{b}_{in} \rangle$, i.e. input power of the probe signal. This will be of relevance when analysing the results. Results will often be presented using the frequency f_p instead of the angular frequency ω_p, and they are as usual related via $\omega_p = 2\pi f_p$.

In order to be able to compare the theoretical results with experiments, the parameters will be chosen such that they match the values of the measured device, namely

$$\begin{cases} \omega_r/2\pi & = 4.715\,\text{GHz} \\ E_C/h & = 290\,\text{MHz} \\ \kappa_L = \kappa_R = \kappa_c & = 2\pi \cdot 11\,\text{MHz} \\ \kappa_i & = 2\pi \cdot 3\,\text{MHz}. \end{cases} \tag{6.4}$$

These can be obtained by fitting a function to the experimental data. For instance in the case of measuring the transmission, the (Lorentzian) function

$$T = |\tilde{t}|^2 = \frac{\kappa_c^2}{(\omega - \omega_r)^2 + \left(\frac{\kappa}{2}\right)^2}, \tag{6.5}$$

where $\tilde{t}$ is from Eq. (4.42) and $\kappa_L = \kappa_R = \kappa_c$ is assumed, can be fitted to the data yielding

κ_c, κ_i and ω_r. This will look essentially as the turquoise line in Fig. 6.1h, but will only work with this system for a very weak probe while the system is still in the linear regime.

As discussed previously in Sec. 3.4, the anharmonicity of the Transmon is determined by the charging energy E_C. This means that also E_C can be determined from measurements, which is most easily done in two-tone measurements where the drive power is changed and the system is weakly probed. More specifically, the separation in the two resonance peaks (a second will appear at sufficiently strong drive on resonance corresponding to the $|1\rangle \leftrightarrow |2\rangle$-transition) will be such that $h\Delta f = E_C$. Alternatively, as we will see later in this section, one can find E_C in a P_p - f_p plot (Fig. 6.1a-c), and the reason for this will become clear when the data is presented.

With this, we are now ready to move on to explaining how the response is calculated numerically in practice.

6.1.1 Lindblad master equation using QuTiP

As previously mentioned, QuTiP is a powerful tool when simulating quantum processes. It can numerically find a steady state solution to the density matrix $\hat{\rho}$ of the system using the Lindblad master equation. For our system the master equation is as previously mentioned of the form Eq. 5.3, where $\kappa = 2\kappa_c + \kappa_i$ and $\hat{H} \to \hat{H}_{\mathcal{S}}$, where $\hat{H}_{\mathcal{S}}$ is the system Hamiltonian in the rotating frame of the probe (Eq. (5.23)), where $\gamma = \sqrt{\kappa_c \dot{N}}$. I repeat them here for readability:

$$\dot{\hat{\rho}} = -\frac{i}{\hbar}[\hat{H}_{\mathcal{S}}, \hat{\rho}] + \kappa \mathcal{D}[\hat{a}]\hat{\rho} \tag{6.6}$$

$$\hat{H}_{\mathcal{S}} = \hbar\Delta\hat{a}^\dagger\hat{a} + \frac{E_C}{2}(\hat{a}^\dagger\hat{a} - \hat{a}^\dagger\hat{a}\hat{a}^\dagger\hat{a}) + \hbar\gamma(\hat{a}^\dagger + \hat{a}). \tag{6.7}$$

Another parameter that has to be chosen in the numerical simulations is where to truncate the Hilbert space. Due to the strong non-linearity of the system, it is only the first few states that have a relevant impact on the system dynamics. The Hilbert space was truncated such that it only contains $\{|0\rangle, \ldots, |5\rangle\}$, i.e the ground state up to the 5th excited state. Another way of phrasing this is that the dimension N of the Hilbert space was chosen such that $N = 6$.

The steady state solution of $\hat{\rho}$ was then found for each probe power P_p and detuning $\Delta = \omega_r - \omega_p$, where $P_p = \hbar\omega_p\dot{N}$, from which the steady state amplitude of $\langle\hat{a}\rangle = \mathrm{tr}\{\hat{\rho}\hat{a}\}$ can easily be extracted and used to determine $P_{out,coh}$ and t by using Eqs. (6.1),(6.2) respectively.

6.1.2 Input-output theory

Now we also want to find the transmitted signal entirely within the input-output theory. The method for this was introduced in Sec. 4.4, and we will utilise the EoM for operators that we got from the input-output formalism. First we want to have the expression for $(\hat{a}^\dagger)^m\hat{a}^n$ (Eq. (4.58)) in a more manageable form, which we achieve by moving to a frame

rotating with the probe and then taking the expectation value. With the unitary operator

$$\hat{U}(t) = e^{i\omega_p \hat{a}^\dagger \hat{a} t}, \tag{6.8}$$

we find, using the results from Sec. 5.2, that

$$\hat{U}(t)(\hat{a}^\dagger)^m \hat{a}^n \hat{U}^\dagger(t) = (\hat{a}^\dagger)^m \hat{a}^n e^{i(m-n)\omega_p t}. \tag{6.9}$$

Performing this transformation on Eq. (4.58) and dividing by $e^{i(m-n)\omega_p t}$ yields the result

$$\begin{aligned}\frac{\mathrm{d}}{\mathrm{d}t}(\hat{a}^\dagger)^m \hat{a}^n = &\Big(i(m-n)(\omega_r - \omega_p) - i\frac{(m-n)(m+n-1)}{2}\omega_C - \frac{m+n}{2}\kappa\Big)(\hat{a}^\dagger)^m \hat{a}^n \\ &- i(m-n)\omega_C (\hat{a}^\dagger)^{m+1}\hat{a}^{n+1} - n\sqrt{\kappa_c}(\hat{a}^\dagger)^m \hat{a}^{n-1}\hat{b}_{in}(t)e^{i\omega_p t} \\ &- m\sqrt{\kappa_c}\hat{b}_{in}^\dagger(t)(\hat{a}^\dagger)^{m-1}\hat{a}^n e^{-i\omega_p t}.\end{aligned} \tag{6.10}$$

Taking the expectation value of this, and defining

$$A_{m,n} \equiv \langle (\hat{a}^\dagger)^m \hat{a}^n \rangle, \tag{6.11}$$

we can rewrite this as

$$\begin{aligned}\frac{\mathrm{d}}{\mathrm{d}t}A_{m,n} = &\Big(i(m-n)(\omega_r - \omega_p) - i\frac{(m-n)(m+n-1)}{2}\omega_C - \frac{m+n}{2}\kappa\Big)A_{m,n} \\ &- i(m-n)\omega_C A_{m+1,n+1} - n\sqrt{\kappa_c \dot{N}}A_{m,n-1} - m\sqrt{\kappa_c \dot{N}}A_{m-1,n},\end{aligned} \tag{6.12}$$

where Eq. (6.3) has been inserted into the relation after using

$$\langle \hat{b}_{in}^\dagger(t)(\hat{a}^\dagger)^{m-1}\hat{a}^n \rangle = \langle \hat{b}_{in}^\dagger(t)\rangle \langle (\hat{a}^\dagger)^{m-1}\hat{a}^n \rangle, \tag{6.13}$$

and

$$\langle (\hat{a}^\dagger)^m \hat{a}^{n-1}\hat{b}_{in}(t)\rangle = \langle (\hat{a}^\dagger)^m \hat{a}^{n-1}\rangle \langle \hat{b}_{in}(t)\rangle. \tag{6.14}$$

The justification for this is the use of a coherent drive, which is the most classical drive so the quantum correlations arise mostly from thermal and vacuum fluctuations and these are assumed to be negligible. Now we have gotten rid of the time dependence from the drive and can find a steady state solution, yielding the equation for $A_{m,n}$ as

$$A_{m,n} = \frac{i(m-n)\omega_C A_{m+1,n+1} + n\sqrt{\kappa_c \dot{N}}A_{m,n-1} + m\sqrt{\kappa_c \dot{N}}A_{m-1,n}}{i(m-n)(\omega_r - \omega_p) - i\frac{(m-n)(m+n-1)}{2}\omega_C - \frac{m+n}{2}\kappa}, \tag{6.15}$$

which allows us to define a vector $\vec{A} = \begin{pmatrix} A_{0,1} & A_{0,2} & \dots & A_{1,0} & \dots & A_{m,n}\end{pmatrix}^T$, such that we can write our recursive relation as a matrix equation

$$\vec{A} = M\vec{A} + C, \tag{6.16}$$

where C is yielded by the special cases arising from the EoM of $\hat{a}$ and $\hat{a}^\dagger$ where we have

$$A_{0,1} = \frac{1}{-i(\omega_r - \omega_p) - \kappa/2}\left(-i\omega_C A_{1,2} + \sqrt{\kappa_c \dot{N}}\right) \tag{6.17}$$

$$A_{1,0} = \frac{1}{i(\omega_r - \omega_p) - \kappa/2}\left(i\omega_C A_{2,1} + \sqrt{\kappa_c \dot{N}}\right). \tag{6.18}$$

Now it only remains to solve for $\vec{A}$ and extract $\langle \hat{a} \rangle = A_{0,1}$, from which we again can get our quantities $P_{out,coh}$ and t.

6.2 Theory and experiment

The result from the two theoretical approaches are represented in Fig. 6.1 together with the experimental result. In Figs. 6.1a-c, you can see the transmitted coherent power $P_{out,coh}$ on a log-scale as a function of the probe frequency f_p and power P_p. The two theoretical methods yield virtually identical results within the numerical accuracy in the calculated range. The theory and experiment show excellent agreement within the measurement accuracy, even capturing areas where the transmission is suppressed. This suppression is caused by the loss of coherence, similarly to the case of the two-level system when this was discussed in Sec. 5.4. This will be discussed more in depth in Sec. 6.3. At the points indicated by coloured arrows in Fig. 6.1b, there are different absorption processes behind the visible features, distinct in the number of photons involved in the excitation process. These multi-photon processes are illustrated in Fig. 6.1d, where the the energy of a photon $E = \hbar\omega_p$ is represented by the length of an arrow. The single photon process excites the system from its ground state to its first excited state ($|0\rangle \rightarrow |1\rangle$), indicated by the purple arrow. Since the next resonance mode has a lower frequency, the photon has too much energy to be able to excite the system further. At lower frequency however, two photons with lower energy can match the energy difference between the ground state and the second excited state (blue arrows), thereby driving the transition $|0\rangle \leftrightarrow |2\rangle$. This process however requires a stronger input field, as the probability for a multi-photon interaction decreases each time another photon is involved in the process. It is thereby only noticeable when there are a lot of photons available, i.e when the drive is strong. Previous studies of systems with similar level structure have shown these features as well, see e.g. Ref. 46.

The data presented in Figs. 6.1e-g is the same as Figs. 6.1a-c, only presented in terms of the transmission coefficient $|t|^2$ instead of the output power. Once again, the agreement is good, both between experiment and theory, as well as between the two methods used for the theoretical predictions. All of these figures clearly show a constant transmission at very low powers ($-140\,\mathrm{dBm}$). This is in the linear response regime where we expect that the transmission behaves as for a linear resonator. At higher powers, already at $-130\,\mathrm{dBm}$ but more clearly at $-120\,\mathrm{dBm}$ the transmission shows saturation. This means that the transmission decreases due to the fact that the system is now more probable to be in an excited state when a photon tries to enter the resonator due to the stronger probe

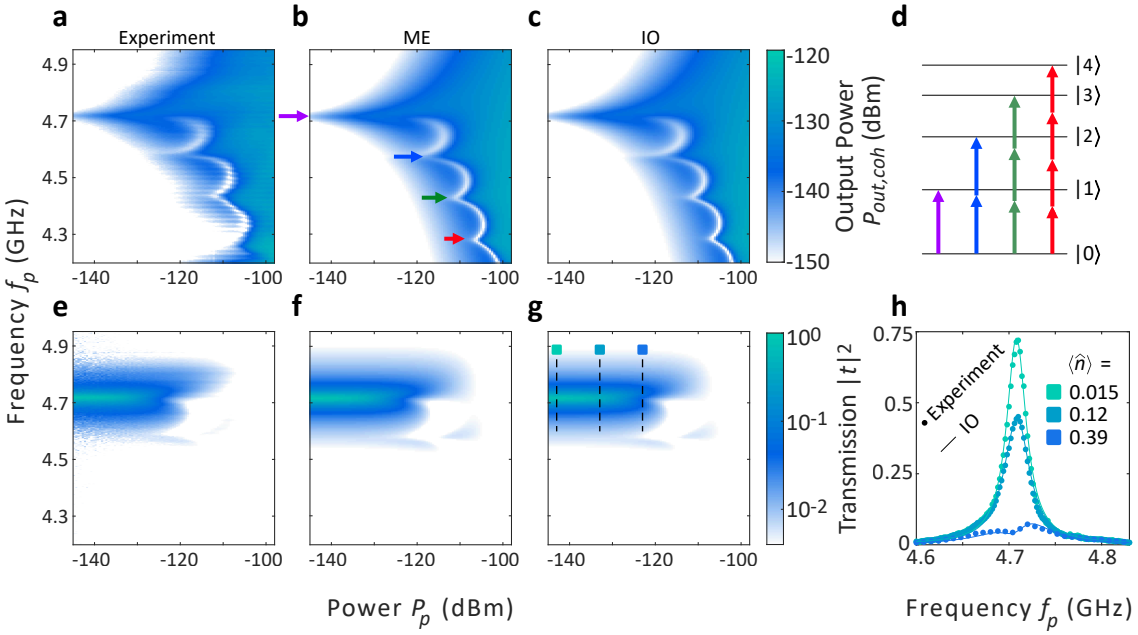

Figure 6.1: **a-c,** The power of the coherent transmitted signal $P_{out,coh}$ as a function of the frequency f_p and power P_p of the probe. Panel **a** shows the experimental data while **b** and **c** show the master equation and input-output theory approaches respectively. The coloured arrows in panel **b** indicate where different types of processes occur. The violet arrow indicates a one-photon process, while blue, green and red indicate 2-, 3- and 4-photon processes respectively, schematically represented in panel **d**. **e-g,** The same data as in **a-c**, but represented in terms of the transmission coefficient $|t|^2$. Panel **e** show experimental data, panel **f** the master equation approach and panel **g** the input-output approach. **h,** Transmission coefficient as a function of probe frequency f_p at probe powers $P_p = -143, -133, -123$ dBm, indicated by dashed lines in panel **g**. The dots are from experimental data and the lines are obtained using the input-output approach. The values for $\langle\hat{n}\rangle = \langle\hat{a}^\dagger\hat{a}\rangle$ are determined theoretically when the system is driven at the resonance frequency.

signal. This is because of the shift in resonance frequency due to the Kerr non-linearity, which in turn prohibits the photon from entering as there is a mismatch in energy for an available transition. Figure 6.1h shows three line-cuts indicated in Fig. 6.1g, where the transmission coefficient is shown as a function of frequency at the three different probe powers $P_p = -143$ (turquoise), -133 (light blue), and -123 dBm (blue). The dots indicate experimental data, while the solid lines are determined theoretically using the input-output approach. The turquoise line-cut is still approximately in the linear regime, and as indicated in the figure, $\langle\hat{n}\rangle = \langle\hat{a}^\dagger\hat{a}\rangle = 0.015$, determined theoretically. Here the agreement with experiment and theory is very good, especially close to the resonance frequency. At the tails, the agreement is slightly worse, but barely visible in the image. At 10 times higher power, saturation is already visible. This is indicated both by the decrease in transmission and that $\langle\hat{n}\rangle$ is slightly less than 10 times the lower power case. Finally at 10 times higher power again (-123 dBm), the transmission is close to 0, meaning that only a very small fraction of the input power is transmitted through the resonator. The saturation of $\langle\hat{n}\rangle$ is also clearer than before, as the increase is now less than a factor of 4. You can also see the loss of coherence on top of the saturation, as there is a valley on the resonance frequency. All of these features are reminiscent of the two-level system,

where similar effects can be concluded from Fig. 5.1.

6.3 Transmission and output power

The coherence of the transmitted photons has been discussed briefly in different places so far (e.g. in Secs. 5.4,6.2). It has mostly just been mentioned that the loss of coherence is a non-linear effect visible especially in a two-level system but also in the Transmon. (Another example of a non-linear system where the loss of coherence is observed is for instance a system where a Transmon qubit is coupled to a CPW, where the system Hamiltonian can be mapped to a typical James-Cummings Hamiltonian giving anharmonic energy levels, see e.g. Ref. 46.) As previously mentioned briefly at the end of Sec. 5.1, for an ideal harmonic oscillator, $\langle \hat{a}^\dagger \hat{a} \rangle = \langle \hat{a}^\dagger \rangle \langle \hat{a} \rangle$ $(= |\langle \hat{a} \rangle|^2)$, which means that all transmitted light is coherent. We have already seen in Sec. 5.4 that this is not the case for a two-level system, where instead if the system was driven strongly enough, all coherence could be lost. This section will go into slightly more detail about the coherence, or rather incoherence, and try to quantify it in the system. For this I define the two quantities

$$\alpha_{inc} \equiv \frac{P_{out,inc}}{P_{out,tot}} = 1 - \frac{|\langle \hat{a} \rangle|^2}{\langle \hat{a}^\dagger \hat{a} \rangle} \tag{6.19}$$

and

$$\beta_{inc} \equiv \frac{P_{out,inc}}{P_p} = \frac{\hbar \omega_p \kappa_c \langle \hat{a}^\dagger \hat{a} \rangle \alpha_{inc}}{P_p}, \tag{6.20}$$

where $P_{out,tot} = \hbar \omega_p \kappa_c \langle \hat{a}^\dagger \hat{a} \rangle$ is the total transmitted output power (as in Eq. (4.45) with $\kappa_R = \kappa_c$) and $P_{out,inc} = P_{out,tot} - P_{out,coh}$ (with $P_{out,coh}$ as defined in Eq. (6.1)) is the incoherent transmitted output power. So α_{inc} is the fraction of the emitted photons that are incoherent and β_{inc} is the fraction of the incoming power that is turned into transmitted incoherent power. This analysis will be made mostly from the theoretical data, since we do not have access to $\langle \hat{a}^\dagger \hat{a} \rangle$ from the experimental data. This is as we did not measure the full signal in the experiments since we did not anticipate a large contribution from the incoherent response. In this section, we aim to quantify the strength of this contribution and make sure that we have accounted for all the output signals of the system.

Using Figs. 6.1a,b as a starting point, Fig. 6.2a shows a line-cut of these figures at $f_p = 4.716\,\text{GHz}$, shown in turquoise where the solid line is the theoretical prediction while the dots are from the experimental data. Furthermore, the figure also has the total output power (blue) from the resonator, determined theoretically by $P_{out,tot} = \hbar \omega_p \kappa_c \langle \hat{a}^\dagger \hat{a} \rangle$. A dashed line indicating when $\langle \hat{n} \rangle = \langle \hat{a}^\dagger \hat{a} \rangle = 0.5$ is indicated to show the saturation point for a two-level system. The theory predicts the coherent transmitted power very well, especially for low powers. while the agreement falls off slightly at higher powers. Note that both the x-axis and the y-axis are on a logarithmic scale so at $P_p = -118\,\text{dBm}$, the total output power is almost 10 times larger than the coherent output power. This is better reflected in Fig. 6.2b, which shows α_{inc} as a function of probe power P_p and frequency

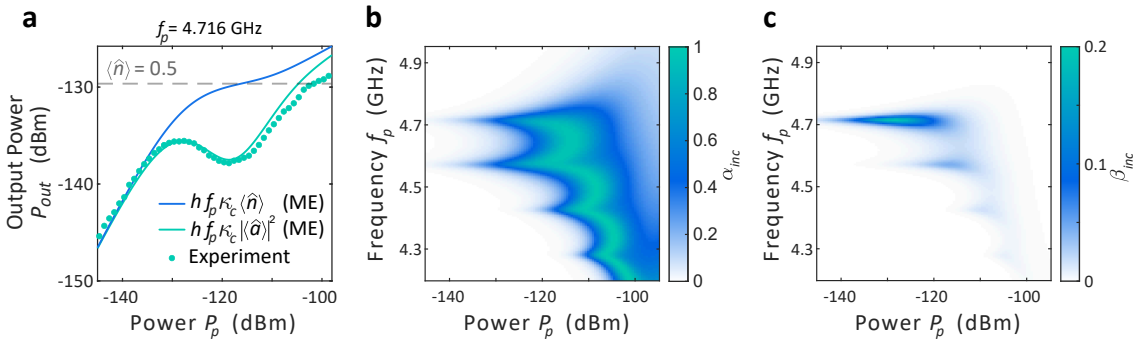

Figure 6.2: **a,** Output power P_{out} as function of probe power P_p, where both all the output power is shown (blue) as well as the coherent output power (turquoise). The solid lines are theoretical predictions using the master equation approach. The dots are the experimental data, which matches the coherent output power prediction over a large range of probe powers. The dashed line indicates the crossing for $\langle\hat{n}\rangle = 0.5$, which is where the two-level system would be saturated. **b,** The defined quantity α_{inc} as a function of probe power P_p and frequency f_p, showing that at certain powers, almost all of the coherence in the system is lost. Note here that the z-axis is linear in contrast to the logarithmic scale used in for instance Fig. 6.1b. **c,** The defined quantity β_{inc} as a function of probe power P_p and frequency f_p. Here you can see the fraction of the probe power P_p that is turned into transmitted incoherent power. It is largest when driving on resonance, reaching close to a fifth of the input power at $P_p = -128\,dBm$.

f_p. Here one can see that for a sizeable region of the two-dimensional parameter space explored, the system emits more than 80 % of the transmitted photons incoherently. The coherence is however starting to be regained when driving the system strongly enough, unlike the case of the two-level system. The extra levels available must therefore play a crucial role in this process. A partial but not fully satisfactory explanation is that multi-photon processes start to give rise to a coherent response again. In Fig. 6.1b for instance, by the blue arrow where 2-photon processes start to occur, you see a similar broadening in frequency as the power is increased, as for the single photon process by the violet arrow. The question then arises about the 'arcs', especially for the base resonance frequency, where the loss of coherence is less at frequencies just above resonance than below. The next section will help to provide some insights into what happens with the photons that lose their coherence, but some of the questions that have arisen will unfortunately not be fully explained.

Moving on to Fig. 6.2c where β_{inc} is shown as a function of probe power P_p and frequency f_p, we see that the arcs are no longer as visible. This is natural, since the arcs in α_{inc} are present off resonance where the probability for excitation is lower as we are further away from resonance. This decrease in probability does not affect α_{inc} but it does affect β_{inc} as this scales with $1/P_p$ and is thus not just dependent on internal dynamics. Another way of putting it is that the detuning Δ affects $P_{out,inc}$ and $P_{out,tot}$ in the same way, cancelling this effect for α_{inc}, while it does not affect P_p, so the detuning causes a smaller amplitude off resonance for β_{inc}. This is naturally what we would expect, as when we are off resonance, most of the power is reflected and thus does not enter the system. β_{inc} reaches its max

value of almost 0.2 on resonance at about $P_p = -128\,\mathrm{dBm}$, a rather high value. You can see that some coherence is lost even at very small powers, but when the power is increased, both saturation effects and reduction in lost coherence results in β_{inc} approaching 0 rather quickly as compared to α_{inc}. β_{inc} is also slightly larger again early on, close to resonance for the multi-photon processes. As seen from α_{inc} the loss of coherence is large within the system when these processes start to occur. In order to gain insight in the question of what happens to the emitted photons whose coherence is lost, the next section will investigate the power spectrum of the emitted photons from system.

Before moving on to what happens to the emitted incoherent photons, an answer to the question of what happens to the reflected signal and what is lost to the environment would be appropriate, to make sure that for instance energy conservation holds for what we have so far considered. Before that, recall that the total reflected output power is

$$P_r = \hbar\omega\langle\hat{b}_{out}^\dagger\hat{b}_{out}\rangle, \tag{6.21}$$

where we now consider the steady state. As the coherent probe is considered only at one frequency ω_p for the input power P_p, we will for now make the assumption when determining the output power also only carries the same frequency, setting $\omega = \omega_p$. The observant reader notices that this assumption was already made in the definition of β_{inc}. By similar arguments as before, the coherent reflected power $P_{r,coh}$ is given by

$$P_{r,coh} = \hbar\omega_p|\langle\hat{b}_{out}\rangle|^2 = \hbar\omega_p|\langle\hat{b}_{in} + \sqrt{\kappa_c}\hat{a}\rangle|^2. \tag{6.22}$$

Since the drive is coherent, we can let $\langle\hat{b}_{in}\rangle = \sqrt{\dot{N}_p}$, note that with this we implicitly assume that we are in a frame rotating with the drive. To get the incoherent reflected power $P_{r,inc}$ we use

$$\begin{aligned} P_{r,inc} &= P_r - P_{r,coh} = \hbar\omega_p\Big(\langle\hat{b}_{out}^\dagger\hat{b}_{out}\rangle - |\langle\hat{b}_{in} + \sqrt{\kappa_c}\hat{a}\rangle|^2\Big) \\ &= \hbar\omega_p\Big(\langle\hat{b}_{in}^\dagger\hat{b}_{in}\rangle + \sqrt{\kappa_c}\Big(\langle\hat{b}_{in}^\dagger\hat{a}\rangle + \langle\hat{a}^\dagger\hat{b}_{in}\rangle\Big) + \kappa_c\langle\hat{a}^\dagger\hat{a}\rangle \\ &\qquad - \Big(|\langle\hat{b}_{in}\rangle|^2 + 2\sqrt{\kappa_c}\,\mathrm{Re}\{\langle\hat{b}_{in}\rangle\langle\hat{a}\rangle\} + \kappa_c|\hat{a}|^2\Big)\Big) \\ &= \hbar\omega_p\kappa_c\Big(\langle\hat{a}^\dagger\hat{a}\rangle - |\langle\hat{a}\rangle|^2\Big), \end{aligned} \tag{6.23}$$

where $\langle\hat{b}_{in}^\dagger\hat{b}_{in}\rangle = |\langle\hat{b}_{in}\rangle|^2$ and $\langle\hat{b}_{in}^\dagger\hat{a}\rangle + \langle\hat{a}^\dagger\hat{b}_{in}\rangle = \sqrt{\dot{N}_p}\langle\hat{a} + \hat{a}^\dagger\rangle$ has been used (see Ref. 39) since $\hat{b}_{in}$ is assumed coherent. If we divide $P_{r,inc}$ by P_p, we see that we have nothing else than β_{inc}, meaning that the transmitted incoherent signal is equal to the reflected incoherent signal. This is what we expect since any interference between the coherent and incoherent photons should be averaged out. To consider the power lost via the resonator

internal losses to the environment P_i, we take similarly as for the transmission

$$P_i = \hbar\omega_p\kappa_i\langle\hat{a}^\dagger\hat{a}\rangle, \tag{6.24}$$

where the difference between the transmitted power and P_i is interchanging $\kappa_c \leftrightarrow \kappa_i$. Energy conservation means that

$$P_p = \hbar\omega_p\langle\hat{b}^\dagger_{out}\hat{b}_{out}\rangle + \hbar\omega_p\langle\hat{c}^\dagger_{out}\hat{c}_{out}\rangle + P_i, \tag{6.25}$$

i.e. that the input power ends up as either one of the output modes $(\hat{b}_{out}, \hat{c}_{out})$ or is dissipated in the system. By substituting $\hat{b}_{out}$ and $\hat{c}_{out}$ with Eqs. (4.25),(4.39) as well carrying out calculations similar to Eq. (6.23) yields the relation

$$\kappa\langle\hat{a}^\dagger\hat{a}\rangle + 2\sqrt{\kappa_c\dot{N}}\ \mathrm{Re}\{\langle\hat{a}\rangle\} = 0, \tag{6.26}$$

where again $\kappa = 2\kappa_c + \kappa_i$. We recognise this as the steady state solution of Eq. (5.7). This shows the consistency with our assumptions. In the numerical calculations this relation holds true with error $< 1\,\%$ in units of $\kappa\langle\hat{a}^\dagger\hat{a}\rangle$. Since the incoherent output power was calculated by subtracting the coherent contribution out from the total output signal, this energy conservation consideration checks that the total output powers to different ports and losses obey energy conservation. It does not test energy conservation between the coherent and incoherent parts. Note that this relation assumes that $\hat{b}_{in}$ is coherent and does not take into account for instance white noise or quantum noise from the input, in which case the correlations would be different [39].

Now going back to the question of only considering the frequency ω_p for all the outgoing photons. This turns out to be a very bold assumption. As we will see next, photons are emitted at other frequencies than ω_p at strong drive. They are however emitted with equal amplitude, and for instance in the case of driving on resonance, they are emitted symmetrically (in frequency) around the resonance frequency, thereby the emitted energy from the photons of different frequencies averages out to the energy of considering photons with just the probe frequency. Therefore the assumption is formally incorrect but the end result in considering steady state averages still holds as the average energy of the output photons is equal to $\hbar\omega_p$. As this is only shown for driving on resonance in the next section (Sec. 6.4), the validity of the equations when this assumption is made for the incoherent output would need to be established for when ω_p is off-resonance. As mentioned, the relation of Eq. (6.26) had a very small error over the entire range considered in Figs. 6.1b,c which suggests that this simplification is a good approximation and this is more to motivate further in depth studies of the validity of the relations. They might

6.4 Power spectrum of emitted photons

As already mentioned briefly in the introduction to this section, we will again build some of our understanding on the foundation of processes occurring in the two-level system. The Mollow triplet will be introduced, as well as some parts of how the spectrum is derived. After this, the spectrum of the Transmon will briefly be analysed numerically. The general method for finding the power spectrum of the emitted photons will be to look at the two-time correlation function $\langle \hat{a}^\dagger(t')\hat{a}(t)\rangle$. We will make the constraint to only consider the case when the system is driven on resonance, and to make calculations simpler we have changed to a frame rotating with the drive frequency. Furthermore the initial condition for the time evolution will be from the steady state, in which case it suffices to look at $\langle \hat{a}^\dagger(\tau)\hat{a}(0)\rangle$ (or $\langle \hat{a}^\dagger(0)\hat{a}(\tau)\rangle$). This is Fourier transformed to give the spectrum.

6.4.1 Two-level system

This section will contain some highlights from Ref. 45, although translated from the atom-light system picture into the cQED Transmon device, to gain some insight in how the Mollow triplet is derived. In order to find the power spectrum of the two-level system, the time evolution of the system will be important. This was derived in Sec. 5.4, and the expressions Eqs. (5.33),(5.34),(5.35) will be handy. Let us first define $\alpha \equiv \langle \hat{a}\rangle$, $\bar{e} \equiv \langle \hat{\sigma}^+\hat{\sigma}^-\rangle$ and $\bar{g} \equiv \langle \hat{\sigma}^-\hat{\sigma}^+\rangle$ which allows us to write the equations slightly simpler. With this definition $\bar{e}$ and $\bar{g}$ become the expectation value for the two-level system to be in the excited state and ground state respectively. Note now that instead of $\langle \hat{\sigma}_z\rangle$ we separate the EoM of the ground state $|0\rangle = |g\rangle$ and the excited state $|1\rangle = |e\rangle$ even though they are coupled. The reason for this becomes apparent later. Now we have the equations as

$$\frac{\mathrm{d}}{\mathrm{d}t}\bar{e} = -i\gamma\alpha^* + i\gamma\alpha - \kappa\bar{e} \tag{6.27}$$

$$\frac{\mathrm{d}}{\mathrm{d}t}\alpha = -\left(\frac{\kappa}{2} + i\Delta\right)\alpha + i\gamma(\bar{e} - \bar{g}) \tag{6.28}$$

$$\frac{\mathrm{d}}{\mathrm{d}t}\alpha^* = -\left(\frac{\kappa}{2} - i\Delta\right)\alpha^* - i\gamma(\bar{e} - \bar{g}) \tag{6.29}$$

$$\frac{\mathrm{d}}{\mathrm{d}t}\bar{g} = -\frac{\mathrm{d}}{\mathrm{d}t}\bar{e}. \tag{6.30}$$

Writing the solution for $\alpha(t+\tau)$ in a very general way, we can say that if we know the solution of all functions $\bar{e}, \bar{g}, \alpha$ and α^* at time t, then $\alpha(t+\tau)$ is just a linear combination of these and some time evolution functions that depend on t and τ:

$$\alpha(t+\tau) = h_{\alpha,\alpha}(\tau,t)\alpha(t) + h_{\alpha,\bar{e}}(\tau,t)\bar{e}(t) + h_{\alpha,\alpha^*}(\tau,t)\alpha^*(t) + h_{\alpha,\bar{g}}(\tau,t)\bar{g}(t). \tag{6.31}$$

Recall that when looking at $\hat{\rho}$ in our master equations, we have been looking at $\hat{\rho} = \mathrm{tr}_E\{\hat{\rho}_{tot}\} = \mathrm{tr}_E\{\hat{\rho}\otimes\hat{\rho}_E\}$, i.e. we have traced out the environment. With this in mind, we can see that if we use the full density matrix the expectation value of the two-time

correlation function is determined formally by

$$\langle \hat{a}^\dagger(0)\hat{a}(\tau)\rangle = \mathrm{tr}\{\hat{\rho}_{tot}(0)\hat{a}^\dagger \hat{U}^\dagger(\tau,0)\hat{a}\hat{U}(\tau,0)\}, \tag{6.32}$$

which can be compared to

$$\alpha(\tau) = \mathrm{tr}\{\hat{\rho}_{tot}(0)\hat{U}^\dagger(\tau,0)\hat{a}\hat{U}(\tau,0)\}, \tag{6.33}$$

where we can see that from $\alpha(\tau)$ we can go to $\langle \hat{a}^\dagger(0)\hat{a}(\tau)\rangle$ by making the substitution $\hat{\rho_{tot}}(0) \to \hat{\rho}_{tot}(0)\hat{a}^\dagger$. Making this substitution in Eq. (6.31) we then find

$$\langle \hat{a}^\dagger(0)\hat{a}(\tau)\rangle = h_{\alpha,\alpha}(\tau,0)\bar{e}(0) + h_{\alpha,\bar{g}}(\tau,0)\alpha^*(\tau). \tag{6.34}$$

Here we now see why it was helpful to divide $\langle \hat{\sigma}_z\rangle$ into its two components. The details will now be skipped, but the functions h can from the obtained from the coupled differential equations (Eqs. (6.27)-(6.30)) and then Fourier transformed. The calculations become quite lengthy and we are interested in the main result which is the spectrum

$$\begin{aligned} S[\omega] &= \mathcal{F}(\langle \hat{a}^\dagger(0)\hat{a}(\tau)\rangle)[\omega] \\ &= 2\pi|\langle \hat{\sigma}^-\rangle_{ss}|^2\delta(\omega-\omega_p) + 4\bar{e}_\infty\kappa\gamma^2\left(\frac{(\omega-\omega_p)^2 + (2\gamma^2+\kappa^2)}{|f(i(\omega-\omega_p))|^2}\right), \end{aligned} \tag{6.35}$$

where $\langle \hat{\sigma}^-\rangle_{ss}$ is the steady state solution of $\langle \hat{\sigma}^-\rangle$ found in Eq. (5.37) and $\bar{e}_\infty$ is given by Eq. (5.42). If the system is driven on resonance

$$|f(i\omega)|^2 = (\omega^2 + s_0^2)(\omega^2 + s_+^2)(\omega^2 + s_-^2), \tag{6.36}$$

in the case when all roots

$$s_0 = -\frac{1}{2}\kappa \tag{6.37}$$

$$s_+ = -\frac{3}{4}\kappa + \sqrt{\frac{1}{16}\kappa^2 - 4\gamma^2} \tag{6.38}$$

$$s_- = -\frac{3}{4}\kappa - \sqrt{\frac{1}{16}\kappa^2 - 4\gamma^2}, \tag{6.39}$$

are real, i.e $\frac{1}{16}\kappa - 4\gamma^2$ is positive. If however $\frac{1}{16}\kappa - 4\gamma^2$ is negative, s_+ and s_- become complex conjugates, in which case they can be re-written as

$$s_0 = -\frac{1}{2}\kappa \tag{6.40}$$

$$s_+ = -\frac{3}{4}\kappa + i\omega_M \tag{6.41}$$

$$s_- = -\frac{3}{4}\kappa - i\omega_M, \tag{6.42}$$

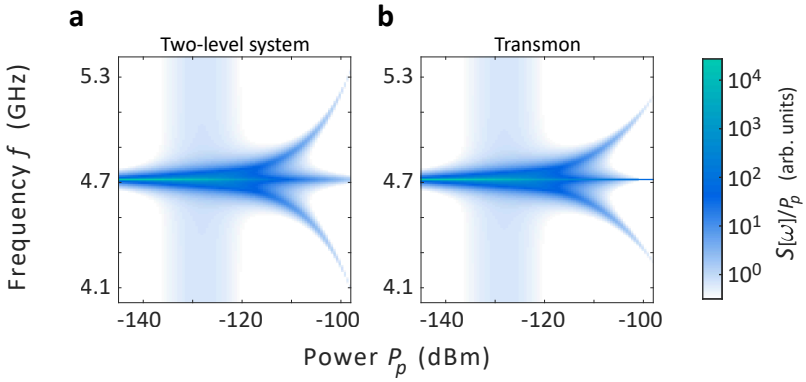

Figure 6.3: The power spectrum $S[\omega]$ of emitted photons when the system is driven on resonance by the probe as function of the probe power P_p. The spectrum is normalised such that it shows $S[\omega]/P_p$ (in some arbitrary units) in order to better resolve the spectrum at lower power. Panel **a** shows the power spectrum for a two-level system, where you can clearly see the splitting into the Mollow triplets. In **b**, the same behaviour is visible, however the non-linear effects are not as strong here, showing a slightly smaller amplitude at higher powers for the Mollow triplets, instead having a stronger coherent response visible in the spectrum as a sharp line on the probe frequency.

where $\omega_M = \sqrt{4\gamma^2 - \frac{1}{16}\kappa}$. In this case

$$|f(i\omega)|^2 = \Big((\omega-\omega_p)^2 + (\kappa/2)^2)\Big)\Big((\omega-\omega_p-\omega_M)^2 + (3\kappa/4)^2\Big)\Big((\omega-\omega_p+\omega_M)^2 + (3\kappa/4)^2\Big). \tag{6.43}$$

By using partial fraction decomposition, we can write the second term of Eq. (6.35) as three separate terms. In the first case, when all roots are real, the three terms will be Lorentzians centered around the resonance frequency, where one of the terms will be negative. In the second case we instead get three Lorentzians centred around three different frequencies (ω_r and $\omega_r \pm \omega_M$). This is the emission spectrum referred to as the Mollow triplet, observed in e.g. Ref. 47. An interesting feature of this is that the splitting in frequency between the emitted photons increases as the drive strength increases, so even though we have a two-level system (so only one resonance mode) we see emission at three different frequencies. This is shown in Fig. 6.3a, where $S[\omega]$ has been normalised with respect to the probe power P_p in order to resolve the spectrum better at lower powers. You can clearly see a splitting into the triplets as the power increases. As the effect eventually saturates in the sense that the three Lorentzian peaks reach an asymptotic value for their maximum [45], you can see that the features start fading due to the normalisation with P_p.

6.4.2 Transmon

Moving on to cover the emission spectrum of the Transmon, I will only consider a similar case as for the two-level system, namely the emission spectrum when driving on resonance. Since attempting an analytical solution would require at least a three-level system and that would become significantly more difficult to deal with, the Transmon case is only done numerically, but using the qualitative results from the two-level system in order to draw conclusions. The Transmon case is indeed very similar, as can be seen in Fig. 6.3

by comparing the two-level system with the Transmon. There are however some subtle differences, for instance that the coherent signal is stronger at higher powers (the $\delta(\omega-\omega_p)$ amplitude) for the Transmon, as well as a lower amplitude on the Mollow triplet spectrum. The splitting appears to be slightly smaller as well, which can be understood by some photons being able to excite the system to higher energy levels reducing the effect from the extreme non-linear case of the two-level system. The higher coherent amplitude in the emission spectrum agrees with the previous result presented in Fig. 6.2a, and explains well what happens with the incoherent part of the signal from the system.

Chapter 7

Two-Tone Measurements

One of the basic rules of the universe is that nothing is perfect. Perfection simply doesn't exist.....Without imperfection, neither you nor I would exist.
- Stephen Hawking

In this section, we will move on to try to model two-tone measurements on our system. Here we will have an input signal containing two amplitudes and frequencies (the drive and the probe), such that

$$\langle \hat{b}_{in} \rangle = \underbrace{\sqrt{\dot{N}_d} e^{-i\omega_d t}}_{\text{drive}} + \underbrace{\sqrt{\dot{N}_p} e^{-i\omega_p t}}_{\text{probe}}. \tag{7.1}$$

So for instance the system Hamiltonian $\hat{H}_{\mathcal{S}}$ that we consider in the master equation will be

$$\begin{aligned} \hat{H}_{\mathcal{S}} = &\left(\sqrt{8E_J E_C} - \frac{E_C}{2} \right) \hat{a}^\dagger \hat{a} - \frac{E_C}{2} \hat{a}^\dagger \hat{a} \hat{a}^\dagger \hat{a} \\ &+ \hbar\gamma_d (\hat{a}^\dagger e^{-i\omega_d t} + \hat{a} e^{i\omega_d t}) + \hbar\gamma_p (\hat{a}^\dagger e^{-i\omega_p t} + \hat{a} e^{i\omega_p t}), \end{aligned} \tag{7.2}$$

where $\gamma_{(d,p)} = \sqrt{\kappa_c \dot{N}_{(d,p)}}$. This turns out to be much more of a challenge, as we are unable to find a frame where we can get rid of all the time dependence (except for the special case of $\omega_d = \omega_p$). We will still however be able to manage using the methods described in Sec. 7.2, but before that the two-level system will be analysed and in this case we are able to find an analytical solution in the perturbative case of a weak probe. In all of the following cases, the probe will be considered weak, such that the response is approximately linear to it, more precisely it will be such that $\dot{N}_p = 10^{-2.5}$ GHz which on resonance corresponds to about -140 dBm. The drive frequency ω_d will always be set to the bare resonance frequency ω_r.

7.1 Two-level system

In order to gain a better understanding for the two-tone measurements done on the Transmon resonator, understanding what happens to a two-level system proves useful as the two systems will share some similarities. Moving to the rotating frame of the drive will modify equation (5.27), giving the form

$$\hat{H}_{\mathcal{S}} = \hbar\gamma_d(\hat{\sigma}^+ + \hat{\sigma}^-) + \hbar\gamma_p(\hat{\sigma}^+ e^{-i\delta\omega t} + \hat{\sigma}^- e^{i\delta\omega t}), \tag{7.3}$$

where γ_d, γ_p are the drive and probe couplings respectively, and $\delta\omega = \omega_p - \omega_d$, where ω_d, ω_p are the drive and probe frequencies respectively. This will then change the equations of motion for the different operators. The result is the coupled set of equations

$$\begin{cases} \dot{\langle\hat{\sigma}^+\rangle} = -\frac{\kappa}{2}\langle\hat{\sigma}^+\rangle - i(\gamma_d + \gamma_p e^{i\delta\omega t})\langle\hat{\sigma}_z\rangle \\ \dot{\langle\hat{\sigma}^-\rangle} = -\frac{\kappa}{2}\langle\hat{\sigma}^-\rangle + i(\gamma_d + \gamma_p e^{-i\delta\omega t})\langle\hat{\sigma}_z\rangle \\ \dot{\langle\hat{\sigma}_z\rangle} = -2i(\gamma_d + \gamma_p e^{-i\delta\omega t})\langle\hat{\sigma}^+\rangle + 2i(\gamma_d + \gamma_p e^{i\delta\omega t})\langle\hat{\sigma}^-\rangle - \kappa(1 + \langle\hat{\sigma}_z\rangle). \end{cases} \tag{7.4}$$

In order to simplify these we can assume that the drive is stronger than the probe, such that the system is driven to a steady state by the drive, then it has a time dependent perturbation from the probe. The probe is then assumed to be weak such that terms with $\mathcal{O}(\gamma_p^2)$ are neglected, implicitly assuming a linear response. In order to achieve this, we make the perturbation

$$\langle\hat{\sigma}(t)\rangle = \langle\hat{\sigma}\rangle_0 + \gamma_p\langle\hat{\sigma}(t)\rangle_1. \tag{7.5}$$

Now the time dependent part sits in the perturbative term and the steady state solutions ($\langle\hat{\sigma}\rangle_0$) are given by equations (5.36),(5.37),(5.40) by setting $\gamma = \gamma_d$ and $\Delta = 0$. The EoM for $\langle\hat{\sigma}^+\rangle$ then becomes

$$\begin{aligned} \gamma_p\dot{\langle\hat{\sigma}^+\rangle}_1 &= -\frac{\kappa}{2}\Big(\langle\hat{\sigma}^+\rangle_0 + \gamma_p\langle\hat{\sigma}^+\rangle_1\Big) - i\Big(\gamma_d + \gamma_p e^{i\delta\omega t}\Big)\Big(\langle\hat{\sigma}_z\rangle_0 + \gamma_p\langle\hat{\sigma}_z\rangle_1\Big) \\ &= -\frac{\kappa}{2}\gamma_p\langle\hat{\sigma}^+\rangle_1 - i\gamma_p\gamma_d\langle\hat{\sigma}_z\rangle_1 - i\gamma_p e^{i\delta\omega t}\langle\hat{\sigma}_z\rangle_0, \end{aligned} \tag{7.6}$$

where, in the second line, $-i\gamma_p^2 e^{i\delta\omega t}\langle\hat{\sigma}_z\rangle_1$ has been neglected, and the (steady state) condition $-\kappa/2\langle\hat{\sigma}^+\rangle_0 - i\gamma_d\langle\hat{\sigma}_z\rangle_0 = 0$ has been imposed. Analogous calculations for the other equations of motion yields our new set of coupled equations which can be represented in matrix form

$$\dot{\vec{\sigma}} = M\vec{\sigma} + C, \tag{7.7}$$

where

$$\vec{\sigma} = \begin{pmatrix} \langle\hat{\sigma}^+\rangle_1 \\ \langle\hat{\sigma}^-\rangle_1 \\ \langle\hat{\sigma}_z\rangle_1 \end{pmatrix}, M = \begin{pmatrix} -\frac{\kappa}{2} & 0 & -i\gamma_d \\ 0 & -\frac{\kappa}{2} & i\gamma_d \\ -2i\gamma_d & 2i\gamma_d & -\kappa \end{pmatrix}, C = \begin{pmatrix} -ie^{i\delta\omega t}\langle\hat{\sigma}_z\rangle_0 \\ ie^{-i\delta\omega t}\langle\hat{\sigma}_z\rangle_0 \\ -2ie^{-i\delta\omega t}\langle\hat{\sigma}^+\rangle_0 + 2ie^{i\delta\omega t}\langle\hat{\sigma}^-\rangle_0 \end{pmatrix}. \tag{7.8}$$

It is more convenient to work in a diagonal basis, which we can achieve by a transformation. Let $\vec{\sigma} = S\vec{x}$, where $\vec{x} = \begin{pmatrix} x_1 & x_2 & x_3 \end{pmatrix}^T$ is in the diagonal basis. Then the equation can be rewritten as

$$\dot{\vec{x}} = S^{-1}MS\vec{x} + S^{-1}C = D\vec{x} + \tilde{C}, \tag{7.9}$$

where D contains the eigenvalues. There is a choice in the ordering of the eigenvalues in D. One choice, and its corresponding transformation matrices, is

$$D = \begin{pmatrix} -\frac{3}{4}\kappa + i\omega_M & 0 & 0 \\ 0 & -\frac{3}{4}\kappa - i\omega_M & 0 \\ 0 & 0 & -\frac{\kappa}{2} \end{pmatrix} \tag{7.10}$$

$$S = \begin{pmatrix} \frac{-i\gamma_d}{-\kappa/4+i\omega_M} & \frac{i\gamma_d}{\kappa/4+i\omega_M} & 1 \\ \frac{i\gamma_d}{-\kappa/4+i\omega_M} & \frac{-i\gamma_d}{\kappa/4+i\omega_M} & 1 \\ 1 & 1 & 0 \end{pmatrix}, \quad S^{-1} = \begin{pmatrix} \frac{-\gamma_d}{\omega_M} & \frac{\gamma_d}{\omega_M} & \frac{-\kappa/4+i\omega_M}{2i\omega_M} \\ \frac{\gamma_d}{\omega_M} & \frac{-\gamma_d}{\omega_M} & \frac{\kappa/4+i\omega_M}{2i\omega_M} \\ \frac{1}{2} & \frac{1}{2} & 0 \end{pmatrix}, \tag{7.11}$$

where $-3\kappa/4 \pm i\omega_M$ and $-\kappa/2$ are the eigenvalues of M and $\omega_M \equiv \sqrt{4\gamma_d^2 - \frac{1}{16}\kappa^2}$ has suggestively been named with the same notation as the Mollow triplets in Sec. 6.4. Note that for $64\gamma_d^2 > \kappa^2$ it makes sense to think of this as a frequency, as then ω_M is real. This is assumed, since the drive is currently assumed to be strong but the expressions themselves are in principle valid for low γ_d as well. One thing to note is that for $64\gamma_d = \kappa^2$, there is a pole in S^{-1}. This is because at this power, we have a degeneracy in the eigenvalues of M, and are unable to find a basis for the transition matrix S. This does not affect the end result. With these we find $\tilde{C}$ to be

$$\tilde{C} = \begin{pmatrix} \left(e^{i\delta\omega t} + e^{-i\delta\omega t}\right)\left(\frac{i\gamma_d}{\omega_M} - \frac{\kappa/4-i\omega_M}{\omega_M}\frac{i\gamma_d}{\kappa/2}\right)\langle\hat{\sigma}_z\rangle_0 \\ \left(e^{i\delta\omega t} + e^{-i\delta\omega t}\right)\left(\frac{-i\gamma_d}{\omega_M} + \frac{\kappa/4+i\omega_M}{\omega_M}\frac{i\gamma_d}{\kappa/2}\right)\langle\hat{\sigma}_z\rangle_0 \\ \langle\hat{\sigma}_z\rangle_0 \sin\delta\omega t \end{pmatrix} = \begin{pmatrix} 2\xi\cos\delta\omega t \\ 2\xi^*\cos\delta\omega t \\ \langle\hat{\sigma}_z\rangle_0 \sin\delta\omega t \end{pmatrix}, \tag{7.12}$$

where the relations (5.36),(5.37) have been inserted and the definition

$$\xi = \frac{i\gamma_d}{\omega_M}\left(\frac{\kappa/4 + i\omega_M}{\kappa/2}\right)\langle\hat{\sigma}_z\rangle_0, \tag{7.13}$$

has been made.

Since the probe is oscillating with $e^{-i\omega_p t}$, this is the signal that will be detected in a measurement which motivates the interest in looking at this particular frequency. We will also see that there is an amplitude oscillating with $e^{i\omega_p t}$. Furthermore, due to the assumed long duration of the measurement, the steady state solution is what is interesting. With

all of this in mind, the ansatz $\vec{x}(t) = \vec{x}_0(t) + \vec{x}_+ e^{+i\delta\omega t} + \vec{x}_- e^{-i\delta\omega t}$ is made, where $\vec{x}_+, \vec{x}_-$ are the steady state amplitudes which are oscillating with the probe frequency. Extracting the terms oscillating with $e^{+i\delta\omega t}$ first, we find the linear differential equations (after dividing by $e^{i\delta\omega t}$) to give

$$\begin{cases} i\delta\omega x_1^+ = \lambda_1 x_1^+ + \xi \\ i\delta\omega x_2^+ = \lambda_2 x_2^+ + \xi^* \\ i\delta\omega x_3^+ = \lambda_3 x_3^+ + \frac{\langle\hat{\sigma}_z\rangle_0}{2i} \end{cases} \Rightarrow \begin{cases} x_1^+ = \frac{\xi}{i(\delta\omega - \omega_M) + 3\kappa/4} \\ x_2^+ = \frac{\xi^*}{i(\delta\omega + \omega_M) + 3\kappa/4} \\ x_3^+ = \frac{\langle\hat{\sigma}_z\rangle_0/2i}{i\delta\omega + \kappa/2} \end{cases} . \tag{7.14}$$

Similarly, one finds

$$\begin{cases} x_1^- = \frac{-\xi}{i(\delta\omega + \omega_M) - 3\kappa/4} \\ x_2^- = \frac{-\xi^*}{i(\delta\omega - \omega_M) - 3\kappa/4} \\ x_3^- = \frac{\langle\hat{\sigma}_z\rangle_0/2i}{i\delta\omega - \kappa/2} \end{cases} . \tag{7.15}$$

Transforming back to the original basis, we are interested in the coherent response of the probe, so $\langle\hat{\sigma}^-\rangle_1$ oscillating with $e^{\pm i\delta\omega}$. These are readily obtained as

$$\langle\hat{\sigma}^-\rangle_1^+ = \frac{\eta}{i(\delta\omega - \omega_M) + 3\kappa/4} - \frac{\eta^*}{i(\delta\omega + \omega_M) + 3\kappa/4} + \frac{\langle\hat{\sigma}_z\rangle_0/2i}{i\delta\omega + \kappa/2} \tag{7.16}$$

$$\langle\hat{\sigma}^-\rangle_1^- = -\frac{\eta}{i(\delta\omega + \omega_M) - 3\kappa/4} + \frac{\eta^*}{i(\delta\omega - \omega_M) - 3\kappa/4} + \frac{\langle\hat{\sigma}_z\rangle_0/2i}{i\delta\omega - \kappa/2}, \tag{7.17}$$

where now $\eta = \frac{i\gamma_d}{\kappa/4 - i\omega_M}\xi$. From these expressions, we see that the signal is split into three resonance modes. The resonance modes with frequencies ω_r and $\omega_r \pm \omega_M$ correspond exactly to the frequencies of the Mollow triplets. One further note is that all of the terms are linear with $\langle\hat{\sigma}_z\rangle_0$. This is interpreted as an effect due to both loss of coherence as well as saturation of the two-level system. The third term in Eqs. (7.16),(7.17) approaches 0 as $\sim 1/\gamma_d^2$ (see Eq. (5.40)), while the first and second term approach 0 rather as $\sim 1/\gamma_d$ (see Eq. (5.37) together with Eq. (5.40)). Putting our result back into equation (7.5), we end up with

$$\langle\hat{\sigma}^-(t)\rangle = \langle\hat{\sigma}^-\rangle_0 + \gamma_p\Big(\langle\hat{\sigma}^-\rangle_1^0(t) + \langle\hat{\sigma}^-\rangle_1^- e^{-i\delta\omega t} + \langle\hat{\sigma}^-\rangle_1^+ e^{i\delta\omega t}\Big), \tag{7.18}$$

where $\langle\hat{\sigma}^-\rangle_1^0(t)$ contains any transients and corrections to the constant term. Note also here the importance of a weak probe, as in the approximation the outgoing signal is linear with γ_p as $\langle\hat{\sigma}^-\rangle_1^\pm$ do not depend on γ_p at all. The system is highly non-linear so the approximation is only valid for when the system responds linearly to the probe.

The question is now how to interpret the terms in the lab frame, as all of the calculations have been done in a frame rotating with the drive. There is therefore an ambiguity in what frequencies $-\delta\omega$ and $+\delta\omega$ would correspond to in the lab frame, as it could

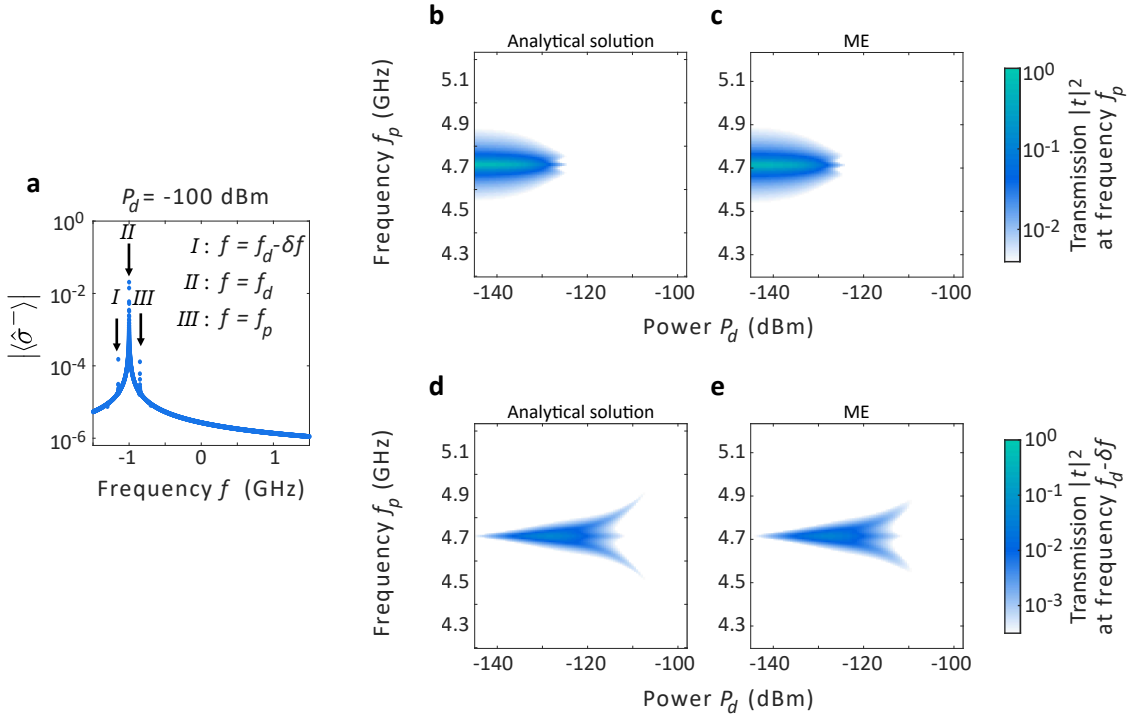

Figure 7.1: a, The modulus of the frequency spectrum for the time evolution of $\langle\hat{\sigma}^-\rangle$ in a frame rotating such that the resonance frequency is at 1 GHz. The drive power $P_d = -100$ dBm and there are three peaks visible corresponding to the frequencies $f_d - \delta f$, f_d and f_p. **b, c,** The amplitude at f_p is extracted and displayed as a transmission coefficient $|t|^2$ (with t defined as in Eq. 7.19) as a function of drive power P_d and probe frequency f_p for both the analytical solution derived in Sec. 7.1 and the master equation (ME) approach discussed in Sec. 7.2. At low drive, the system response is approximately linear, until at around -130 dBm where the response quickly vanishes due to the saturation from the drive. **d, e,** The amplitude at $f_d - \delta f$ is displayed in terms of the transmission coefficient $|t|^2$ as a function of drive power P_d and probe frequency f_p, again both for the analytical solution and the ME approach. Note that the scale of the z-axis is slightly different in order to better resolve the features. The signal is here low for weak drive, but then increases and eventually splits into the Mollow triplets before vanishing.

be some classical signal like a beating, or coming from the $e^{+i\delta\omega t}$ term in the system Hamiltonian (7.3) corresponding to rotating with $e^{i\omega_p t}$ in the lab frame. We are no longer able to make a transformation with operators, as we have taken the expectation values and are therefore only working with numbers. What we can do however, is to evolve the system numerically using master equations, then Fourier transform the response and extract the amplitude at the probe frequency. Doing this in the lab frame can be computationally quite heavy, and for the purpose of understanding where the amplitudes come from it is a bit unnecessary. We can work in some intermediate frame, such that in this frame the resonance frequency is 1 GHz. This is shown in Fig. 7.1a, where we see three peaks. Peak *II* is at the drive frequency and not very interesting in our case, however peaks *I* and *III* are more interesting, as peak *III* is at the probe frequency f_p. This amplitude is naturally interpreted as corresponding to $\gamma_p\langle\hat{\sigma}^-\rangle_1^-$. Peak *I* however, is at frequency $f_d - \delta f$, where $\delta f = f_p - f_d$, so this is then interpreted as the amplitude corresponding to $\gamma_p\langle\hat{\sigma}^+\rangle_1^+$.

With this interpretation, we can now plot the transmission $|t|^2$ at the different frequencies. This is shown in Fig. 7.1b-e, where both the analytical solutions originating from Eqs. 7.16,7.17 and the master equation solution is shown. It is important to stress here that the master equation figures were simulated in the frame rotating with the drive, so Eq. 7.3 was used here as well. Furthermore $|t|^2$ refers to the definition

$$t \equiv \frac{\kappa_c \langle \hat{a} \rangle}{\langle \hat{b}_{in} \rangle}, \tag{7.19}$$

which means that at the probe frequency $\omega_p = 2\pi f_p$, it makes sense to think of it as the fraction of power transmitted, however in Figs. 7.1d,e the view of it as fraction of number of photons transmitted since then the photons are emitted at a different frequency. Figures 7.1c,e are in other words determined by time evolving the system in the frame rotating with the drive, then Fourier transforming the signal and extracting the amplitudes at $\pm\delta\omega$. It will also be explained in more detail in the next section. The above method was only to aid in the interpretation of the amplitudes. We see that the response at the probe frequency f_p (Figs. 7.1b,c) at low powers has a shape similar to the one-tone measurement shown in Figs. 6.1e-g. You can also see that transmission quickly vanishes, as the two-level system is saturated by the drive. At frequency $f_d - \delta f$ (Figs. 7.1d,e) we see that the transmission is lower for lower drive powers, but initially increases, splitting into the Mollow triplets, before vanishing again. Note that the two cases have different limits on the z-axis. This is in order to resolve more of the response at $f_d - \delta f$, which has lower amplitude.

The agreement between the perturbative analytical solution and the numerical solution is very good in this limit of a weak probe. Now with the interpretations and understanding gained from the two-level system, we are ready to move on to the more complicated Transmon.

7.2 Method

As we have already seen, solving for the response from a two-tone measurement becomes quite a bit more challenging than for a one-tone measurement as we can no longer move to a rotating frame that gets rid of all time dependencies. The treatment required will therefore be a bit different than the one-tone case, both for the master equation and the input-output approach. The restriction of using a weak probe just as in Sec. 7.1 will help to simplify the problem in the case of the input-output theory, but before that, let us treat the method used for determining the two-tone response using master equations.

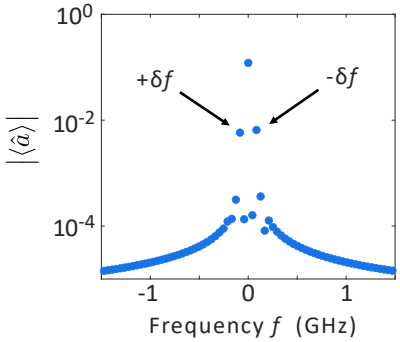

Figure 7.2: The Fourier spectrum of $\langle\hat{a}(t)\rangle$ at $P_p = -113\,\text{dBm}$ and $\delta\omega = -0.5$. We see a strong amplitude on resonance, and two smaller ones at frequencies $\pm\delta f = \pm\delta\omega/2\pi$. The amplitude at $-\delta f$ is interpreted as the steady state amplitude for the probe, corresponding to the measured amplitude in the experiment.

7.2.1 Lindblad master equation using QuTiP

In order to simplify the numerical simulation, we move to a frame rotating with the drive, such that we end up with the system Hamiltonian

$$\hat{H}_S = \frac{E_C}{2}(\hat{a}^\dagger\hat{a} - \hat{a}^\dagger\hat{a}\hat{a}^\dagger\hat{a}) + \hbar\gamma_d(\hat{a}^\dagger + \hat{a}) + \hbar\gamma_p(\hat{a}^\dagger e^{-i\delta\omega t} + \hat{a}e^{i\delta\omega t}), \tag{7.20}$$

where again $\delta\omega = \omega_p - \omega_d$. The steady state solution for the density matrix $\hat{\rho}$ is first found for $\gamma_p = 0$, which is then used as initial condition for the time evolution in order to reduce the amount of time needed to approach a steady state solution for the system. Now we have some $\hat{\rho}(t)$, from which we can easily get $\langle\hat{a}(t)\rangle$. Since we are interested in the coherent amplitude of the signal in the heterodyne detection, we want the amplitude oscillating with $e^{-i\delta\omega t}$. This we can extract by Fourier transforming $\langle\hat{a}(t)\rangle$ and taking the amplitude at the desired frequency. An example of such a spectrum is shown in Fig. 7.2, where we see an amplitude at $-\delta\omega = -2\pi\delta f$. As we saw in the two-level system, there is also an amplitude at $\delta\omega = 2\pi\delta f$. This one is also extracted and is what we have already seen in Fig. 7.1e.

7.2.2 Input-output theory

For the input-output approach it will again be done as in Ref. 25, only adding an amplitude rotating with $e^{i\delta\omega t}$ in the frame of the drive. As in the one-tone case we will use Eq. 4.58 just as in the one-tone case. Now we will however use Eq. 7.1 as the input. Once again moving to a frame rotating with the drive, defining

$$A_{m,n} \equiv \langle(\hat{a}^\dagger)^m\hat{a}^n\rangle, \tag{7.21}$$

and making the same approximations as before we end up with the EoM for $A_{m,n}$ as

$$\begin{aligned}\frac{\mathrm{d}}{\mathrm{d}t}A_{m,n} = &\Big(i(m-n)(\omega_r-\omega_p) - i\frac{(m-n)(m+n-1)}{2}\omega_C - \frac{m+n}{2}\kappa\Big)A_{m,n} \\ &- i(m-n)\omega_C A_{m+1,n+1} - n\sqrt{\kappa_c}\left(\sqrt{\dot{N}_d} + \sqrt{\dot{N}_p}e^{-i\delta\omega t}\right)A_{m,n-1} \\ &- m\sqrt{\kappa_c}\left(\sqrt{\dot{N}_d} + \sqrt{\dot{N}_p}e^{i\delta\omega t}\right)A_{m-1,n},\end{aligned} \tag{7.22}$$

where we unfortunately still have a time-dependence. Here we will do a similar trick as for the two-level case where we make an ansatz

$$A_{m,n}(t) = A^0_{m,n} + A^{1,+}_{m,n}e^{i\delta\omega t} + A^{1,-}_{m,n}e^{-i\delta\omega t}, \tag{7.23}$$

where $A^0_{m,n}$ is the steady state solution from the drive and $A^{1,+}_{m,n}$ as well as $A^{1,-}_{m,n}$ are assumed to be perturbations from the probe. In other words we make the approximation that $\dot{N}_p$ is small (equivalent to γ_p being small), so that we can neglect the terms proportional to $\sqrt{\dot{N}_p}A^1_{m,n}$. The restriction of looking at terms oscillating with $e^{\pm i\delta\omega t}$ and not $e^{i\pm(m-n)\delta\omega t}$ is that we are only interested in $A_{0,1}(t)$ in the end and the amplitudes that are oscillating with those frequencies.

The approach for the steady state solution is the same as in Sec. 6.1.2. The ansatz allows us to find steady state solutions for terms that are proportional to $e^{i\pm\delta\omega t}$ by separating those terms and solve for them separately. This yields one set of equations by only considering the terms proportional to $e^{i\delta\omega t}$:

$$\begin{aligned}i\delta\omega A^{1,+}_{m,n} = &\Big(-i\frac{(m-n)(m+n-1)}{2}\omega_C - \frac{m+n}{2}\kappa\Big)A^{1,+}_{m,n} \\ &- i(m-n)\omega_C A^{1,+}_{m+1,n+1} - n\sqrt{\kappa_c\dot{N}_d}A^{1,+}_{m,n-1} \\ &- m\sqrt{\kappa_c}\left(\sqrt{\dot{N}_d}A^{1,+}_{m-1,n} + \sqrt{\dot{N}_p}A^0_{m-1,n}\right),\end{aligned} \tag{7.24}$$

as well as one set of equations by considering the terms proportional to $e^{-i\delta\omega t}$:

$$\begin{aligned}-i\delta\omega A^{1,-}_{m,n} = &\Big(-i\frac{(m-n)(m+n-1)}{2}\omega_C - \frac{m+n}{2}\kappa\Big)A^{1,-}_{m,n} \\ &- i(m-n)\omega_C A^{1,-}_{m+1,n+1} - n\sqrt{\kappa_c}\left(\sqrt{\dot{N}_d}A^{1,-}_{m,n-1} + \sqrt{\dot{N}_p}A^0_{m,n-1}\right) \\ &- m\sqrt{\kappa_c\dot{N}_d}A^{1,-}_{m-1,n}.\end{aligned} \tag{7.25}$$

There will again be some special cases that we need to deal with:

$$i\delta\omega A^{1,+}_{1,0} = -\frac{\kappa}{2}A^{1,+}_{1,0} - i\omega_C A^{1,+}_{2,1} - \sqrt{\kappa_c \dot{N}_p} \tag{7.26}$$

$$i\delta\omega A^{1,+}_{0,1} = -\frac{\kappa}{2}A^{1,+}_{0,1} + i\omega_C A^{1,+}_{1,2} \tag{7.27}$$

$$-i\delta\omega A^{1,-}_{1,0} = -\frac{\kappa}{2}A^{1,-}_{1,0} - i\omega_C A^{1,-}_{2,1} \tag{7.28}$$

$$-i\delta\omega A^{1,-}_{0,1} = -\frac{\kappa}{2}A^{1,-}_{0,1} + i\omega_C A^{1,-}_{1,2} - \sqrt{\kappa_c \dot{N}_p}, \tag{7.29}$$

after which we can write a matrix equation similar to the form of Eq. 6.16 for each case. With all of this taken care of this section is concluded.

7.3 Transmon

The transmission $|t|^2$ at the probe frequency $f_p = \omega_p/2\pi$ from the experiments as well as the two theoretical methods just described is shown in Fig. 7.3a-c. Starting with describing the experimental measurement, we see at low drive power P_d that the transmission $|t|^2$ looks just as in the linear case that we saw in Fig. 6.1e-g. This is expected as the rate with which photons enter the cavity is to low to start saturating the system and having any significant effect. At higher powers there are several interesting features. For instance at $f_p = 4.4\,\text{GHz}$ we start seeing the $|1\rangle \leftrightarrow |2\rangle$ transition (second mode) appearing due to a photon residing in the resonator for a significant amount of the time, such that the photon from the probe at 4.4 GHz is resonant with the second transition. The first mode ($|0\rangle \leftrightarrow |1\rangle$ transition) splits at higher power into two; one dominant feature splitting downwards in frequency and one faint feature splitting upwards in frequency, both corresponding to the Mollow triplet frequencies. Furthermore there is also a splitting of the second mode at high powers. Both of these features can be explained by a phenomenon known as 'dressed states' [48]. This is something that has been observed in similar systems, see for instance Refs. [22, 25, 49]. It can be understood as an effect that the environment has on the perceived energy levels of the system, and is in special cases known as Autler-Townes splitting [23, 50]. The photons in the environment that couple to the system can be seen as changing the potential of the system, in a semi-classical picture similar to a strong oscillating electric field perturbing the potential of an atom in the so-called ac-Stark effect. Take for instance a two-level system driven on resonance in the frame of the drive and consider the Hamiltonian where the environment is traced out, such that you have Eq. 5.27 with $\Delta = 0$:

$$\hat{H}_{\mathcal{S}} = \hbar\gamma(\hat{\sigma}^+ + \hat{\sigma}^-), \tag{7.30}$$

then the eigenenergies of the system Hamiltonian will change due to the drive term, and one has to diagonalise it again in order to receive effective eigenenergies which describe the system better. This gives new eigenstates which will instead be superpositions of the bare states. This is mostly in order to gain some intuition for the phenomenon and there are some more details that need to be considered which are beyond the scope of this thesis,

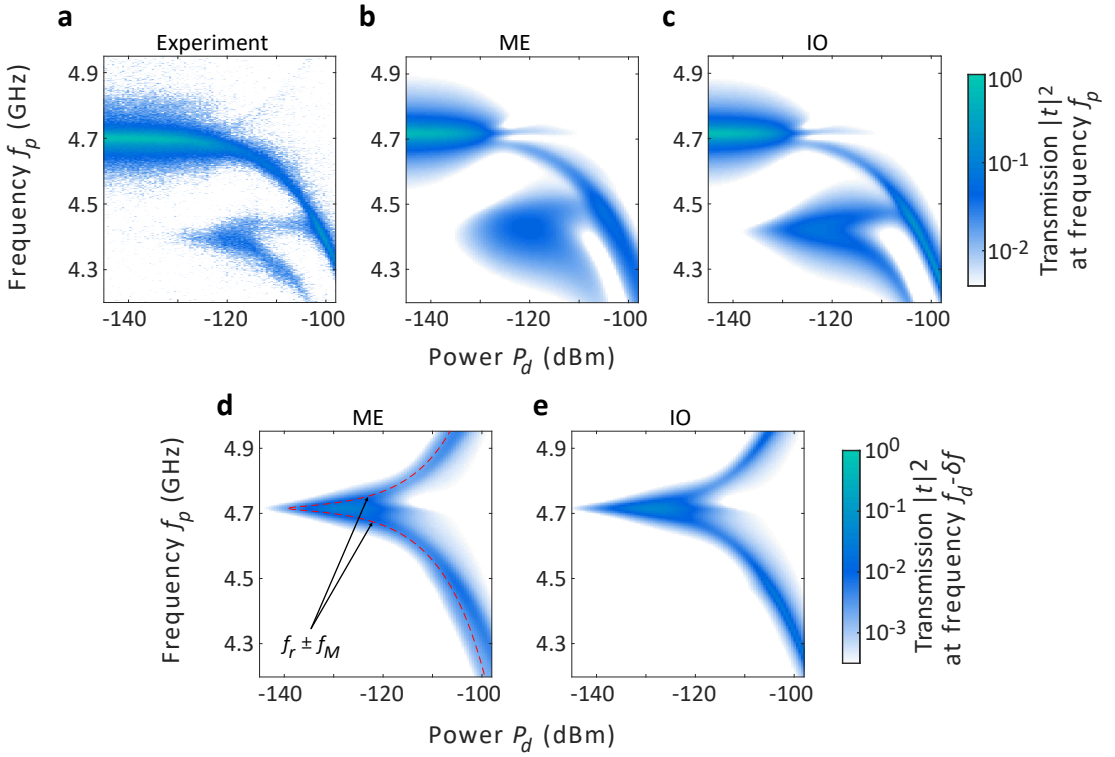

Figure 7.3: **a,** The transmission $|t|^2$ of the probe in the two-tone measurements as function of drive power P_d and probe frequency f_p. The drive frequency f_d is fixed at the bare resonance frequency $f_r = 4.715\,\text{GHz}$ and the probe power $P_p = -144\,\text{dBm}$. At low drive power the response is the same as with no drive. At around $-130\,\text{dBm}$ the second resonance mode starts appearing as well, corresponding to the $|1\rangle \leftrightarrow |2\rangle$ transition. The main resonance mode splits at $-120\,\text{dBm}$ into two signals, one very faint going upwards in frequency. This corresponds to one of the Mollow triplets. The other is stronger and goes downward in frequency, corresponding to the other split frequency of the Mollow triplet. At about $-115\,\text{dBm}$, the second transition also splits. Both of these splittings are due to dressed states, meaning that the strong drive causes the effective eigenenergies of the system to change. **b, c,** The theoretical results received for the prediction of panel **a**, determined using the methods described in Sec. 7.2. Qualitatively a lot of the features are present such as the signal going downwards in frequency at strong drive P_d and the splitting of the second transition due to the dressed states, however they deviate a bit quantitatively from the experimental data. There is also some deviance between the two theoretical methods where the ME gives a more smeared feature from the second transition mode. **d, e,** The predicted response at frequency $f_d - \delta f = 2f_d - f_p$ as function of probe frequency f_p and drive power P_d, which shows features at the Mollow triplet frequencies. The two splitting frequencies of the Mollow triplet are indicated in the figure as $f_d \pm f_M$ by dashed red lines. Note that the z-axis has a different scale in order to better resolve the features.

these can be found in for instance Ref. 48.

Turning to the theoretical results, they do no replicate the two-tone measurements as well as the one-tone measurements. They do however contain most of the main features, such as an approximately linear response at low drive power P_d, the downwards splitting signal of the first mode and the appearance of the second mode and its splitting. Even between the two methods, there are some discrepancies. The discrepancies are mainly around the second mode, where the approach using the Lindblad master equation shows more 'smeared' features in contrast to the input-output result which has slightly sharper features that seem to agree better with the experimental data. The exact reason is unknown, but

a possible explanation is that the system had not been evolved for long enough in order to get rid of transients and end up at a steady state. Since the probe was weak, the approximation made in the input-output theory approach is not enough to explain this as in the relevant regime this approximation is justified. There will be some discussion in Chapter 8 about ways that could potentially explain the difference between experiments and theory.

Moving on to the output at angular frequency $\omega_d - \delta\omega = 2\omega_d - \omega_p$, the theoretically predicted transmission $|t|^2$, with t defined in Eq. 7.19, is shown as function of drive power P_d and probe frequency $f_p = \omega_p/2\pi$ in Figs. 7.3. Here the z-axis has a different scale as compared to Figs. 7.3a-c, in order to resolve the features better. The features appearing correspond to the frequencies of the Mollow triplet. One weak at resonance and two stronger features at frequencies $f_r \pm f_M$ where f_r is the resonance frequency and $f_M = \omega_M/2\pi$ is the frequency of the sidebands of the Mollow triplet. These frequencies are indicated in Fig. 7.3 with red dashed lines. A satisfactory explanation for this phenomenon of coherent emission at frequency $2\omega_d - \omega_p$ was not achieved within the scope of this thesis, however there will be some suggestion on future directions in studying this phenomenon in the next section. The reason for there not being an experimental figure is that we were unaware of the possibility of observing a signal at a frequency other than ω_d and ω_p.

Chapter 8

Conclusions and Outlook

It doesn't matter how beautiful your theory is, it doesn't matter how smart you are. If it doesn't agree with experiment, it's wrong.
- Richard P. Feynman

We have seen that the theoretical framework of cQED, input-output theory and master equations together are effective for explaining the behaviour of the measured device; a microwave resonator consisting of a single Josephson junction capacitively coupled to input- and output transmission lines. The view that has been presented is from the perspective of a non-linear resonator, rather than the more common approach of viewing it as an artificial atom or qubit stemming from the energy level structure of the Transmon. The difference in the view is quite subtle, but starting with the view of an artificial atom it would be that the Transmon absorbs a photon causing Cooper pairs to tunnel, similarly to how electrons in an atom can absorb a photon causing it to transition to a different energy level. This photon is then emitted by the system (Transmon or atom) as it decays back to its ground state. If we instead consider the view of a photon, we can think of CPW resonators which are also superconducting systems. These are distributed elements, meaning that the size is comparable to or larger than the wavelength of the photons, rather than lumped elements such as the Transmon, where the wavelength is large compared to the component. The view in CPW resonators is that the photons 'jump' from the transmission lines into the resonators, just like a cavity made from semi-transparent mirrors used in cavity QED, so that the photons really are residing in the resonator. The view of the Transmon as a resonator raises the question of whether or not a similar picture can be used here as well, where photons are residing in the Transmon cavity. The theoretical framework used in the thesis does not necessarily make a significant distinction in the end when working almost exclusively with ladder operators, so in this sense the distinction is a matter of taste and which interpretation better fits the situation. As long as one is aware of the underlying physics when relevant, the system can be understood in both ways, for instance the 'photons' in CPW resonators should really be called plasmons if one wants to be more precise [51]. Sometimes one picture has an advantage when trying

to explain a certain behaviour, such as the non-linear behaviour observed in two-tone measurements that can be explained in the picture of dressed states, in which the picture is that the bare states of an atom get 'dressed' by the photons in the surrounding field. In order to keep the picture of a cavity with photons, these observed phenomena in the two-tone measurements would need a satisfying explanation without resorting to the picture of an artificial atom.

The theory and experiments show overall good agreement, especially for the one-tone measurements where both the qualitative and quantitative agreement is very good. The two-tone measurements show similar qualitative agreement overall, however it is lacking in quantitative agreement. Some discrepancies between the two theoretical methods used were found which could be verified more in detail. Furthermore the theoretical simulation of the two-tone measurements of the Transmon showed a coherent amplitude at a third frequency, related via the probe frequency f_p and drive frequency f_d as $2f_d - f_p$, however no physical explanation was presented although suggestions will come in the outlook.

The thesis opens up several areas where further work can be done. As mentioned several times already, there are discrepancies between theory and experiment. There are processes that occur in experiments that have not been captured in the theoretical model used here, for instance leakage between the couplers - that some photons can leak from the left to the right coupler - an effect that should become more relevant for a stronger drive and lead to a larger output in experiments than in theory. This can be added to the heterodyne amplitude A in Eq. (4.67) as a term proportional to $\langle \hat{b}_{in} \rangle$ similarly as to how it is done in Ref. 46. Furthermore pure dephasing can be added to see how the signal would change due to that, which can easily be done with the Lindblad master equation approach. The Transmon is insensitive to low frequency charge noise, one of the main dephasing mechanisms [16]. However it could be of interest to see if this would have any effect on the response.

There were also some terms thrown away in the RWA when deriving the Hamiltonian for the Transmon in Sec. 3.4, and it would be interesting to further investigate how this effects the end result if one tries to keep these terms, as this is something that is rarely done when studying the system.

The loss of coherence was only investigated in the single tone measurements in Sec. 6.4.2 for the case when the probe drives the system on resonance, however as seen from Figs. 6.2b there is also significant loss of coherence at other frequencies forming arc-like shapes. The reason for this loss of coherence could be further explored, for instance by analysing the emission spectrum at those frequencies as well. This could show for instance if the loss of coherence is due to sequential decay of for instance the first and second transitions, or some other process. It could also show if an effect similar to that of the Mollow triplet splitting occurs then as well due to the saturation of the second excited state.

It was mentioned in Chapter 2 that the probe and LO were phase locked to each other but

not to the drive. This is not captured within the theoretical model presented in the thesis, as lack of phase locking can lead to for instance phase drifting. This is something that could be added to the model as well, appearing in the drive term as $e^{-i\omega_d t+i\varphi(t)}$, where $\varphi(t)$ can be some stochastic process or a constant phase drift, in order to try to capture this effect. Experiments were however performed with phase locking to the drive as well, without observation of any significant difference [1].

The method for the two-tone measurements could also be adapted to have the operators for the probe in the dressed state basis similarly to how some have done it in previous works (see e.g. Refs. 22, 24) rather than in the bare state basis. This is an additional alternative that has potential to improve on the agreement between experiment and theory.

Future experimental work of interest is to try to measure the response at frequency $2f_d - f_p$ shown in Figs. 7.3d,e. If a signal is detected then this would motivate further investigation into the underlying physical process causing this effect. For instance, as it seems to be an effect that is strong along the Mollow triplet frequencies, a dressed states picture might be appropriate to use. For instance where a photon from the probe causes a de-excitation at f_p, then energy conservation forces another photon at $2f_d - f_p$ to be emitted, which is then the frequency at the opposite side Mollow triplet. This does not explain why it would be coherent though. Another picture is that of a scattering process, where two incoming photons at frequency f_d scatter at the system, emitting two photons at frequencies $2f_d - f_p$ and f_p with this process becoming more likely somehow due to resonance with the Mollow triplet frequencies as well as presence of a photon with frequency f_p. The answer might even already exist in previous work or literature.

In summary, a lot of the needed basic theory for quantum optics and in particular superconducting circuits for describing the system was presented quite detailed, as well as derivations for the particular system that was studied. Furthermore instructive examples and in places detailed calculations were presented in order to get acquainted with methods of how the theoretical tools can be used. Some of the theory showed excellent agreement with theoretical data while other parts of the approaches used motivate further studies for improved understanding. It was also proposed to perform an experiment in order to verify theoretical results not yet measured in experiments.

Bibliography

[1] S. Andersson, H. Havir, A. Ranni, S. Haldar, and V. F. Maisi. High-impedance microwave resonators with two-photon nonlinear effects, 2024. URL https://doi.org/10.48550/arXiv.2403.03779.

[2] C.P. Wen. Coplanar waveguide: A surface strip transmission line suitable for nonreciprocal gyromagnetic device applications. *IEEE Transactions on Microwave Theory and Techniques*, 17(12):1087–1090, 1969. doi: 10.1109/TMTT.1969.1127105.

[3] M. Göppl, A. Fragner, M. Baur, R. Bianchetti, S. Filipp, J. M. Fink, P. J. Leek, G. Puebla, L. Steffen, and A. Wallraff. Coplanar waveguide resonators for circuit quantum electrodynamics. *Journal of Applied Physics*, 104(11), December 2008. ISSN 1089-7550. doi: 10.1063/1.3010859. URL http://dx.doi.org/10.1063/1.3010859.

[4] Conrad Clauss, Martin Dressel, and Marc Scheffler. Optimization of coplanar waveguide resonators for esr studies on metals. *Journal of Physics: Conference Series*, 592: 012146, March 2015. ISSN 1742-6596. doi: 10.1088/1742-6596/592/1/012146. URL http://dx.doi.org/10.1088/1742-6596/592/1/012146.

[5] R. Bianchetti, S. Filipp, M. Baur, J. M. Fink, M. Göppl, P. J. Leek, L. Steffen, A. Blais, and A. Wallraff. Dynamics of dispersive single-qubit readout in circuit quantum electrodynamics. *Physical Review A*, 80(4), October 2009. ISSN 1094-1622. doi: 10.1103/physreva.80.043840. URL http://dx.doi.org/10.1103/PhysRevA.80.043840.

[6] T. Frey, P. J. Leek, M. Beck, A. Blais, T. Ihn, K. Ensslin, and A. Wallraff. Dipole coupling of a double quantum dot to a microwave resonator. *Phys. Rev. Lett.*, 108: 046807, Jan 2012. doi: 10.1103/PhysRevLett.108.046807. URL https://link.aps.org/doi/10.1103/PhysRevLett.108.046807.

[7] Subhomoy Haldar, Drilon Zenelaj, Patrick P. Potts, Harald Havir, Sebastian Lehmann, Kimberly A. Dick, Peter Samuelsson, and Ville F. Maisi. Microwave power harvesting using resonator-coupled double quantum dot photodiode. *Physical Review B*, 109(8), February 2024. ISSN 2469-9969. doi: 10.1103/physrevb.109.l081403. URL http://dx.doi.org/10.1103/PhysRevB.109.L081403.

[8] R.N. Simons. *Coplanar Waveguide Circuits, Components, and Systems*. Wiley Series

in Microwave and Optical Engineering. Wiley, 2004. ISBN 9780471463931. URL https://books.google.se/books?id=XgNMZ5YVJdgC.

[9] S. M. Girvin. 113Circuit QED: superconducting qubits coupled to microwave photons. In *Quantum Machines: Measurement and Control of Engineered Quantum Systems: Lecture Notes of the Les Houches Summer School: Volume 96, July 2011*. Oxford University Press, 06 2014. ISBN 9780199681181. doi: 10.1093/acprof:oso/9780199681181.003.0003. URL https://doi.org/10.1093/acprof:oso/9780199681181.003.0003.

[10] A. Wallraff, D. I. Schuster, A. Blais, L. Frunzio, R.-S. Huang, J. Majer, S. Kumar, S. M. Girvin, and R. J. Schoelkopf. Strong coupling of a single photon to a superconducting qubit using circuit quantum electrodynamics. *Nature*, 431 (7005):162–167, September 2004. ISSN 1476-4687. doi: 10.1038/nature02851. URL http://dx.doi.org/10.1038/nature02851.

[11] B.D. Josephson. Possible new effects in superconductive tunnelling. *Physics Letters*, 1(7):251–253, 1962. ISSN 0031-9163. doi: https://doi.org/10.1016/0031-9163(62)91369-0. URL https://www.sciencedirect.com/science/article/pii/0031916362913690.

[12] M. A. Castellanos-Beltran, K. D. Irwin, G. C. Hilton, L. R. Vale, and K. W. Lehnert. Amplification and squeezing of quantum noise with a tunable josephson metamaterial. *Nature Physics*, 4(12):929–931, October 2008. ISSN 1745-2481. doi: 10.1038/nphys1090. URL http://dx.doi.org/10.1038/nphys1090.

[13] R. Vijay, D. H. Slichter, and I. Siddiqi. Observation of quantum jumps in a superconducting artificial atom. *Physical Review Letters*, 106(11), March 2011. ISSN 1079-7114. doi: 10.1103/physrevlett.106.110502. URL http://dx.doi.org/10.1103/PhysRevLett.106.110502.

[14] N. Bergeal, F. Schackert, M. Metcalfe, R. Vijay, V. E. Manucharyan, L. Frunzio, D. E. Prober, R. J. Schoelkopf, S. M. Girvin, and M. H. Devoret. Phase-preserving amplification near the quantum limit with a josephson ring modulator. *Nature*, 465 (7294):64–68, May 2010. ISSN 1476-4687. doi: 10.1038/nature09035. URL http://dx.doi.org/10.1038/nature09035.

[15] V Bouchiat, D Vion, P Joyez, D Esteve, and M H Devoret. Quantum coherence with a single cooper pair. *Physica Scripta*, 1998(T76):165, jan 1998. doi: 10.1238/Physica.Topical.076a00165. URL https://dx.doi.org/10.1238/Physica.Topical.076a00165.

[16] Jens Koch, Terri M. Yu, Jay Gambetta, A. A. Houck, D. I. Schuster, J. Majer, Alexandre Blais, M. H. Devoret, S. M. Girvin, and R. J. Schoelkopf. Charge-insensitive qubit design derived from the cooper pair box. *Phys. Rev. A*, 76:042319, Oct 2007. doi: 10.1103/PhysRevA.76.042319. URL https://link.aps.org/doi/10.1103/PhysRevA.76.042319.

[17] Christian Kraglund Andersen and Alexandre Blais. Ultrastrong coupling dynamics

with a transmon qubit. *New Journal of Physics*, 19(2):023022, feb 2017. doi: 10.1088/1367-2630/aa5941. URL https://dx.doi.org/10.1088/1367-2630/aa5941.

[18] A. Stockklauser, P. Scarlino, J. V. Koski, S. Gasparinetti, C. K. Andersen, C. Reichl, W. Wegscheider, T. Ihn, K. Ensslin, and A. Wallraff. Strong coupling cavity qed with gate-defined double quantum dots enabled by a high impedance resonator. *Physical Review X*, 7(1), March 2017. ISSN 2160-3308. doi: 10.1103/physrevx.7.011030. URL http://dx.doi.org/10.1103/PhysRevX.7.011030.

[19] Jay M. Gambetta, Jerry M. Chow, and Matthias Steffen. Building logical qubits in a superconducting quantum computing system. *npj Quantum Information*, 3(1), January 2017. ISSN 2056-6387. doi: 10.1038/s41534-016-0004-0. URL http://dx.doi.org/10.1038/s41534-016-0004-0.

[20] Nicholas A. Masluk, Ioan M. Pop, Archana Kamal, Zlatko K. Minev, and Michel H. Devoret. Microwave characterization of josephson junction arrays: Implementing a low loss superinductance. *Phys. Rev. Lett.*, 109:137002, Sep 2012. doi: 10.1103/PhysRevLett.109.137002. URL https://link.aps.org/doi/10.1103/PhysRevLett.109.137002.

[21] Antti Ranni, Subhomoy Haldar, Harald Havir, Sebastian Lehmann, Pasquale Scarlino, Andreas Baumgartner, Christian Schönenberger, Claes Thelander, Kimberly A. Dick, Patrick P. Potts, and Ville F. Maisi. Dephasing in a crystal-phase defined double quantum dot charge qubit strongly coupled to a high-impedance resonator, 2023. URL https://doi.org/10.48550/arXiv.2308.14887.

[22] K. Koshino, H. Terai, K. Inomata, T. Yamamoto, W. Qiu, Z. Wang, and Y. Nakamura. Observation of the three-state dressed states in circuit quantum electrodynamics. *Phys. Rev. Lett.*, 110:263601, Jun 2013. doi: 10.1103/PhysRevLett.110.263601. URL https://link.aps.org/doi/10.1103/PhysRevLett.110.263601.

[23] Io-Chun Hoi, C. M. Wilson, Göran Johansson, Tauno Palomaki, Borja Peropadre, and Per Delsing. Demonstration of a single-photon router in the microwave regime. *Phys. Rev. Lett.*, 107:073601, Aug 2011. doi: 10.1103/PhysRevLett.107.073601. URL https://link.aps.org/doi/10.1103/PhysRevLett.107.073601.

[24] Emely Wiegand, Ping-Yi Wen, Per Delsing, Io-Chun Hoi, and Anton Frisk Kockum. Ultimate quantum limit for amplification: a single atom in front of a mirror. *New Journal of Physics*, 23(4):043048, April 2021. ISSN 1367-2630. doi: 10.1088/1367-2630/abf1d8. URL http://dx.doi.org/10.1088/1367-2630/abf1d8.

[25] T. Yamaji, S. Kagami, A. Yamaguchi, T. Satoh, K. Koshino, H. Goto, Z. R. Lin, Y. Nakamura, and T. Yamamoto. Spectroscopic observation of the crossover from a classical duffing oscillator to a kerr parametric oscillator. *Phys. Rev. A*, 105:023519,

Feb 2022. doi: 10.1103/PhysRevA.105.023519. URL https://link.aps.org/doi/10.1103/PhysRevA.105.023519.

[26] P. Y. Wen, A. F. Kockum, H. Ian, J. C. Chen, F. Nori, and I.-C. Hoi. Reflective amplification without population inversion from a strongly driven superconducting qubit. *Physical Review Letters*, 120(6), February 2018. ISSN 1079-7114. doi: 10.1103/physrevlett.120.063603. URL http://dx.doi.org/10.1103/PhysRevLett.120.063603.

[27] D.F. Walls and G.J. Milburn. *Quantum Optics*. Springer Berlin Heidelberg, 2008. ISBN 9783540285731. URL https://books.google.se/books?id=LiWsc3Nlf0kC.

[28] H. Zu, W. Dai, and A.T.A.M. de Waele. Development of dilution refrigerators—a review. *Cryogenics*, 121:103390, 2022. ISSN 0011-2275. doi: https://doi.org/10.1016/j.cryogenics.2021.103390. URL https://www.sciencedirect.com/science/article/pii/S001122752100148X.

[29] M. Tinkham. *Introduction to Superconductivity*. Dover Books on Physics Series. Dover Publications, 2004. ISBN 9780486134727. URL https://books.google.se/books?id=VpUk3NfwDIkC.

[30] J. Bardeen, L. N. Cooper, and J. R. Schrieffer. Theory of superconductivity. *Phys. Rev.*, 108:1175–1204, Dec 1957. doi: 10.1103/PhysRev.108.1175. URL https://link.aps.org/doi/10.1103/PhysRev.108.1175.

[31] N A Court, A J Ferguson, and R G Clark. Energy gap measurement of nanostructured aluminium thin films for single cooper-pair devices. *Superconductor Science and Technology*, 21(1):015013, November 2007. ISSN 1361-6668. doi: 10.1088/0953-2048/21/01/015013. URL http://dx.doi.org/10.1088/0953-2048/21/01/015013.

[32] Vinay Ambegaokar and Alexis Baratoff. Tunneling between superconductors. *Phys. Rev. Lett.*, 10:486–489, Jun 1963. doi: 10.1103/PhysRevLett.10.486. URL https://link.aps.org/doi/10.1103/PhysRevLett.10.486.

[33] Uri Vool and Michel Devoret. Introduction to quantum electromagnetic circuits. *International Journal of Circuit Theory and Applications*, 45(7):897–934, June 2017. ISSN 1097-007X. doi: 10.1002/cta.2359. URL http://dx.doi.org/10.1002/cta.2359.

[34] J. J. Sakurai and Jim Napolitano. *Modern Quantum Mechanics*. Cambridge University Press, 3 edition, 2020.

[35] Roy J. Glauber. Coherent and incoherent states of the radiation field. *Phys. Rev.*, 131:2766–2788, Sep 1963. doi: 10.1103/PhysRev.131.2766. URL https://link.aps.org/doi/10.1103/PhysRev.131.2766.

[36] Wei-Min Zhang, Da Hsuan Feng, and Robert Gilmore. Coherent states: Theory and some applications. *Rev. Mod. Phys.*, 62:867–927, Oct 1990. doi: 10.1103/RevModPhys.62.867. URL https://link.aps.org/doi/10.1103/RevModPhys.62.867.

[37] Alexandre Blais, Arne L. Grimsmo, S. M. Girvin, and Andreas Wallraff. Circuit quantum electrodynamics. *Reviews of Modern Physics*, 93(2), May 2021. ISSN 1539-0756. doi: 10.1103/revmodphys.93.025005. URL http://dx.doi.org/10.1103/RevModPhys.93.025005.

[38] A. A. Clerk, M. H. Devoret, S. M. Girvin, Florian Marquardt, and R. J. Schoelkopf. Introduction to quantum noise, measurement, and amplification. *Rev. Mod. Phys.*, 82:1155–1208, Apr 2010. doi: 10.1103/RevModPhys.82.1155. URL https://link.aps.org/doi/10.1103/RevModPhys.82.1155.

[39] C. W. Gardiner and M. J. Collett. Input and output in damped quantum systems: Quantum stochastic differential equations and the master equation. *Phys. Rev. A*, 31:3761–3774, Jun 1985. doi: 10.1103/PhysRevA.31.3761. URL https://link.aps.org/doi/10.1103/PhysRevA.31.3761.

[40] Bernard Yurke. Use of cavities in squeezed-state generation. *Phys. Rev. A*, 29:408–410, Jan 1984. doi: 10.1103/PhysRevA.29.408. URL https://link.aps.org/doi/10.1103/PhysRevA.29.408.

[41] Bernard Yurke and John S. Denker. Quantum network theory. *Phys. Rev. A*, 29:1419–1437, Mar 1984. doi: 10.1103/PhysRevA.29.1419. URL https://link.aps.org/doi/10.1103/PhysRevA.29.1419.

[42] M. J. Collett and C. W. Gardiner. Squeezing of intracavity and traveling-wave light fields produced in parametric amplification. *Phys. Rev. A*, 30:1386–1391, Sep 1984. doi: 10.1103/PhysRevA.30.1386. URL https://link.aps.org/doi/10.1103/PhysRevA.30.1386.

[43] Lev S. Bishop. Circuit quantum electrodynamics, 2010. URL https://doi.org/10.48550/arXiv.1007.3520.

[44] Daniel Manzano. A short introduction to the lindblad master equation. *AIP Advances*, 10(2), February 2020. ISSN 2158-3226. doi: 10.1063/1.5115323. URL http://dx.doi.org/10.1063/1.5115323.

[45] B. R. Mollow. Power spectrum of light scattered by two-level systems. *Phys. Rev.*, 188:1969–1975, Dec 1969. doi: 10.1103/PhysRev.188.1969. URL https://link.aps.org/doi/10.1103/PhysRev.188.1969.

[46] Lev S. Bishop, J. M. Chow, Jens Koch, A. A. Houck, M. H. Devoret, E. Thuneberg, S. M. Girvin, and R. J. Schoelkopf. Nonlinear response of the vacuum rabi resonance. *Nature Physics*, 5(2):105–109, December 2008. ISSN 1745-2481. doi: 10.1038/nphys1154. URL http://dx.doi.org/10.1038/nphys1154.

[47] O. Astafiev, A. M. Zagoskin, A. A. Abdumalikov, Yu. A. Pashkin, T. Yamamoto, K. Inomata, Y. Nakamura, and J. S. Tsai. Resonance fluorescence of a single artificial

atom. *Science*, 327(5967):840–843, February 2010. ISSN 1095-9203. doi: 10.1126/science.1181918. URL http://dx.doi.org/10.1126/science.1181918.

[48] Stephen M. Barnett and Paul M. Radmore. Dressed States. In *Methods in Theoretical Quantum Optics*. Oxford University Press, 11 2002. ISBN 9780198563617. doi: 10.1093/acprof:oso/9780198563617.003.0006. URL https://doi.org/10.1093/acprof:oso/9780198563617.003.0006.

[49] Fahad Aziz, Kuan Ting Lin, Ping Yi Wen, Samina, Yu Chen Lin, Emely Wiegand, Ching-Ping Lee, Yu-Ting Cheng, Ching-Yeh Chen, Chin-Hsun Chien, Kai-Min Hsieh, Yu-Huan Huang, Ian Hou, Jeng-Chung Chen, Yen-Hsiang Lin, Anton Frisk Kockum, Guin Dar Lin, and Io-Chun Hoi. Microwave amplification via interfering multi-photon processes in a half-waveguide quantum electrodynamics system, 2023. URL https://doi.org/10.48550/arXiv.2302.07442.

[50] S. H. Autler and C. H. Townes. Stark effect in rapidly varying fields. *Phys. Rev.*, 100:703–722, Oct 1955. doi: 10.1103/PhysRev.100.703. URL https://link.aps.org/doi/10.1103/PhysRev.100.703.

[51] J. E. Mooij and Gerd Schön. Propagating plasma mode in thin superconducting filaments. *Phys. Rev. Lett.*, 55:114–117, Jul 1985. doi: 10.1103/PhysRevLett.55.114. URL https://link.aps.org/doi/10.1103/PhysRevLett.55.114.